Institut für Geodäsie und Geoinformation

Professur für Astronomische, Physikalische und Mathematische Geodäsie

Development of an experimental gravimetric geoid model for Nigeria

Dissertation

zur Erlangung des Grades

Doktor der Ingenieurwissenschaften (Dr.-Ing.)

der Landwirtschaftlichen Fakultät

der Rheinischen Friedrich-Wilhelms-Universität Bonn

vorgelegt von

Michael Bako

aus Minna, Nigeria

Bonn 2024

igg

UNIVERSITÄT BONN

Referent: Prof. Dr.-Ing. Jürgen Kusche
Korreferent: Prof. Dr.-Ing. Michael Schindelegger

Tag der mündlichen Prüfung: 13. Dezember, 2024.
Angefertigt mt Genehmigung der Landwirtschaftlichen Fakultät der Universität Bonn

Abstract

Due to the increasing demand for precise mapping, surveying, geodesy, and large-scale infrastructure projects, the establishment of a precise national geoid model for Nigeria is essential. In this doctoral thesis, an experimental gravimetric geoid model customized for Nigeria has been developed. This model integrates various data sources, including terrestrial gravity data, shipborne gravity measurements, satellite altimetry-derived gravity data, and contributions from Global Geopotential Models (GGMs). One of the objective of this research is to conduct validation of geoid height from GGM using GNSS/levelling data over Nigeria**.** The results of this evaluation confirm that the application of the Spectral Enhancement Method (SEM) has improved the assessment of GGM solutions in an unbiased manner. Integrating XGM2019e_2159 and SRTM data to constraint the high-frequency component of geoid heights in GOCE-based GGMs leads to an approximately 10% improvement in reducing the standard deviation (SD) relative to when the SEM was not applied. TIM_R6 at spherical harmonics (SH) up to degree and orders (d/o) 260 demonstrates the least SD when compared with DIR_R6 and SPW_R5, with a reduction from 0.380 m without SEM application to 0.342 m with SEM implementation. Additionally, four transformation models comprise: linear, four-parameter, five-parameter, and seven-parameter models were evaluated. The objective is to mitigate reference system offsets between the GNSS/levelling data and the GGMs, and to identify the particular parametric model with smallest SDs across all GGMs. This effort reduced the GGMs' misfits to GNSS/levelling to 0.30 m, a 15.3% decrease in SD. Notably, the XGM2019e_2159 model provides this improvement. As an independent validation, recent high-degree combined global gravity-field models were evaluated against terrestrial gravity data to determine the most adequate/suitable global model within the study area. The results indicate that XGM2019e_2159 outperformed other evaluated models, achieving accuracies of 6.24 mGal in term of SD. Furthermore, an evaluation and homogenization of a marine gravity database from shipborne and satellite altimetry-derived gravity data over the coastal region of Nigeria was carried out. The analysis showed that DTU21GRA outperformed the other models in the same region when compared with shipborne data. The refined shipborne data were merged with the DTU21GRA data using Least-Squares Collocation (LSC) to create a combined dataset. An independent validation against 100 randomly selected shipborne gravity points that are not included in the LSC procedures confirmed the improvement after the integration procedure. Additionally, comparisons between the complete refined shipborne data and the combined dataset revealed that the mean offset and SD values decreased from 0.43 to -0.02 mGal and 3.14 to 2.69 mGal, respectively, which reveal an improvement in the final combined data. Gravimetric geoid models were generated using refined shipborne data and combined gravity datasets. The Mean Dynamic Topography (MDT) was derived using the Technical University of Denmark (DTU) 21 Mean Sea Surface (MSS) and validated against the Center National d'Etudes Spatiales (CNES-CLS22) MDT. The geoid model constructed with the combined gravity data showed slight improvement in the mean values, decreasing from 0.924 to 0.923 m when evaluated against the CNES-CLS22 MDT. Finally, an experimental gravimetric geoid model customized for Nigeria, designated as Nigeria-Experimental Geoid Model (NG-EGM2024), was computed. This computation employed the Fast Fourier Transformation (FFT) method within the Remove-Compute-Restore (RCR) procedure. NG-EGM2024 integrate various datasets, including gravity anomalies from the combined global geopotential model XGM2019e_2159 up to SH d/o 360, along with terrestrial gravity datasets comprising 1055 gravity field anomalies and approximately 2026 and 3371 shipborne and satellite-altimetry gravity anomalies respectively. The results of comparisons between the 10 GNSS/levelling geoid undulations and the computed geoid model NG-EGM2024 revealed that the gravimetric geoid over Nigeria exhibits an accuracy of 10.8 cm accuracy in terms of SD.

Zusammenfassung

Aufgrund des zunehmenden Bedarfs an präziser Kartierung, Vermessung, Geodäsie und großen Infrastrukturprojekten ist die Erstellung eines präzisen nationalen Geoidmodells für Nigeria unerlässlich. In dieser Dissertation wurde ein experimentelles gravimetrisches Geoidmodell entwickelt, das speziell auf Nigeria zugeschnitten ist. Dieses Modell integriert verschiedene Datenquellen, darunter terrestrische Schwerefelddaten, schiffsgestützte Schwerefeldmessungen, von der Satellitenaltimetrie abgeleitete Schwerefelddaten und Beiträge von globalen Geopotentialmodellen (GGMs). Eines der Ziele dieser Forschung ist die Validierung der Geoidhöhe aus dem GGM unter Verwendung von GNSS-Nivellierungsdaten uber Nigeria. Die Ergebnisse dieser Auswertung bestätigen, dass die Anwendung der Spectral Enhancement Methode (SEM) die Bewertung der GGM-Lösungen auf unvoreingenommene Weise verbessert hat. Die Integration von XGM2019e_2159 und SRTM-Daten zur Einschränkung der Hochfrequenzkomponente der Geoidhöhen in GOCE-basierten GGMs führt zu einer ca. 10% Verbesserung bei der Verringerung der Standardabweichung (SD) im Vergleich zur Nichtanwendung der SEM. TIM_R6 weist bei sphärischen Harmonischen (SH) bis zu Grad und Ordnungen 260 die geringste SD im Vergleich zu DIR_R6 und SPW_R5 auf, mit einer Reduzierung von 0,380 m ohne SEM-Anwendung auf 0,342 m mit SEM-Implementierung. Zusätzlich wurden vier Transformationsmodelle bewertet: lineare, Vier-Parameter-, Fünf-Parameter- und Sieben-Parameter-Modelle. Ziel ist es, die Abweichungen des Referenzsystems zwischen den GNSS-/Nivellierdaten und den GGMs zu verringern und das parametrische Modell mit der geringsten Abweichung für alle GGMs zu ermitteln. Dadurch konnte die Abweichung der GGMs von den GNSS-/Nivellierungsdaten auf 0,30 m reduziert werden, was einer Verringerung der SD um 15,3 % entspricht. Diese Verbesserung wurde insbesondere durch das Modell XGM2019e_2159 erzielt. Als unabhängige Validierung wurden aktuelle kombinierte globale Schwerefeldmodelle hohen Grades mit terrestrischen Schwerefelddaten verglichen, um das geeignetste globale Modell für das Untersuchungsgebiet zu ermitteln. Die Ergebnisse zeigen, dass XGM2019e_2159 die anderen bewerteten Modelle mit einer Genauigkeit von 6,24 mGal l für SD. Darüber hinaus wurde eine Bewertung und Harmonisierung einer marinen Schwere-Datenbank durchgeführt, die aus schiffsgestützten und satellitengestützten Schwere-Daten über dem Nigeria-Meer abgeleitet wurde. Die Analyse zeigte, dass DTU21GRA im Vergleich zu anderen Modellen in der gleichen Region besser abschneidet als die anderen Modelle, wenn sie mit schiffsgestützten Daten verglichen werden. Die verfeinerten schiffsgestützten Daten wurden mit den DTU21GRA-Daten unter Verwendung der Kleinste-Quadrate-Kollokation (LSC) zusammengeführt, um einen kombinierten Datensatz zu erstellen. Eine unabhängige Validierung anhand von 100 zufällig ausgewählten schiffsgestützten Schwerepunkten, die nicht in die LSC-Verfahren einbezogen wurden, bestätigte die Verbesserung nach dem Integrationsverfahren. Darüber hinaus ergaben Vergleiche zwischen den vollständigen verfeinerten schiffsgestützten Daten und dem kombinierten Datensatz, dass der mittlere Offset und die SD-Werte von 0,43 auf −0,02 mGal bzw. von 3,14 auf 2,69 mGal zurückgingen, was eine Verbesserung der endgültigen kombinierten Daten erkennen lässt. Gravimetrische Geoidmodelle wurden mit den verfeinerten schiffsgestützten Daten und den kombinierten Datensätzen erstellt. Die mittlere dynamische Topographie (Mean Dynamic Topography, MDT) wurde aus dem Model DTU21-MSS der mittleren Meeresoberfläche (Mean Sea Surface, MSS) der Technischen Universität Dänemark (DTU) abgeleitet und anhand der MDT des Center National d'Etudes Spatiales (CNES-CLS22) validiert. Das Geoidmodell, das mit den kombinierten Schwerefelddaten erstellt wurde, zeigte eine Verbesserung der Offset-Werte, die von 0,924 auf 0,923 m sanken, wenn es mit dem CNES-CLS22 MDT verglichen wurde. Schließlich wurde ein experimentelles gravimetrisches Geoidmodell für Nigeria berechnet, das als NG-EGM2024 bezeichnet wird. Bei dieser Berechnung wurde die Methode der schnellen Fourier-Transformation (FFT) im Rahmen des Remove-Compute-Restore (RCR)-Verfahrens verwendet. Das Nigeria-Experimental Geoid Model (NG-EGM2024) integriert verschiedene Datensätze,

darunter Schwereanomalien des kombinierten globalen Geopotentialmodells (XGM2019e_2159) bis zum SH-Grad und der Ordnung 360, sowie terrestrische Schweredatensätze, die 1055 Schwerefeldanomalien und etwa 2026 bzw. 3371 schiffsgestützte und satellitengestützte Schwereanomalien umfassen. Die Ergebnisse der Vergleiche zwischen den 10 GNSS/Nivellier-Geoid-Wellen und dem berechneten Geoidmodell NG-EGM2024 zeigten, dass das gravimetrische Geoid über Nigeria eine Genauigkeit von 10,8 cm in Bezug auf die SD aufweist.

Acknowledgements

I would like to begin by expressing my profound gratitude to God almighty for bestowing upon me the privilege to embark on my Ph.D. journey in Germany. I extend my sincere appreciation to my esteemed supervisor, Prof. Dr.-Ing. Jurgen Kusche, for graciously accepting the responsibility of guiding and mentoring me throughout this endeavor. Your mentorship has been an immense honor, marked by your meticulous guidance from the inception of this academic pursuit, and your ever-attentive ear to my queries. I am still amazed by how little information you need to formulate relevant questions. Furthermore, I acknowledge the extensive effort you devoted to reviewing my manuscripts, an effort that has not gone unnoticed. I am confident that my sentiment is shared by numerous colleagues who have had the privilege of your mentorship. I extend my gratitude to Prof. Dr.-Ing Michael Schindelegger, PD Dr.-Ing Luciana Fenoglio-Marc, Dr.-Ing Basem Elsaka, Dr.-Ing Bernd Uebbing and Dr. Fupeng Li for their valuable enlightening correspondence and sharing their experience with me during the course of my Ph.D. research. I am also appreciative of the unwavering support I received from the entire departmental staff, with a mention of Mrs. Catherine van Eckeren, the secretary of the APMG research group, who provided invaluable assistance in administrative matters and facilitated my access to conference travel grants from the university. I also appreciate the University of Bonn for awarding me the get finished scholarship.

I wish to convey my heartfelt thanks to the management of the Federal University of Technology (FUT) Minna for releasing me to pursue my studies at the Institute of Geodesy and Geoinformation, University of Bonn, Germany. My gratitude extends to the entire management and staff of Surveying and Geoinformatics Department, FUT Minna for their support at various junctures. I reserve a special place in my heart for my family, particularly my late parents, Mr. and Mrs. Raphael Bako, who held unwavering aspirations of witnessing this momentous day. Words cannot adequately express my appreciation for all that you have done. To my brothers and the entire extended family, I extend my heartfelt gratitude.

Lastly, I express my deep appreciation to my wife, Mariam Michael, and my daughter, Agnes Michael, for their unwavering support and tranquility throughout my Ph.D. pursuit.

Contents

List of Figures

List of Table

List of Plates

List of Abbreviations

Abbreviations	Meanings
BGI	Bureau Gravimetrique International
BVP	Boundary Value Problem
CHAMP	CHAllenging Minisatellite Payload
CNES	Centre National d'Etudes Spatiales
XO	Cross-over
d/o	Degree and Order
DIR	Direct solution
DLR	DeutschesZentrumfurLuft-und Raumfahrt
DNSC	Danish National Space Centre
DTU	Technical University of Denmark
EGG	Electrostatic Gravity Gradiometer
EGM2008	Earth Geopotential Model 2008
EIGEN	European Improved Gravity models of the Earth By New techniques
ESA	European Space Agency
FFT	Fast Fourier Transform
GECO	GOCE and EGM2008 combination model
GGMs	Global Geopotential Models
GNSS	Global Navigation Satellite System
GOCE	Gravity field and steady-state Ocean Circulation Explorer
GOCO	Gravity Observation Combination
GRACE	Gravity Recovery and Climate Experiment
GRACE-FO	Gravity Recovery and Climate Experiment Follow-On
GRS80	Geodetic Reference System 1980
ICGEM	International Centre for Global Earth Models
IAG	International Association of Geodesy
LEOs	Low Earth Orbiting Satellite
LSC	Least Squares Collocation
MSL	Mean Sea Level
MDT	Mean Dynamic Topography
MSS	Mean Sea Surface
NG-EGM2024	Nigeria-Experimental Geoid Model 2024
RCR	Remove-Compute-Restore
RTM	Residual Terrain Modelling
SA	Satellite Altimetry
SEM	Spectral Enhancement Method
SGG	Satellite Gravity Gradiometer
SGG-UGM-2	Satellite Gravity Gradiometer-Universal Geopotential Model-2

SH	Spherical Harmonics
SLR	Satellite Laser Ranging
SPW	Space-wise solution
SRTM	Shuttle Radar Topography Mission
SST	Space borne Satellite Tracking
SWOT	Surface Waters and Ocean Topography altimeter mission
TIM	Time-Wise solution
XV	Cross validation
XGM2019e_2159	Combined global gravity field model

Chapter 1

Introduction

1.1 Background to the Study

Geodesy is a scientific discipline focused on comprehending the Earth through three fundamental pillars: The Earth’s time-dependent geometric shape, its time-dependent gravitational field, and its rotation, including variations (Torge & Muller, 2012). Addressing one of these pillars namely, the determination of Earth's gravitational field, results in a representation of Earth's physical figure. An indispensable component for unravelling Earth as a dynamic system lies in our understanding of Earth's gravitational field, and changes in it, as these aspects reflect on the distribution and movement of mass in geophysical fluids and within the solid Earth. The Earth's gravitational field is of particular significance in defining the geoid. The geoid is an equipotential surface of the Earth’s gravity field which best fits to the mean sea level (MSL). This surface approximates the hypothetical undisturbed state of the ocean's surface, disregarding influences such as currents and tides. Precise knowledge of Earth's gravitational field carries far-reaching implications, benefiting, e.g., geodynamics, sea-level science, ice mass determination, and ocean circulation studies. A comprehensive overview can be found in Ilk et al. (2005).

The principal area of application for geoids is their use as a reference surface in geodetic levelling. In such activities, the elevation measured by levelling is relative to that of the geoid (Odumusu, 2019). Obtaining accurate marine and terrestrial gravity data is of paramount importance for determining geoid shape and high-resolution mean dynamic topography (MDT), connecting offshore and land height systems, identifying the distribution of mineral resources, and conducting gas and petroleum exploration (Sandwell and Smith, 1997; Li et al., 2021; Bako and Kusche, 2024).

Multiple data sources, including shipborne, airborne, and satellite-derived gravity data, are available for determining the marine gravity fields. However, relying solely on a single data source may not provide an accurate and high-resolution representation of desired results (Zamri et al., 2024). To address this, it is essential to merge gravity datasets from various sources such as global geopotential models (GGMs), shipborne observations, and altimetry-derived gravity data. Combining satellite gravimetry observations with terrestrial data and other sources has

led to the development of combined GGMs, such as the Satellite Gravity Gradiometer-Universal Geopotential Model (SGG-UGM-2), combined global gravity field model (XGM2019e_2159), and Earth Gravitational Model (EGM2008), which improves the medium-to-short wavelength characteristics of the gravity field (Liang et al., 2020; Zingerle et al., 2019 and Pavlis et al.,2012).

Satellite altimetry missions have become instrumental in providing regional and global marine gravity data, offering high resolution and easy accessibility, particularly in regions with limited shipborne gravity data, such as the coastal region of Nigeria. However, the precision of altimetry measurements is affected near coastlines and in shallow waters because of challenges such as inadequate tidal modelling, substantial sea surface variations, and interference from onshore reflectors (Zhang et al., 2017).

Recent missions, such as CryoSat-2 and Sentinel-3A/B, have played a crucial role in enhancing the quality and accessibility of altimetry-derived gravity data. These missions employ synthetic aperture radar (SAR) altimeters, enabling precise sea surface height measurements up to a few kilometers near the coast. CryoSat-2, with its long repeat cycle, provides dense cross-track spacing, making it well suited for deriving marine gravity data (Abulaitijiang et al., 2015). CryoSat-2 operates in different modes, including low-resolution mode (LRM), SAR mode, and SAR interferometry (SARIn) mode (Calafat et al., 2017). Sentinel-3A/B, which inherits SAR altimeter technology from CryoSat-2, offers denser along-track measurements than conventional altimetry, including the LRM mode. As a result, SAR altimetry data achieves high accuracy levels, ranging from centimeters to decimeters, particularly near coastlines and lakes (Nielsen et al., 2015). DTU13GRA (Andersen and Knudsen, 2013), DTU15GRA (Andersen et al., 2017), DTU17GRA (Andersen and Knudsen, 2019), and DTU21GRA (Andersen and Knudsen 2021) utilized CryoSat-2 data, which operated in the LRM mode over the coastal region of Nigeria. However, these models did not incorporate SAR altimetry data. In contrast, DTU21GRA (Andersen and Knudsen, 2021) integrated SAR altimeter measurements from Sentinel-3A/B over the coastal region of Nigeria to improve the quality of the gravity data in the region. The forthcoming availability of novel datasets characterized by unprecedented resolution facilitated by the recently launched Surface Waters and Ocean Topography (SWOT) altimeter mission is anticipated.

Over the past two decades, significant progress has been made in modelling regional and local geoid models and acquiring gravity data through terrestrial, airborne, and satellite-based measurements. Consequently, achieving the precision of a regional or local geoid model at the

level of 1 centimeter has emerged as a prominent objective pursued by various research groups and surveying and mapping agencies on a global scale.

Over the past 20 years, the understanding of various Earth processes has significantly improved through the launch of several satellite missions dedicated to measuring the Earth's gravitational field, including the Challenging Minisatellite Payload (CHAMP) (Reigber, 1999), Gravity Ocean Circulation Explorer (GOCE) (Drinkwater et al., 2003), Gravity Recovery and Climate Experiment (GRACE) (Tapley, 2004) and Gravity Recovery and Climate Experiment Follow-On (GRACE-FO) (Kornfeld et al., 2019). For instance, CHAMP provides an almost continuous set of high-quality space borne satellite tracking (SST) observations combined with high-precision accelerometers and star sensor data. These observations were used to develop GGMs with a spatial resolution of 133 km, corresponding to spherical harmonics (SH) up to a degree and order (d/o) of 150 (Flechtner et al., 2010).

The GOCE mission provided unprecedented data on static gravity fields (Drinkwater et al., 2003). It became operational from 2009 to 2013, flew at an orbital altitude of 260 km, and was the first mission to carry a gradiometer as its primary instrument consisting of six accelerometers positioned along three perpendicular axes. GOCE observations have allowed scientists to improve the accuracy of the Earth's gravity field determination, achieving an accuracy of approximately 1–2 cm for geoid undulations at a spatial resolution of approximately 100 km. Consequently, numerous GGMs have been developed using coefficients derived from the solutions of the Stokes boundary value problem (BVP), represented as a series of SH (Ince et al., 2019). The GRACE mission, which operated from 2002 to 2017, enabled a more accurate determination of the Earth's gravity field compared to CHAMP, and was the first mission to detect time-variable changes in the gravity field at monthly intervals. The GRACE has a spatial resolution of approximately 1° × 1°. Following the success of GRACE, GRACE-FO (Kornfeld et al., 2019) has continued its objectives since its launch in May, 2018. As discussed by Bako et al., 2024.

1.2 Geoid modelling research in Nigeria and related region

Over the past thirty years, very little research has been conducted on modelling geoid heights within the Nigerian region. Few studies have been undertaken to this end, including those by Ezeigbo (1989) and Moka et al. (2018). To address the problem of determining a geoid model for Nigeria, Ezeigbo (1989) conducted a comprehensive study using doppler satellite observations. However, the limited distribution of doppler stations, totaling only approximately ten, employed in geoid computation renders it challenging to achieve the required level of

accuracy in geoid determination. Consequently, Ezeigbo (1986) highlighted in their research that the optimal geoid solution remains elusive owing to data limitations.

Currently, there is no official gravity database available for Nigeria. Efforts have been made to develop a gravimetric geoid model for Nigeria using airborne and shipborne gravity data from the Bureau Gravimétrique International (BGI, 2018) database and local Digital Terrain Models (DTMs) (Moka et al., 2018). However, the developed geoid model does not include gravity data derived from altimetry in its computations. With the introduction of new gravity data, such as marine gravity data calculated from the altimetry-based Technical University of Denmark (DTU) 21 Mean Sea Surface (MSS) (Andersen et al., 2023), hereafter referred to as the DTU21 Gravity (GRA) (Andersen and Knudsen, 2021), it is necessary to revisit the development of a geoid model for Nigeria to address these limitations. Moreover, this study differs from previous studies in that it provides new combined marine gravity datasets for geoid modelling based on a marine gravity database established using shipborne and satellite altimetry-derived gravity datasets (Bako and Kusche, 2024).

In addition, several researchers have developed geoid models in regions of comparable areas, topography, density, and conditions of gravimetric networks, such as Egypt, Cameron, Turkey, and the entire African region. In a study conducted by Saadon et al. (2021), two gravimetric geoid models were computed for Egypt using Least-Squares Collocation (LSC) and Fast Fourier Transformation (FFT) methodologies. Both techniques incorporate the remove-compute-restore (RCR) procedures into the computation process. Various datasets were employed in this analysis, including gravity contributions from the GOCE-based space-wise (SPW_5) model (Gatti et al., 2016) and EGM2008 (Pavlis et al.,2012) as reference model, terrestrial gravity data, and SRTM 30 data. The resulting geoid models, denoted as EGY-FLGM2019 (derived using the LSC method) and EGY-FFGM2019 (derived using the FFT method), were compared and validated against six Global Navigation Satellite System (GNSS)/levelling datasets. The outcomes of this comparison yielded standard deviations (SD) of 18.46 cm and 7.57 cm, respectively. Barzaghi et al. (2021) computed a new gravimetric quasi-geoid of Cameroon using recent GGMs and a detailed DTM of the region. In addition, terrestrial, shipborne and marine gravity data over Cameroon were incorporated into the computation. Three quasi-geoid models were developed based on the global GOCE-dir5, EGM2008, and XGM2019e_2159 models. The RCR technique was applied, and Fast Collocation was employed to estimate the residual quasi-geoid component from gridded gravity data. The developed geoid models were compared with GNSS/levelling data distributed across Cameroon, and the results show that the SD of the gravimetric quasi-geoid based on

EGM2008 is 14.4 cm while the geoid model computed using XGM2019e_2159 GGM showed an SD of 11.8 cm, In addition, the result of the gravimetric quasi-geoid obtained based on the satellite-only model, the GOCE-dir5 to d/o 300, showed an SD of 18.0 cm. Isik et al. (2022) conducted computations for the gravimetric geoid model in Turkey using two distinct reference models: the GOCE-only model (GO_CONS_GCF_2_TIM_R6) (Brockmann et al., 2021) and the combined model (EIGEN-6C4) (Förste et al., 2014). This analysis led to a noteworthy 23% improvement in the accuracy of the regional geoid model. The most precise result obtained in this study yielded an accuracy level of 7.7 cm.

Finally, Abd-Elmotaal et al. (2019) computed a geoid model for Africa, designated AFRgeo_v1.0. This computation relies on terrestrial gravity and gravity anomaly data acquired from shipborne and satellite altimetry sources. The computation of the geoid model for Africa followed two distinct methodologies. First, the tailored reference model, extending to degree and order 2160, was used to compute the geoid model. This process involves the application of the RCR technique, which employs the Stokes integral in the frequency domain using the 1D FFT technique. The second approach used the topographic-isostatic reduction method, incorporating the recent GGM EIGEN-6C4 (Förste et al., 2014), extended to d/o 2190 as a reference model. These two geoid models, generated using different methodologies, underwent a comparative analysis, which revealed significant differences between them. However, when the AFRgeo-v1.0 geoid model for Africa was juxtaposed with the AGP2003 geoid model (Merry et al., 2005), significant improvements in accuracy and precision were observed.

1.3 Statement of research Problem

Nigeria currently lacks an officially endorsed national or regional geoid model that holds uniform recognition throughout the country (Nwilo, 2013). Consequently, geodetic scientists in Nigeria encounter challenges when converting ellipsoidal heights obtained from GNSS observations into their corresponding orthometric heights. Without a dedicated or officially approved geoid model explicitly designed for Nigeria, particularly for extensive-scale applications, researchers must use pre-existing combined GGMs, such as EGM2008 (Pavlis et al.,2012) with a spatial resolution of 9 km or more recent models. However, a geopotential model that most accurately approximates the local gravity field has remained elusive (Nwilo, 2013). This deficiency necessitates frequent spirit-level observations, particularly in engineering projects. However, spirit levelling can be difficult and time-consuming, especially over large and rugged terrains or in coastal regions.

An officially accepted geoid model in Nigeria is necessary for various challenges, such as difficulties in connecting land and marine datum, assessing sea level rise, and implementing infrastructure projects (Bako and Kusche, 2024; Mahmud et al., 2023; Bako et al., 2020). Incompatible height systems, would cause complications for engineers who require orthometric heights referenced to the geoid. The availability of GNSS technology could simplify the determination of orthometric measurements if well-established and precise geoid model for Nigeria would be available.

1.4 Aim and objectives of the study

This research aims to develop an experimental gravimetric geoid model for Nigeria (NG-EM2024). The gravimetric geoid model for Nigeria will be developed by combining the available terrestrial free-air gravity anomaly data with accurate gravimetric information obtained from GGM. In addition, SRTM data (USGS, 2017), DTU21GRA (Andersen & Knudsen, 2021) and shipborne gravity data (BGI, 2018). In pursuit of this dissertation's aim, a series of research objectives have been delineated, each geared towards the research's core purpose:

i) To validate the geoid heights derived from GGMs by using GNSS/levelling data across Nigeria.

ii) To assess the efficacy of recent high-degree combined global gravity-field models for geoid modelling within the Nigerian region.

iii)To evaluate and homogenized a marine gravity database from shipborne gravity measurements and satellite-derived gravity data over the coastal region of Nigeria.

iv) To develop a gravimetric geoid model tailored explicitly to the Nigeria region, leveraging the available terrestrial gravity measurements, marine gravity data (shipborne and satellite-altimetric), SRTM data, and GGMs-derived data.

v) To evaluate the precision of the developed gravimetric geoid model for Nigeria, using five combined GGMs and 10 GNSS/levelling data not used in the fitting.

1.5 Outline of the Thesis

This thesis comprises six chapters, each addressing distinct aspects of the research. The ***second chapter*** overviews the GRACE/GOCE and Combined GGMs used in the study, highlighting their roles in advancing our understanding of the Earth's gravity field. Furthermore, this chapter provides comprehensive details in the fundamental theory of the Earth's gravity field and the geoid, presenting concepts relevant to the thesis. Within this context, the chapter expounds upon the computational methodologies employed in geoid determination, with particular

emphasis on the application of the FFT approach, which was used in the estimation of the developed gravimetric geoid for the Nigeria region.

The ***third chapter*** discusses the methodology and data used for the study in detail. It presents several methods of numerical analysis that have been carried out to validate and evaluate GGMs using ground truth data. Different procedures are discussed to overcome the spectral band inconsistency between gravity functional determined from GGMs and the corresponding functional obtained from ground truth data. Furthermore, this chapter offers insight into the computational framework governing the development of the gravimetric geoid model.

The results of the various validations and evaluations of GGMs using ground-based data are presented and discussed in the ***fourth chapter***. This chapter is organized into three sections to facilitate a comprehensive understanding of the research findings. The initial section showcases the results of validating the geoid heights over Nigeria from GGMs using GNSS/levelling data. Within this section, the first subsection delineates the validation results that do not incorporate spectral consistency considerations. By contrast, the second subsection presents findings obtained after accounting for spectral consistency via applying the Spectral Enhancement Method (SEM) Forsberg, 1985; Gruber, 2009; Hirt et al., 2011; Elsaka et al., 2016 and Bako et al., 2024. The SEM technique augments the alignment between GGMs and ground-based geoid heights by encompassing the high and very-high-frequency components of the gravity functional. Subsequently, the third subsection offers insights into the outcomes stemming from the examination of linear, four-, five-, and seven-parameter transformation parameters, which are examined to determine a better fit of geoid heights obtained from the studied GGMs to those from GNSS/levelling data over Nigeria. The second section of this chapter is devoted to recent high-degree combined global gravity-field models concerning their use in geoid modelling over Nigeria. The initial subsection presents result from evaluating free-air gravity anomalies vis-à-vis GGMs. In the subsequent subsection, the focus shifts to evaluating Bourguer gravity anomalies in conjunction with GGMs. The third subsection discuses findings derived from a comparative assessment of geoid heights sourced from GGMs, utilizing GNSS/levelling data as an independent check within the Federal Capital Territory (FCT), Abuja, Nigeria. The third section of this chapter is devoted to an in-depth analysis of the results from evaluation and homogenization of shipborne and satellite altimetry-derived gravity data over the coastal region of Nigeria.

The ***fifth chapter*** adopts a dual focus, delving into the outcomes derived from two primary areas of investigation. The first section unveils the results from the computation of the

gravimetric geoid model, which is computed using various datasets. Concurrently, the second section represents an analysis of the accuracy of the gravimetric geoid model developed for Nigeria. The assessment comprises a comparison with the complete spectrum of GNSS/levelling data, serving as a reference framework for evaluation.

Finally, the new achievement of this work is summarized. An outlook to further possible investigations and recommendations for future research conclude this ***chapter six***.

Chapter 2

Global Geopotential Models, Earth's gravity field and the geoid

This chapter introduces the GRACE and GOCE-based GGMs used in this research, the fundamental theory of the Earth's gravity field and the geoid determination essential to this thesis are discussed.

2.1 The GRACE/GOCE and combined GGMs

GGMs are representation of long-to-short-wavelength parts of the gravity field and are comprised of fully normalized SH coefficients. These were accessible via the ICGEM web front (Ince et al., 2019*).* When computing the geoid heights from the GGMs, the Geodetic Reference System 1980 ellipsoid (GRS80) was employed and the zero-tide convention was consistently applied (Ince et al., 2019).

A set of SH coefficients can signify geoid heights (*N*) within the global gravity field analysis in the spherical approximation. The SH coefficients in Eq. (2.1) are derived from GGMs and the GRS80 ellipsoid (Heiskanen & Moritz, 1967; Barthelmes, 2013).

$$N(\varphi,\lambda) \approx R\sum_{n=2}^{N_{\max}}\sum_{m=0}^{n}\overline{P}_{nm}(\sin\varphi)\left[\overline{C}_{nm}\cos m\lambda + \overline{S}_{nm}\sin m\lambda\right], \tag{2.1}$$

when (φ,λ) is the computation position of geocentric colatitude and longitude where *N* will be determined, *R* is the Earth's mean radius, $\overline{P}_{nm}$ is the fully normalized Legendre functions, and $\overline{C}_{nm}$ $\overline{S}_{nm}$ are the SH coefficients for degree n and order m, respectively. The series coefficients allow the determination of the geoid heights using Eq. (2.1). This finite series are usually up to a maximum degree of expansion, $n = N_{\max}$.

Within the context of this thesis, three GOCE-based GGMs are used. These include the fifth release of the space-wise solution GO_CONS_GCF_2_SPW_R5 (SPW_R5) (Gatti et al., 2016), the sixth release of the time-wise solution GO_CONS_GCF_2_TIM_R6 (TIM_R6) (Brockmann et al., 2021), and the sixth release of the direct solution GO_CONS_GCF_2_DIR_R6 (DIR_R6) (Bruinsma et al., 2014). Additionally, six combined GGMs have been incorporated, namely EGM2008 (Pavlis et al., 2012), EIGEN-6C4 (Förste et

al., 2014), GECO (Gilardoni et al., 2016), GOCO05c (Fecher et al., 2016), XGM2019e_2159 (Zingerle et al., 2020), and SGG-UGM-2 (Liang et al., 2020). A summary of the primary characteristics of these models and the data employed for their computation is presented below. See also Bako et al. (2024).

GO_CONS_GCF_2_SPW_R5: The SPW solution represents a GOCE-based GGM designed for satellite-only applications, extending to d/o 330. Within the SPW solution, the transition occurs from the original data positioned at the actual satellite locations to a standardized spherical grid located at the mean altitude of the satellites. This prediction process is accomplished by applying LSC, taking advantage of the spatial correlations inherent in the functional representation of the gravity field. Subsequently, the SH coefficients are computed based on the data predicted assumed grid in the final step. The model is based on four years of GOCE observations (Gatti et al., 2016).

GO_CONS_GCF_2_TIM_R6: The time-wise solution constitutes a satellite-only GGM derived from GOCE data, encompassing d/o up to 300. An established approach for the analysis of GOCE observations is the so-called time-wise solution.

This GGM solely depends on GOCE observations obtained throughout four and a half years of the mission from 2009 to 2013 (Brockmann et al., 2021). The time-wise solution nicely meets the official GOCE mission requirements with a global mean accuracy of about 2 cm in terms of geoid height and 0.6 mGal in terms of gravity anomalies at ESA's target spatial resolution of 100 km. Compared to its TIM_R5 predecessor, three kinds of improvements are shown, i.e., the mean global accuracy increases by 10-25%, a more realistic uncertainty description, and a local reduction of systematic errors in the order of centimeters (Brockmann et al., 2021).

GO_CONS_GCF_2_DIR_R6: In the direct approach, the partial derivatives are determined by integrating the virational equations specifically for low-degree recovery based on GNSS orbit tracking. These partial derivatives are calculated without applying any approximations at the precise satellite locations relevant to the gradiometer observations. Subsequently, both the partial derivatives and the gradiometer observations are jointly employed in the least-squares method (Bruinsma et al., 2014).

EGM2008: This is Earth Gravitational Model, representing the gravity field up to a maximum degree of 2190 (Pavlis et al., 2012). This model was developed by merging the GRACE standard equations sourced from the ITG-GRACE03S satellite-only model and its associated error covariance matrix, with the gravitational information obtained from a global set of area-mean free-air gravity anomalies defined on a 5 arc-minute equiangular grid. This grid was formed by merging terrestrial, altimetry-derived, and airborne gravity data. The spectral

content over areas where only lower resolution gravity data were available, was supplemented with gravitational information implied by the topography (Pavlis et al., 2012).

EIGEN-6C4: This is "European Improved Gravity model of the Earth by New techniques". It is a static global gravity field model collaboratively computed by GRGS Toulouse and GFZ Potsdam. The model integrates diverse ground and satellite altimetry derived gravity data, comprising four years of GOCE-SGG data, ten years of GRACE RL03 GRGS data (degree 2-130), twenty-five years of LAGEOS data (degree 2-30), DTU13 GRA altimetry derived gravity data, and EGM2008 geoid height grid (maximum 370 degrees) (Förste et al., 2014).

GECO: This is a global gravity field model spanning complete d/o 2190. It was generated by combining the fifth release of the time-wise (TIM_R5) GOCE-only solution with EGM2008. GECO's SH coefficients are computed by analyzing the combined global geoid grids up to degree 359, corresponding to a spatial resolution of 0.5° (Gilardoni et al., 2016). **GOCO05C:** This is a global combined gravity field model, complete up to d/o 720. It was computed using data from the entire mission duration of the GOCE gradiometry solution (November 2009 to October 2013), along with ten years of GRACE data and supplementary orbit information from low Earth-orbiting satellites (LEOs) and satellite laser ranging (SLR) (Fecher et al., 2016).

XGM2019e_2159 is a global combined gravity field model expanded to d/o 2190. It is derived from three primary data sources: a ground gravity anomaly dataset with a 15-minute resolution, the satellite-only GOCO06s model capturing longer wavelengths up to a d/o of 300, and a combination of ground gravity grid and 1-minute augmentation datasets. The augmentation datasets include topography data over continents and altimetry-derived gravity anomalies from DTU13GRA (Andersen et al., 2013), with a 1-minute resolution over the ocean. All computations were performed in the spheroidal harmonic domain (Zingerle et al., 2020).

SGG-UGM-2 is a precise high resolution global gravity field model expanded to d/o 2190. The model is computed using the advanced theory of ellipsoidal harmonic analysis and coefficient transformation. It is constructed by integrating various data sources, including GOCE observations, 15 years of GRACE observations, marine gravity data from satellite altimetry, and EGM2008-derived continental gravity data (Liang et al., 2020).

2.2 Datasets used in the GGMs over Nigeria and its Coastline

The combined GGMs used terrestrial and altimetry data from the land and sea. For instance, in EGM2008 (Pavlis et al.,2012), fill-in gravity anomalies from the residual terrain model (RTM) forward modelling and proprietary gravity data were used over land areas, whereas altimetry-derived gravity anomalies from the Danish National Space Center (DNSC07) computed using

the following satellite mission (e.g., ERS-1 and Geosat data) (Andersen and Knudsen, 1998) were utilized over the seas.

The surface gravity data utilized in the computation of SGG-UGM-2 (Liang et al., 2020), GECO (Gilardoni et al., 2016) and EIGEN-6C4 (Förste et al., 2014) over Nigeria were the same as those utilized in EGM2008 (Pavlis et al., 2012) for terrestrial regions. Marine gravity data obtained through satellite altimetry were used to compute SGG-UGM-2 (Liang et al., 2020) and GECO (Gilardoni et al., 2016), whereas the Technical University of Denmark (DTU)10 Gravity (GRA) (Andersen et al., 2010) satellite altimetry gravity data computed using satellite missions (e.g., ERS-1, ERS-2, Geosat, T/P, GFO, Jason-1, and Envisat data) contributed to the computation of EIGEN-6C4 over the seas (Andersen et al., 2010). GOCO05C (Fecher et al., 2015) used high-quality gravity anomalies with a spatial resolution of 15'×15', combined with GOCO05s satellite-only model over land and DTU13 (Andersen et al., 2013) satellite altimetry data over the seas computed using the following satellite mission (e.g., ERS-1, ERS-2, Geosat, T/P, GFO, Jason-1, Envisat, and Cryosat-2 data). Finally, XGM2019e_2159 (Zingerle et al., 2020) used terrestrial gravity anomaly data obtained from the United States (US) National Geospatial-Intelligence Agency (NGA) over Nigeria's Land and DTU13GRA (Andersen et al., 2013) satellite altimetry data over the seas. Table 2.1 summarizes the characteristics of the nine GGMs employed in this study, encompassing the ICGEM product names for the GRACE- and GOCE-based models.

2.3 The Earth's gravity field and geoid

2.3.1 The gravity potential of the Earth

The Earth's gravity potential, denoted as W, at a specific location P on the Earth's surface or outside is always under the effect of the gravitational potential V induced by the Earth's mass, and the centrifugal potential Φ arising from the Earth's rotation (Hofmann-Wellenhof and Moritz, 2005).

$$W = V + \Phi \tag{2.2}$$

With

$$V = G\iiint_{\Omega} \frac{\rho \mathrm{d}\Omega}{\mathrm{d}} \tag{2.3}$$

and

$$\Phi = \frac{1}{2}\omega^2 . \mathrm{r}^2 \sin^2\theta \tag{2.4}$$

Where G is the Newtonian gravitational constant, which has value:

Table 2.1: Characteristics of nine GGMs that were used in this research. S is satellite-based, G is for ground data (e.g., terrestrial, shipborne, and airborne measurements), A is for altimetry, and T is for topographic-based data (Ince et al., 2019).

GGMs	Data type	Max. Degree	Year of release	References
DIR_R6	S(GOCE, GRACE, LAGEOS)	300	2019	Bruinsma et al., 2014
SPW_R5	S(GOCE)	330	2017	Gatti et al., 2016
TIM_R6	S(GOCE)	300	2019	Brockmann et al., 2021
EGM2008	S (GRACE), A, G	2190	2008	Pavlis et al.,2012
EIGEN-6C4	S(GOCE,GRACE, LAGEOS), A, G	2190	2014	Förste et al., 2014
GECO	S(GOCE), EGM2008	2190	2016	Gilardoni et al., 2016
GOCO05C	S(GOCE), A, G	720	2016	Fecher et al., 2015
XGM2019e_2159	S (GOCO06s), A, G, T	2190	2020	Zingerle et al., 2020
SGG-UGM-2	S (GRACE, GOCE), EGM2008, A,	2190	2020	Liang et al., 2020

$\left(\left(\approx 6,674 \pm 0.001\right)\times 10^{-11} m^3 kg^{-1} s^{-2}\right)$ (Torge, 2001), the Earth's body is Ω, ρ is the density at differential volume element of the Earth's body $d\Omega$, d is the distance of that element from the computation point P, ω is the angular velocity of the Earth's rotation, r is the distance to the geocenter, and θ is geocentric co-latitude $\left(90-\varphi\right)$ (Torge and Muller, 2012).

The geometry of the gravity field can be described by surfaces which are defined by a uniform gravity potential W, the so-called equipotential or level surfaces. One of the surfaces is the geoid, which is considered as the equipotential surface $W_{(r,\theta,\varphi)} = W_0 = \text{Constant}$. In geodetic sense, this is the most important level surface, as it serves as a reference for the definition of height systems.

If the Laplace operator Δ is applied to the gravitational potential, it can be shown that V satisfies the Poisson's equation inside the Earth masses, where the density changes discontinuously (Hofmann-Wellenhof and Moritz, 2005):

$$\Delta V = -4\pi G\rho \tag{2.5}$$

If considered outside the attracting masses where the density ρ becomes zero, the Poisson's equation turns into the Laplace's equation (Hofmann-Wellenhof and Moritz, 2005):

$$\Delta V = 0 \tag{2.6}$$

Where Δ represents the Laplacian operator and is defined by (Hofmann-Wellenhof and Moritz, 2005):

$$\Delta = \frac{\mathrm{d}^2}{\mathrm{d}x^2} + \frac{\mathrm{d}^2}{\mathrm{d}y^2} + \frac{\mathrm{d}^2}{\mathrm{d}z^2} \tag{2.7}$$

2.3.2 The disturbing potential and its functionals

An ellipsoid of revolution serves as an approximation to model the Earth's shape. This approximation is advantageous due to the limited deviations observed in the actual gravity field compared to the normal gravity field generated by the reference ellipsoid of revolution (Heiskanen & Moritz, 1967). In terms of potential, these deviations are denoted as the disturbing potential or anomalous potential T. The differences between the normal potential U and the actual gravity potential W, is useful in physical geodesy (Heiskanen & Moritz, 1967):

$$T = W - U \tag{2.8}$$

From the differences (Eq. 2.8), we can see that the centrifugal part, which is the same in W and U, cancels and thus does not have to be considered. Therefore, the disturbing potential T still satisfies the Laplace equation $\Delta T = 0$ outside the Earth's masses, so that it can be expanded into a spherical harmonics' series.

The function T is a harmonic outside the Earth, i.e., it satisfies the Laplace's equation (Heiskanen & Moritz, 1967):

$$\Delta T = \frac{\mathrm{d}^2 T}{\mathrm{d}x^2} + \frac{\mathrm{d}^2 T}{\mathrm{d}y^2} + \frac{\mathrm{d}^2 T}{\mathrm{d}z^2} = 0 \tag{2.9}$$

In addition, some substantial functional that holds significance in physical geodesy are the gravity anomaly, gravity disturbance, geoid height and height anomaly. They play pivotal roles in determining the Earth's figure (geoid).

Assuming the point P on the geoid (Fig. 2.1) is projected onto the point of a reference ellipsoid along the ellipsoidal normal. The above anomalous quantities are defined as follows:

The gravity anomaly Δg : the difference between the gravity value g_P at point P on the geoid surface $W(P)$ and the normal gravity γ_Q at a point Q on the corresponding potential surface $U(Q)$ such that $U(Q) = W(P)$ and Q is an orthogonal projection of P on to, $U(Q)$ particularly the ellipsoid. The gravity anomaly is expressed in Eq. (2.10):

$$\Delta g = g_P - \gamma_Q \tag{2.10}$$

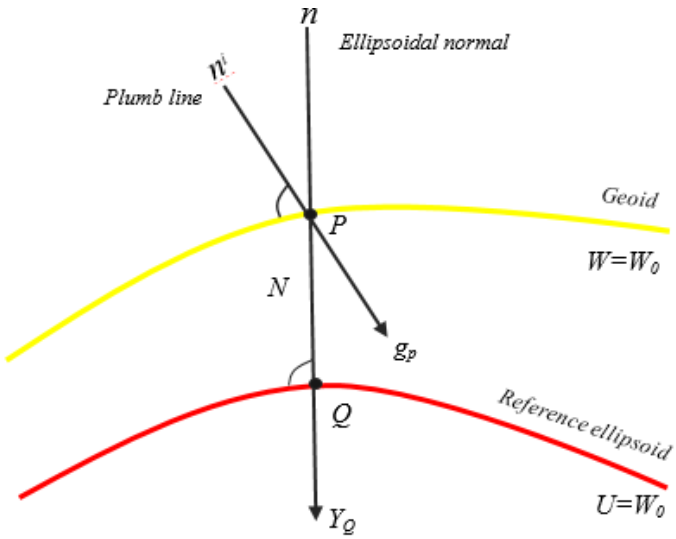

Fig 2.1: Geoid and reference ellipsoid.

In geodesy, gravity anomaly (on the geoid) is the same as when gravity disturbance is corrected for normal gravity on the ellipsoid rather than on the geoid and is mathematically described by Jekeli (2015) as Eq. (2.11):

$$\Delta g = -\frac{\mathrm{d}T}{\mathrm{d}h} + \frac{1}{\gamma_Q}\frac{\mathrm{d}\gamma}{\mathrm{d}h}T \tag{2.11}$$

Were, $\frac{\mathrm{d}\gamma}{\mathrm{d}h}T$ is the correction for evaluation of normal gravity on the ellipsoid rather than on the geoid, $\frac{\mathrm{d}T}{\mathrm{d}h}$ is the gravity disturbance obtained by taking derivative of the gravity potential with respect to the ellipsoidal height, T is the Anomalous potential, h is the ellipsoidal height and γ_Q is the normal gravity.

Due to the difficulties associated with taking partials of gravitational quantities, gravity anomaly is expressed as the differences between the Earth's gravity on the geoid as well as normal gravity on the ellipsoidal and is mathematically, described by Eq. (2.10) and given by Hofmann-Wellenhof and Moritz (2005). Where Δg is the gravity anomaly, g_P is the observed gravity value reduced for instrumental drift, Earth tide correction, Eotvos correction, atmospheric effect, Free-air correction and Bouguer correction, terrain correction and γ_Q is normal gravity (latitude correction).

By the application of the above stated corrections, the terrain observed gravity is reduced to the geoid. Extensive discussion on the correction factors have been given by Idowu (2005), in this study, only the atmospheric effect, free-air correction, bouguer correction and terrain correction will be further discussed (see section 2.5), considering the requirement that all masses must be condensed below the geoid in gravimetric geoid modelling.

Normal gravity: Normal gravity is utilized to eliminate errors arising from centrifugal acceleration on observed gravity values. Specifically, the latitude correction compensates for the effects of centrifugal acceleration by considering the error as a function of the latitude of the observation point on an ellipsoidal Earth surface (Odumuso, 2019; Hackney and Featherstone, 2003). This correction is computed using an international gravity formula adopted by the International Association of Geodesy (IAG). In this study, the Geodetic Reference System 1980 (GRS80) model, as outlined by Moritz (1980), is employed. The correction is applied using Somigliana's closed-form formula, which provides an expression for calculating normal gravity, as discussed by Yilmaz et al., (2018) (see Eq. 2.12).

$$\gamma_Q = \gamma_e \left(\frac{1 + k \sin^2 \varphi}{1 - e^2 \sin^2 \varphi} \right) \tag{2.12}$$

Where γ_e is the normal gravity at the equator, φ is the geodetic station latitude on the mean Earth ellipsoid, k is the function of the ellipsoidal parameters and the normal gravity at the equator and e^2 is the Square of the first eccentricity. The constants from Moritz (1980) are given in Table 2.2.

When the GRS80 reference parameters was applied as presented in Table 2.2, the Chebychev's approximation for Eq. (2.12) becomes Eq. (2.13):

Table 2.2: Physical and geometric constant of GRS80 used in the gravity reduction

Constant	Value
γ_e	9.7803185015 ms^{-2}
k	0.001931851353
e^2	0.00669438002290
a	6378137 m
f	0.00335281068118
m	0.00344978600308

$$\gamma_Q = 978031.85(1 + 0.00527889 Sin^2\varphi + 0.000023462 \mathrm{Sin}^4 \varphi) \tag{2.13}$$

GRS80 was defined using satellite-derived data. This means that the GRS80 model includes the mass of the atmosphere, whereas observations made at the surface of the Earth do not. The atmospheric correction accounts for the mass-inconsistency between the GRS80 normal ellipsoid and the gravity observed on the Earth's surface, as well as the atmosphere above the gravity observation point. The atmospheric correction δg_{AC} is added to the gravity anomalies to account for these differences and to therefore make them consistent with those derived from GGM. The atmospheric correction recommended by the IAG is given in Eq. (2.14) where, H is the orthometric height (in meters). The correction has unit of mGal.

$$\delta g_{AC} = 0.871 - [(1.0298 \times 10^{-4}) \times H] \tag{2.14}$$

The normal gravity and consequently gravity anomalies were therefore computed using Eq. (2.13)

The geoid height N : The distance of separation *PQ* between the geoid surface and the reference ellipsoid measured along the ellipsoidal normal. It is also called geoid undulation. The mathematical relationship between the disturbing potential *T* and the geoid height *N*, which is a geometrical quantity, is given by Brun's formula (Hofmann-Wellenhof and Moritz, 2005).

$$N = \frac{T_P}{\gamma_Q} \tag{2.15}$$

Where T_P is the disturbing potentials at the geoid surface and γ_Q is the normal gravity values at the reference ellipsoid.

The fundamental equation of physical geodesy can be derived using the Bruns' formula in Eq. (2.15) and the definition of gravity anomaly Eq. (2.10). It describes the relationship between the measured gravity anomaly and the disturbing potential (Hofmann-Wellenhof and Moritz, 1967).

$$\frac{\mathrm{d}T}{\mathrm{d}h} - \frac{1}{\gamma_Q}\frac{\mathrm{d}\gamma}{\mathrm{d}h}T + \Delta g = 0 \tag{2.16}$$

Or in the spherical approximation as

$$\frac{\mathrm{d}T}{\mathrm{d}r} + \frac{2\bar{g}}{R}N + \Delta g = 0 \tag{2.17}$$

Where the mean radius of the Earth is R, the mean value of gravity over the Earth is $\overline{g}$, the partial differentials along the ellipsoid normal and the radial are $\frac{\mathrm{d}}{\mathrm{d}h}$ and $\frac{\mathrm{d}}{\mathrm{d}r}$ respectively. This is a fundamental property in geodesy, since it implies that the gravitational potential can be represented by harmonic functions.

2.3.3: The Earth's gravitational potential in spherical harmonics

The Earth's gravitational potential *V* (see Eq. 2.3) at any point $P(\varphi,\lambda,r)$ on the Earth's surface and in the exterior space is expressed as a series of spherical harmonic expansions (Torge & Muller, 2012).

$$V(\varphi,\lambda,\mathrm{r})=\frac{GM}{r}\left(1+\sum_{n=1}^{\infty}\left(\frac{a}{r}\right)^{n}\sum_{m=0}^{n}\overline{f}_{nm}\overline{Y}_{nm}(\theta,\lambda)\right) \tag{2.18}$$

With

$$\overline{f}_{nm}\begin{cases}\overline{C}_{nm} & m\geq 0\\ \overline{S}_{nm} & m<0\end{cases} \tag{2.19}$$

and

$$\overline{Y}_{nm}\begin{cases}\overline{P}_{nm}(\sin\theta)\cos m\lambda & m\geq 0\\ \overline{P}_{nm}(\sin\theta)\sin m\lambda & m<0\end{cases} \tag{2.20}$$

Where *M* is the Earth's Mass, a is the semi-major axis of the reference ellipsoid, the geographical longitude is λ (Torge & Muller, 2012).

$$U(\varphi,\lambda,\mathrm{r})=\frac{GM}{r}\left(1-\sum_{n=1}^{\infty}\left(\frac{a}{r}\right)^{2n}J_{2n}P_{2n}(\cos\varphi)+\frac{1}{2}\omega^{2}r^{2}\sin^{2}\varphi\right) \tag{2.21}$$

Where the coefficients J_{2n} are

$$J_{2n}=(-1)^{n+1}\frac{3e^{2n}}{(2n+1)(2n+3)}\left(1-n+5n\frac{C-A}{ME^{2}}\right) \tag{2.22}$$

The first and linear eccentricities are e and E, respectively, C is the principal moment of inertia along the rotation axis, and A is the equatorial moment of inertia along the x-axis in the equatorial plane.

By inserting Eq. (2.18) and (2.21) into Eq. (2.8), the disturbing potential *T* is written as

$$T(\varphi,\lambda,\mathrm{r}) = \frac{GM}{r}\sum_{n=2}^{\infty}\left(\frac{a}{r}\right)^{n}\sum_{m=0}^{n}\overline{R}_{nm}\overline{Y}_{nm}(\theta,\lambda) \tag{2.23}$$

with

$$\overline{R}_{nm} = \begin{cases} \Delta\overline{C}_{nm} & m \geq 0 \\ \Delta\overline{S}_{nm} & m < 0 \end{cases} \tag{2.24}$$

Where $\Delta\overline{C}_{nm}$ and $\Delta\overline{S}_{nm}$ are residual fully normalized spherical harmonic coefficients (It is the original coefficient minus one of the normal potentials) (Torge & Muller, 2012). Using the Bruns' formula in Eq. (2.15) and Eq. (2.16), the geoid undulation *N* and gravity anomaly Δg are expressed in spherical approximation as follows:

$$N(\varphi,\lambda,\mathrm{r}) = \frac{GM}{r\gamma_Q}\sum_{n=2}^{\infty}\left(\frac{a}{r}\right)^{n}\sum_{m=0}^{n}\overline{R}_{nm}\overline{Y}_{nm}(\theta,\lambda) \tag{2.25}$$

$$\Delta g(\varphi,\lambda,\mathrm{r}) = \frac{GM}{r^2}\sum_{n=2}^{\infty}(n-1)\left(\frac{a}{r}\right)^{n}\sum_{m=0}^{n}\overline{R}_{nm}\overline{Y}_{nm}(\theta,\lambda) \tag{2.26}$$

It should be noted that in the case of calculating quasi-geoid heights or height anomalies with the use of Eq. (2.25), the terms r and γ_Q are referred to point *P* at the Earth's physical surface.

2.4 Gravimetric geoid determination

Several methods and theories have been developed to determine geoid heights and quasi-geoid heights. The gravimetric geoid can be obtained by solving the BVP for the disturbing potential (Moritz, 1980). Various types of BVPs depend on the boundary surfaces and conditions (Hofmann-Wellenhof & Moritz, 2005). Robin's, Drichlet's and Neumann's problems are the main three BVPs in potential theory (Martensen & Ritter, 1997).

The most widely accepted methodologies for modelling the functionals of disturbing potentials comprise the Stokes integral solution, the Molodenski approach, and LSC method. These methodologies are detailed below.

2.4.1 Integral formulae

2.4.1.1 Stokes' integral formula

Stokes' integral formula are foundation in physical geodesy. In this field, determining the geoid from gravity data is regarded as a solution to the third BVP in potential theory. This solution is achieved because the disturbing potential T is harmonic. In the stokes original formulation, the gravity anomalies were corrected as if measured on the geoid. This also means that the

topographic mass outside the geoid needs to be removed (otherwise the Laplace equation would not old) and the effect of this mass layer must be added back to the computed geoid.

The corresponding formulation of this BVP is well-established and described by Heiskanen and Moritz (1967).

$$\begin{cases} \Delta T = 0 \\ \dfrac{\partial T}{\partial r} + \dfrac{2}{r} T - \Delta g \,|_s = 0 \\ T \geq 0 \text{ for } r \geq \infty \end{cases} \tag{2.27}$$

Geoid heights *N* can be determined from gravity data using Stokes' formula. It is expressed as follows:

$$N = \frac{R}{4\pi\gamma_Q} \iint_\sigma \Delta g S(\psi) \mathrm{d}\sigma \tag{2.28}$$

Where γ_Q, Δg and R are explain in Eq. (2.10), ψ is the spherical distance between the computational point *P* and the running point *Q*, $d\sigma$ is the infinitesimal surface element of integration over a unit sphere. The integral kernel $S(\psi)$ is called Stokes' kernel or Stokes's function, which is given by:

$$s(\psi) = \frac{1}{\sin(\psi/2)} - 6\sin\frac{\psi}{2} + 1 - 5\cos\psi - 3\cos\psi In\left(\sin\frac{\psi}{2} + \left(\sin\frac{\psi}{2}\right)^2\right) \tag{2.29}$$

$$s(\psi) = \sum_{n=2}^{\infty} \frac{2n+1}{n-1} \overline{p_n}(\cos\psi) \tag{2.30}$$

Stokes' formula requires gravity anomalies and their integration across the entirety of the Earth's surface. However, these data are typically confined to a spherical cap encompassing the computation point. This limitation results in a truncation error. In response, examining this error led to the developing of a modified version of Stokes' formula. This adaptation accounts solely for terrestrial gravity anomalies originating from restricted regions near the computation point, denoted by the cap size. This modified formula was introduced as proposed by Molodenski et al. (1962).

Practically, the mases above the geoid are mathematically remove by using different reduction methods (see section 2.5). Then a topography restoring process is applied afterwards. This remove-restore procedure introduces errors because the topographic density effect cannot be modelled exactly.

2.4.1.2 Molodenski integral formula

In the mid-20th century, Russian physicist M.S. Molodensky proposed an alternative scalar BVP for solving the disturbing potential outside of the Earth (Molodensky et al., 1962). He critiqued Stokes' approach by highlighting that the geoid, as an equipotential surface internal to the Earth and as such requires detailed knowledge of internal (topographical) Earth mass density, which we will never have. Furthermore, stokes' method involves complex processes such as removing topographic masses and reducing gravity measurements from the Earth's surface to the geoid, introducing additional challenges. He then proceeded to replace stoke's choice of the boundary (geoid) by a different surface called telluroid. The telluroid is the surface which approximates the Earth's physical surface and is formed by all points with $U(Q)=W(P)$ (Torge & Muller, 2012).

The primary objective of the Molodensky method is to directly determine the Earth's physical surface using gravimetric techniques (Molodensky et al., 1962). In this approach, the boundary conditions are defined not on the geoid, but on the Earth's physical surface. Instead of referencing heights to the geoid, an equipotential surface, the method introduces a new reference surface known as the quasi-geoid. Importantly, determining the quasi-geoid and the associated heights does not require knowledge of the Earth's internal mass density distribution. The expression for the determination of the disturbing potential T and quasi-geoid heights or height anomalies is presented as a series of expansions (Torge & Muller, 2012):

$$\Delta T_A = \sum_{i=0}^{\infty} T_A^{(i)} = T_A^{(0)} + T_A^{(1)} + ... \tag{2.31}$$

The quasi-geoid height for point A is obtained as follows:

$$\zeta_A = \frac{\Delta T_A}{\overline{\gamma}_B} = \sum_{i=0}^{\infty} \zeta_A^{(i)} = \zeta_A^{(0)} + \zeta_A^{(1)} + ... \tag{2.32}$$

with

$$\zeta_A^{(0)} = \frac{R}{4\pi\gamma}\iint_{\sigma} \Delta g S(\psi)\,\mathrm{d}\sigma \;\;, \zeta_A^{(1)} = \frac{R}{4\pi\gamma}\iint_{\sigma} G_1 S(\psi)\,\mathrm{d}\sigma \tag{2.33}$$

The first-order correction term in Molodenski's series expansions is denoted as G_1 , which is in the close approximation is given by (Heiskanen & Moritz, 1967).

$$G_1 = \frac{R^2}{2\pi}\iint_{\sigma}\frac{H^* - H_A^*}{l_0^3}\Delta g \mathrm{d}\sigma, \qquad l_0 = 2R\sin\frac{\psi}{2} \tag{2.34}$$

where H_A^* is the normal height at point A

2.4.1.3 The least squares collocation (LSC)

In geoid determination, the LSC method is commonly employed when integrating data of various types. Additionally, the LSC method proves to be particularly suited for least squares prediction. The mathematics of the LSC method are rooted in functional analysis, with a specific emphasis on the theory of reproducing kernel Hilbert space. The derivation of the approximation for the disturbing potential within a reproducing kernel Hilbert space was initially conducted by Krarup (1969), while the introduction of the LSC method itself is attributed to Moritz. The mathematical model characterizing the LSC method within the field of geodesy is formally expressed as (Moritz, 1980).

$$\mathbf{I = AX + t + n} \tag{2.35}$$

Where **I** is the vector comprising all observations**, A** is the design matrix, **X** is the unknown parameters that are estimated in the least squares adjustment, while the signal **t** is predicted at points other than the measured points and **n** is the noise filtered and removed from observations so that LSC can be viewed as a combination of filtering, prediction and adjustment (Balmino, 1978; El-Fiky et al., 1997).

The observation **I** can be regarded as random quantities (i.e. "signals + noise"), which have a mathematical expectation (or mean $M\{\,\mathbf{.}\,\}$) value equal to zero (Heiskanen and Moritz, 1967), have a mean value to zero $M\{\,\mathbf{I}\,\} = 0$, and so that the systematic part will also be equal to zero **AX = 0**, then Eq. (2.35) becomes

$$\mathbf{I = t + n} \tag{2.36}$$

Eq. (2.36) refers to the so-called least-squares collocation without parameters (El-Fiky, et al., 1997). Where the observation vector **I** consist of m values of gravity anomalies.

$$\mathbf{I} = \begin{pmatrix} l_{\Delta g1} \\ \vdots \\ \vdots \\ l_{\Delta gm} \end{pmatrix} \tag{2.37}$$

The estimated signals $\hat{\mathbf{s}}$ are written as:

$$\hat{\mathbf{S}} = \mathbf{C_{st}} \left(\mathbf{C_{tt}} + \mathbf{C_{nn}} \right)^{-1} \mathbf{l} \qquad (2.38)$$

Where $\mathbf{c_{st}}$ is the cross-covariance matrix between the observation and the estimated signal ($\mathbf{c_{st}}$ equal to $\mathbf{c_{ts}}$), $\mathbf{C_{tt}}$ is the auto-covariance matrix between the observation signal components, and $\mathbf{c_{nn}}$ is the variance-covariance matrix of the noise, which is the standard error of the observed gravity anomalies (in practice a diagonal matrix). The error covariance matrix of the estimated signals $\mathbf{E_{ss}}$ is given by (Heikanen and Moritz, 1967 ; El-Fiky, et al., 1997).

$$\mathbf{E_{ss}} = \mathbf{C_{ss}} - \mathbf{C_{st}} \left(\mathbf{C_{tt}} + \mathbf{C_{nn}} \right)^{-1} \mathbf{C_{ts}} \qquad (2.39)$$

Where $\mathbf{c_{ss}}$ is the auto-covariance matrix of the estimated signals. It should be noticed that the quantities **t** and **s** are related to the Earth's gravitational field, which are linear functional of the anomalous potential T . Hence, the matrices $\mathbf{C_{tt}}$, $\mathbf{c_{st}}$, and $\mathbf{c_{ss}}$ can be obtained from the basic covariance function of the anomalous potential by covariance propagation (Heiskanen and Moritz, 1967).

The estimation of covariance matrices Eq. (2.39), $\mathbf{C_{tt}}$, $\mathbf{c_{st}}$ and $\mathbf{c_{nn}}$ is essential for the gravimetric geoid/quasi-geoid determination using LSC method; they are estimated from one of the essential covariance functions, which are usually taken as the covariance function "reproducing kernel Hilbert space" $K(P,Q)$ of the disturbing potential T (Heikanen and Moritz and El-Fiky, et al., 1997).

Let $T(P)$ and $T(Q)$ denote the disturbing potential T at two points $P(\theta,\lambda)$ and $Q(\theta',\lambda')$ separated by a spherical distance $\psi\left\{\cos\psi = \cos\theta\cos\theta' + \sin\theta\sin\theta'\cos(\lambda' - \lambda)\right\}$; then, the covariance function $K(P,Q)$ of the disturbing potential is defined as

$$K(P,Q) = K(\psi) = M\left\{T(P)T(Q)\right\}$$

$$= \frac{1}{8\pi^2} \int_{\lambda=0}^{2\pi} \int_{\theta=0}^{\pi} \int_{\alpha=0}^{2\pi} T(\theta,\lambda)T(\theta'\lambda')\sin\theta \mathrm{d}\theta \mathrm{d}\lambda \mathrm{d}\alpha \qquad (2.40)$$

The covariance function of T is an isotropic function, i.e. depending only on the spherical distance ψ between the two points P and Q, and it can be expressed in terms of spherical harmonic expansions as follows:

$$K(\psi)=\sum_{n=2}^{\infty}k_n\left(\frac{R_B^2}{rr'}\right)^{n+1}P_n(\cos\psi) \tag{2.41}$$

The disturbing potential degree variance is given as

$$K_n=\sum_{m=0}^{n}\left(\bar{a}_{nm}^{2}+\bar{b}_{nm}^{2}\right) \tag{2.42}$$

where R_B is the radius of the Bjerhammar sphere (see, e.g., Bjerhammer, 1975) and $\bar{a}_{nm},\bar{b}_{nm}$ are the fully normalized harmonic coefficients. The gravity anomaly, geoid height, and gravity disturbance are represented as linear functionals of the disturbing potential *T, and* the covariance function of those functionals are derived using Eq (2.40) by the covariance propagation law as shown below:

$$l_i=L_i^pT(P) \qquad \text{and} \qquad l_j=L_i^QT(Q) \tag{2.43}$$

Where, L_i^p and L_j^Q are the linear operators

$$\begin{aligned}Cov(l_il_j)&=M\{l_il_j\}=M\{L_i^pT(P)L_j^QT(Q)\}\\&=L_i^PL_j^QM\{T(P)T(Q)\}=L_i^PL_j^QK(P,Q)\end{aligned} \tag{2.44}$$

By employing Eq. (2.40) and (2.41), all essential covariance functions necessary for the calculation of the gravimetric geoid/quasi-geoid, as outlined in Eq. (2.40), are determined. This is achieved by applying Bruns' formula and the fundamental equation of physical geodesy, as described in Eq (2.15) and (2.16). These equations establish the connection between the gravity anomaly and the disturbing potential.

$$\operatorname{cov}(N(P),\Delta g(Q))=\frac{1}{\gamma}\left(-\frac{\partial}{\partial r}-\frac{2}{r}\right)\left(-\frac{\partial K}{\partial r'}-\frac{2}{r'}K\right) \tag{2. 45}$$

$$C(\Delta g(P),\Delta g(Q))=\operatorname{cov}(\Delta g(P),\Delta g(Q))=\left(-\frac{\partial}{\partial r}-\frac{2}{r}\right)\left(-\frac{\partial K}{\partial r'}-\frac{2}{r'}K\right)$$

$$=\frac{\partial^2K}{\partial r\partial r}+\frac{2}{r'}\frac{\partial K}{\partial r}+\frac{2}{r}\frac{\partial K}{r}+\frac{4}{rr'}K \tag{2.46}$$

The gravity anomaly Δg covariance function $C(\Delta g(P),\Delta g(Q))$ is expressed in spherical harmonics expansions series as

$$C\left(\Delta g_P, \Delta g_Q\right) = C\left(\psi\right) = \sum_{n=2}^{\infty} c_n \left(\frac{R_B^2}{rr'}\right)^{n+1} P_n\left(\cos\psi\right) \tag{2.47}$$

With the so-called gravity anomaly degree variance

$$C_n = \left(\frac{n-1}{R}\right)\sum_{m=0}^{n}\left(\bar{\alpha}_{nm}^2 + \bar{b}_{nm}^2\right) \tag{2.48}$$

Prior to the estimation of the gravity anomaly or disturbing potential, one has to compute the degree covariance function and their degree variances C_n K_n . This is not easy because it requires the computation of the sum of infinite series. A mathematical model can replace the degree variance C_n for the gravity anomaly or K_n for the disturbing potential. Five types of models for gravity anomalies and disturbing potential have been derived by Tscherning and Rapp (1974). The empirical covariance function was determined using mean gravity anomalies. The model for the degree variance of gravity anomalies and the degree variance of disturbing potential is shown in Eq. (2.49) and (2.50), respectively. However, in this thesis we used FFT in the computation of gravimetric geoid model for Nigeria.

$$C_n = \frac{A(n-1)}{(n-2)(n+B)} \tag{2.49}$$

$$K_n = \frac{AR^2}{(n-1)(n-2)(n+B)} \tag{2.50}$$

where the model parameters are A and B

Eq. (2.49) and (2.50) depict the global properties of the Earth's anomalous gravity field. When the LSC method is employed to determine geoids/quasi-geoids gravimetrically, the availability of anomalous gravity data is typically constrained to specific geographical regions or local areas. Consequently, applying a localized covariance function becomes necessary to accurately represent the regional features of the anomalous field within the specific region or local area under consideration. Fashir et al (1998) presented the anomaly degree variance modelling approach for computing the covariance function and further presented a closed form numerical solution to the empirical local and global covariance function. His approach is more numerically stable for empirical covariance determination compared to the conventional closed form solution presented by Moritz (1976); Saadon et al. 2021.

The gravity anomaly parameters of the local covariance function are the variance C_0 , the curvature parameter χ or the variance of the horizontal gradient, and the correlation length ξ defined as follows (Moritz, 1980; Zaki et al. 2021):

Variance C_0 : This is the value of the covariance function $C(\psi)$ when the distance ψ between points *P* and *Q* is equal to zero.

$$C_0 = C(0) \tag{2.51}$$

The correlation length ξ : This is the value of the argument ψ that $C(\psi)$ equals half of its value at ψ = 0

$$C(\xi) = \frac{1}{2} C_0 \tag{2.52}$$

The curvature parameter χ **:** This is a dimensionless quantity related to the curvature k of the covariance function at $\psi = 0$

$$\chi = \frac{k\xi^2}{C_0} \tag{2.53}$$

2.5 Effects of the potential of topography in the geoid/quasi-geoid determination

The potential of the topography at point $P(x_p, y_p, H_p)$ on the physical surface of the Earth can be expressed in planar approximation as follows:

$$T(x_p, y_p, H_p) = G \int_x \int_y \int_0^H \left(\frac{\rho(x, y, H)}{\left((x_p - x)^2 + (y_p - y)^2 + (H_p - H)^2 \right)^{1/2}} \mathrm{d}x\mathrm{d}y\mathrm{d}H \right) \tag{2.54}$$

Where the 3-dimensional density function is $\rho(x, y, H)$ .Gravity anomalies must be available on the geoid surface to employ Stokes's integral for solving the third geodetic BVP and determine gravimetric geoid heights. This procedure assumes the absence of external masses beyond the geoid, apart from requiring that gravity must be reduced to the geoid surface. Within the Molodenski approach, the computation of quasi geoid height, also known as height anomaly, entails a series of integrations. This method requires free-air anomalies, which characterize the disparity between the gravity measured at the Earth's surface and the

normal gravity value on the telluroid. Furthermore, the heights stemming from the topography at the computation points must be considered. Importantly, this technique does not rely on any assumptions concerning mass density within the computation zone.

In applying the LSC method for gravimetric geoid or quasi-geoid modelling, it is imperative to employ a harmonic function to represent the disturbing potential. Consequently, the gravity anomalies must be adjusted to the geoid surface by compensating for or eliminating any masses located above this surface. Various techniques can be employed to achieve this, including free-air reduction, bouguer reduction, topographic-isostatic reductions, Rudzki inverse reduction, helmert's condensation reduction, and residual terrain modelling (RTM) reduction, as documented in references such as Heiskanen and Moritz (1967), Forsberg (1984) and Yilmaz et al., (2018). However, we applied FFT method for gravimetric geoid computation in this thesis and free-air gravity anomaly data and RTM reduction was used.

In principle, the ultimate objective of all data reduction methods is to yield an equivalent geoid model. Any discrepancies that may arise result from the specific approach used to consider the influence of topography's potential during the geoid computation. This dissertation explains numerous techniques for addressing the topographic potential in the geoid/quasi geoid heights computation. These methodologies encompass free-air reduction, bouguer reduction, the RTM method, and the Helmert condensation method (alternatively known as the application of Faye anomalies). A concise overview of these techniques is provided below:

2.5.1 Free-air anomalies

The Free-air correction δg_{FC} is the process that involves reducing the gravity readings taken on the Earth's surface to the geoid level, assuming that no masses exist above the geoid. The free-air reduction method δg_{FC} is employed using the standard vertical gradient of gravity proposed by Hofmann-Wellenhof and Moritz, 2005, and discussed in Yilmaz et al., (2018) and Odumosu, (2019). The simplified formula of free-air correction is expressed in Eq. (2.55)

$$\delta g_{FC} = \frac{\mathrm{d}g}{\mathrm{d}h} H = 0.3086H \quad \text{[mGal]} \tag{2.55}$$

and the free-air gravity anomaly on the geoid is given by

$$\Delta g_{FA} = g_p + \delta g_{FC} + \delta g_{AC} - \gamma_Q \tag{2.56}$$

where H is the orthometric height above the geoid (in meters), Δg_{FA} , is the free-air gravity anomaly, the observed gravity is g_p , δg_{FC} is the free-air correction, δg_{AC} is the

atmospheric correction (for detailed computation process of atmospheric correction, see Eq. 2.14 in section 2.3.2) and γ_Q is the normal gravity or latitude correction.

2.5.2 The simple and complete Bouguer reduction

The bouguer reduction method account for removal of all masses located above the geoid within the bouguer plate. This is achieved using integral, as proposed by Hofmann-Wellenhof and Moritz in 2005.

$$\delta g_{BC} = G\int_x\int_y\int_0^{H_P} \frac{\rho\left(H_p - H\right)\left(H_p - z\right)}{\left(\left(x_p - x\right)^2 + \left(y_p - x\right)^2 + \left(H_p - z\right)^2\right)^{3/2}} \mathrm{d}x\mathrm{d}y\mathrm{d}z \,. \tag{2.57}$$

The bouguer reduction method, as illustrated in Fig. 2.2, assumes that the vicinity surrounding the gravity station is completely flat, and the masses associated with the topography are approximated by a bouguer plate characterized by an infinite radius. This bouguer plate is represented as a horizontal cylinder featuring a uniform density denoted as ρ (with ρ = 2670 $kg\ m^{-3}$) and a thickness equivalent to H_p. Therefore, the calculation of the simple bouguer reduction, denoted as δg_{BC}, is achieved using the formula (Heiskanen & Moritz, 1967).

$$\delta g_{BC} = 2\pi G\rho H \approx 0.1119 H_p \quad \text{[mGal]} \tag{2.58}$$

the bouguer gravity anomalies are given by

$$\Delta g_{BA} = g_p + \delta g_{FC} - \gamma_Q - \delta g_{BC} + T_c \tag{2.59}$$

where Δg_{BA} is the bouguer anomaly, the observed gravity is g_{obs}, δg_{FC} is the free-air correction, is the normal gravity or latitude correction, δg_{BC} is the bouguer correction and T_C is the terrain correction.

The consideration of terrain effects is important in enhancing the precision of the bouguer plate attraction method. This comprises the distinction between the actual topographical features and the bouguer plate model, culminating in the computation of the refined (or complete) bouguer anomaly associated with the corresponding gravity anomaly. At the designated computation point denoted as $P\left(x_p, y_p, H_p\right)$, the classical terrain correction, identified as ς is determined through an integral encompassing the irregularities of the topographic mass relative to the bouguer plate. These irregularities are represented by the terms $\Delta m+$ and $\Delta m-$, in accordance with the methodology introduced by Tziavos and Sideris, 2013.

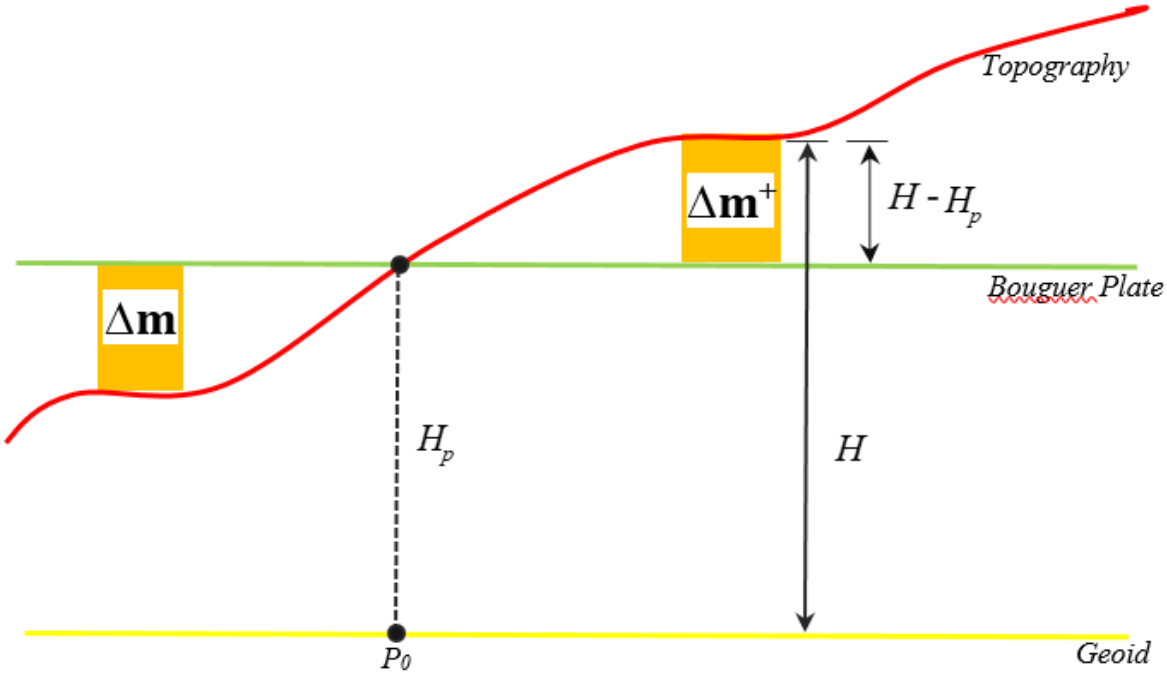

Fig. 2.2: The geometry of the planar bouguer reduction and the terrain

$$\varsigma = G\int_{x}\int_{y}\int_{H}^{H_P} \frac{\rho\left(H_p - H\right)\left(H_p - z\right)}{\left(\left(x_p - x\right)^2 + \left(y_p - x\right)^2 + \left(H_p - z\right)^2\right)^{3/2}} \mathrm{d}x\mathrm{d}y\mathrm{d}z \tag{2.60}$$

2.5.3 Residual terrain modelling (RTM) reduction

2.5.3.1 RTM reduction over Nigeria land

The RTM reduction method, as delineated in Fig (2.3), involves the utilization of two distinct topographical surfaces: a detailed surface and a reference surface over the data region. The effect of the detailed topographic surface was estimated from the SRTM 30" x 30." The reference surface representing the mean elevation of the area was obtained by applying a suitable low-pass filter to the detailed surface. In this study, the reference surface, in meters, was smoothed into a grid with a 5 × 5 arc-minute resolution, corresponding to the resolution of the gravity model XGM2019e_2159, and was estimated from the detailed grid SRTM30"x30", which we named SRTM5 in this study (Forsberg and Tscherning, 1981). The spatial resolution of SRTM 5'x5', measured in kilometers, commences where the spatial resolution of XGM2019e_2159 ends (Bako et al., 2024) The RTM computation used the TC toolbox of the GRAVSOFT package (Forsberg & Tscherning, 2008), with inner and outer integration radii of 10 km and 100 km, respectively, and a standard crustal density of 2.67 g/cm³. The RTM results,

for the region, demonstrate mean and SD values of -1.84 cm and 0.348 cm, respectively (Bako et al., 2024).

2.5.3.2 RTM reduction over the coastal region of Nigeria

In this study, the General Bathymetric Chart of the Oceans (GEBCO) with a spatial resolution of 15 arc-second (Dorschel et al. 2022) was used to compute the topographic potential effect over the coastal region of Nigeria, which represents a very short wavelength signal from the terrain data. RTM reduction (Forsberg, 1984) was computed using GEBCO data. RTM computations within the ocean domain were executed using the TC toolbox in the GRAVSOFT package (Forsberg and Tscherning, 2008). Given that bathymetry correction pertains to the disparities between ocean crust/sediment density and seawater density, we adopted a seawater density value of 1.028 g/cm³ and an ocean crust reference density of 2.9 g/cm³, resulting in a density difference of 1.872 g/cm³ (Chen et al., 2014). We employed inner and outer integration radii of 10 km and 200 km, respectively. RTM reduction utilizes two distinct bathymetry surfaces: a detailed surface and a reference surface over the data region. The effect of the detailed bathymetry surface was estimated from the GEBCO 15 arc seconds data (Dorschel et al. 2022). The reference surface representing the mean elevation of the area was obtained by applying a suitable low-pass filter to the detailed surface. In our study, a smoothed grid of 5 minutes (a resolution corresponding to the gravity model SGG-UGM-2) was estimated from the detailed grid GEBCO 15 arc seconds data, which we named GEBCO 5' in this study (Forsberg and Tscherning, 1981). The RTM results, utilizing the 1.872 g/cm³ density for the coastal region of Nigeria exhibit mean and SD of 0.36 mGal and 0.24 mGal respectively Bako and Kusche (2024).

The effect of topography on gravity in the RTM reduction method is estimated using the formula provided by Forsberg (1984) δg_{RTM} .

$$\delta g_{RTM} = 2\pi G\rho\left(H - H_{ref}\right) - \varsigma \tag{2.61}$$

The symbol ς refers to the classical terrain correction calculated using Eq. (2.60). At the same time, *H* represents the height of the gravity point with respect to the topographic surface and H_{ref} the height of the smooth reference surface.

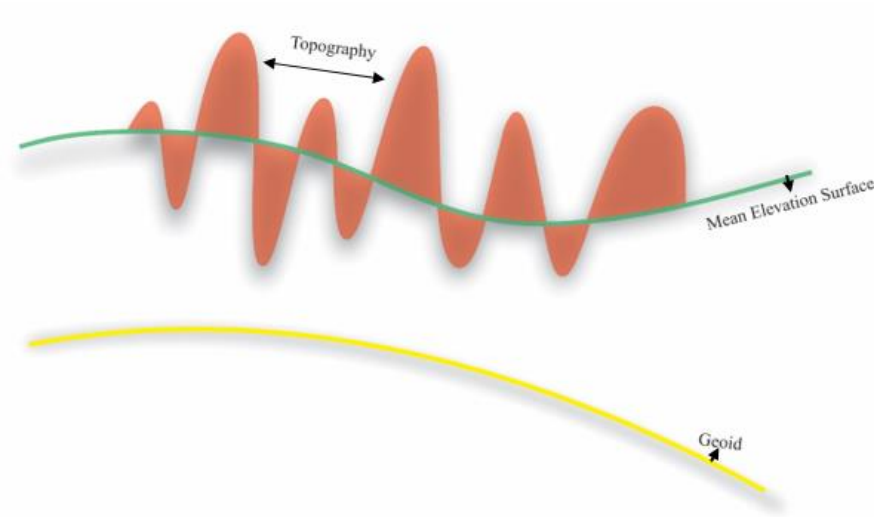

Fig 2.3: The residual terrain model (RTM) method.

The RTM anomaly Δg_{RTM} is given by (Forsberg, 1984):

$$\Delta g_{RTM} = g_p - \delta g_{FC} - \gamma_Q \tag{2.62}$$

The RTM effects on the geoid are expressed in planar approximation as:

$$N_{RTM} = \frac{G\rho}{\gamma_Q}\int_{-\infty}^{\infty}\int_{H_{ref}}^{H}\frac{1}{r}\mathrm{d}x\mathrm{d}y\mathrm{d}H = \frac{G\rho\left(H-H_{ref}\right)}{\gamma_Q}\int_{-\infty}^{\infty}\int_{H_{ref}}^{H}\frac{1}{r_0}\mathrm{d}x\mathrm{d}y\mathrm{d}H \approx$$

$$\frac{G\rho\left(H-H_{ref}\right)}{\gamma_Q}.\frac{1}{r_0} \tag{2.63}$$

The provided equations ρ represent the density of the Earth's crust, H_{ref} represents the height of the reference surface, ensuring that N_{RTM} contains only topographic potential not already included in the $N_{XGM2019e\_2159}$. Additionally, r_0 represents the distance between the computation point and the current point being incorporated. In the context of this study, the computation of N_{RTM} is based on SRTM30_PLUS (30" x 30") data, featuring a spatial resolution of approximately 0.9 km.

2.6 Geoid-quasi separation

The disparity between the geoid and the quasi-geoid leads to variations in the two height systems, specifically, the orthometric and standard heights. Consequently, it becomes imperative to assess the separation between these surfaces.

Estimating the difference between the geoid and the quasi-geoid necessitates the evaluation of the separation between these two height systems. This separation can be approximated as articulated by Heiskanen and Moritz (1967) in Eqn (2.64)

$$N - \zeta \approx \frac{\Delta g_B}{\gamma_Q} H \tag{2.64}$$

where Δg_B is the bouguer anomaly, γ_Q is the mean normal gravity, and H is the height above sea level. The error of the approximation ranges between 1-1.5 cm for flat and mountainous terrain (Saadon et al. 2021).

Chapter 3

Methodology

3.1 Introduction

This section outlines the datasets and research methods employed throughout the study. The objectives are (i) validation of geoid heights derived from GGMs using GNSS/levelling data, (ii) assessment of recent high-degree combined global gravity-field models for geoid modelling over Nigeria, and (iii) evaluation and homogenization of a marine gravity database derived from shipborne gravity and satellite altimetry-derived gravity data over the coastal region of Nigerian. Additionally, the methods of gravimetric geoid modelling over the study area are discussed. Fig 3.1 provides an overview of the sequence of work packages (objectives) in this study. Furthermore, assessing the accuracy of the newly developed gravimetric geoid model are also discussed.

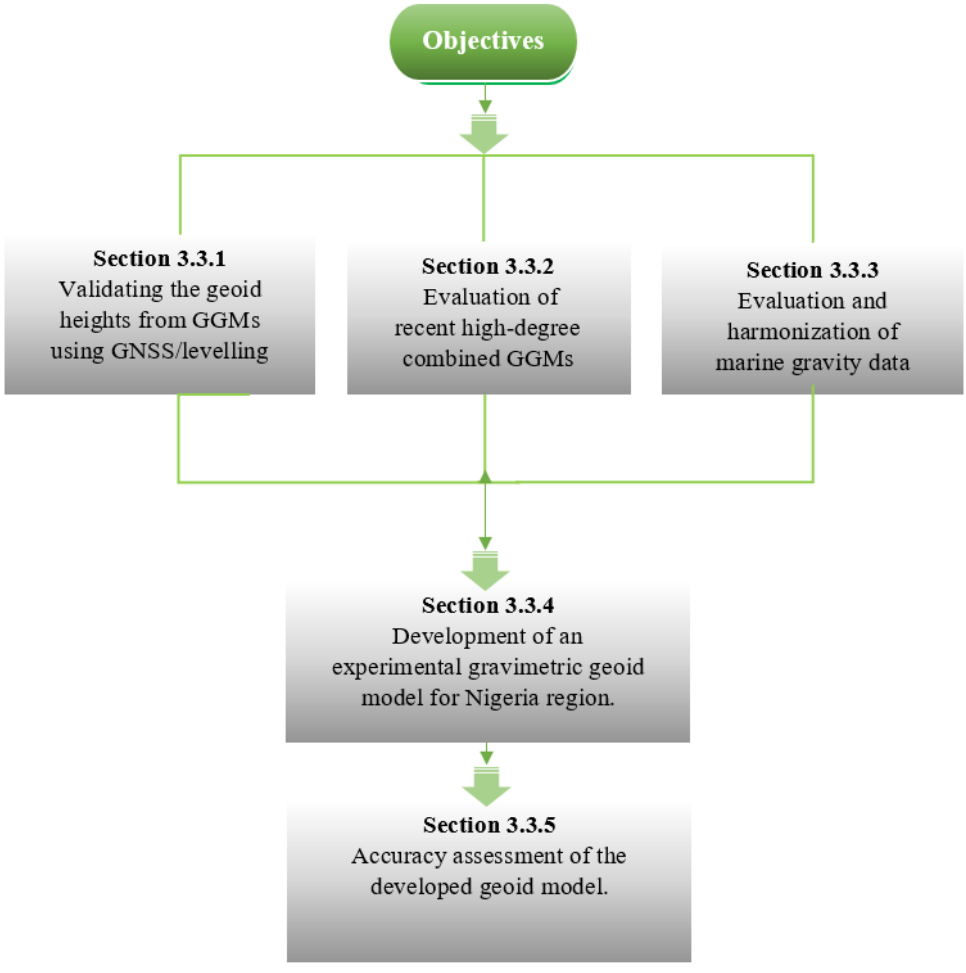

Fig 3.1: Sequence of work packages (objectives) in this study

3.2 Datasets used for the study

The study used five fundamental datasets: (1) the GGM (Ince et al., 2019), (2) Terrestrial and Marine gravity data, (3) GNSS and levelling data obtained from Office of Surveyor General of the Federation (OSGOF) (4) a high-resolution digital terrain model obtained from SRTM (USGS, 2017) (5) DTU21 MSS and CNES-CLS22 MDT

3.2.1 Global Geopotential Models

Prior to geoid computation, the GGM was used as a reference model in the RCR procedures. Hence, the selection of ideal GGMs is crucial to produce precise gravimetric geoid models. In this study, the XGM2019e_2159 (Zingerle et al., 2019) GGM at a SH degree truncated up to d/o 360 was selected for geoid computation to recover the long-to-short wavelength component of the gravity signal when modelling the gravimetric geoid, as it approximates the gravity field well over Nigeria (Bako et al., 2024). Notably, Moka et al. (2018) applied EGM2008 up to d/o 2190, whereas we used the recent XGM2019e_2159 GGM. In addition, it should be noted that we applied only d/o 360 of XGM2019e_2159 (and not 2190) over Nigeria, because beyond d/o 715, XGM2019e_2159 is mostly based on topography (Zingerle et al., 2019).

3.2.2 Gravity data

This research relies on gravity data, including free-air gravity anomalies, shipborne free-air gravity anomalies, and satellite-altimetry-derived gravity data, which were obtained from various sources. Fig 3.2 to 3.3 shows the spatial distribution of the diverse gravity observation points utilized in this study.

3.2.2.1 Cross-validation of gravity data

To ensure the reliability and accuracy of the gravity data, the cross-validation (XV) approach was adopted, following the method described by Bako and Kusche, 2024; Zaki et al., 2021. The XV method aims to provide an unbiased statistical estimate of error. This process involves excluding one observation at a time, utilizing each excluded point for validation while the remaining data are utilized for interpolation (Arlot & Celisse, 2010). The 2-sigma approach as rejection criteria was used, where points exhibiting differences between the interpolated and observed values exceeding twice the SD of the residuals were removed as outliers and gross errors. The XV approach was implemented using Golden Software (Surfer version 8.0).

The residuals obtained from the XV techniques depend on the quality of the interpolation technique and the geographical distribution of gravity observations (Kamguia et al., 2007). Consequently, selecting an appropriate interpolation technique forms an important aspect of

XV. Kriging is a widely employed interpolation method for detecting biased values (Matheron, 1963).

3.2.2.2 Terrestrial free-air gravity data

The available land gravity dataset comprises 1055 gravity data points sourced from the Geological Survey of Nigeria and other sources, which was collected within 3-5 km spacing using Lacoste & Romberg gravimeter. The free-air gravity anomalies are computed using Eq. (2.56) with corrections made for atmospheric effects as discussed in section 2.3.2. To ensure data quality, a gross error and outlier detection scheme employing cross-validation was applied to the gravity data (refer to section 3.2.2.1). The gross errors technique was implemented iteratively until the standard deviation of the residuals (the difference between data and estimated values) reached 1.5 mGal. After removing gross errors and outliers, the dataset was reduced to 846 gravity data points. Fig (3.1) visually represents the distribution of free-air gravity anomalies for Nigeria, as utilized in this study. The measured land gravity values were linked to 2 International Gravity Standardization Network (IGSN) gravity stations and 63 Nigeria Gravity Standardization Network (NGSN) stations. The terrestrial free-air gravity anomalies spanned from −26.20 mGal to 63.33 mGal, with a mean value of approximately 6.71 mGal and a standard deviation of 14.29 mGal.

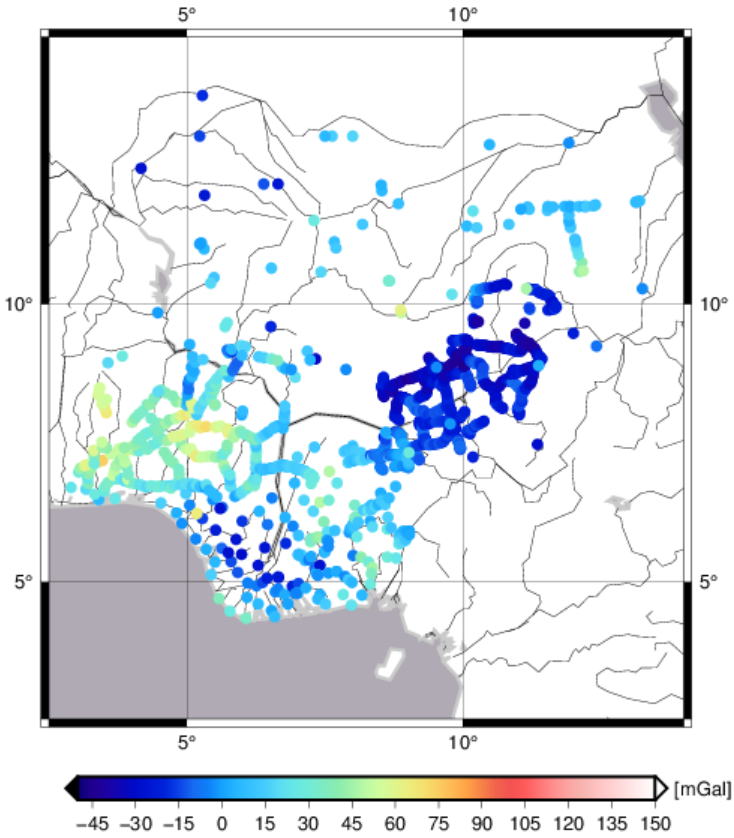

Fig 3.2: Free-air anomalies distributions over the area of Nigeria [mGal]

3.2.2.3 Marine gravity data

3.2.2.3.1 Shipborne Free-air gravity data

This study utilized shipborne gravity data from the BGI. The dataset comprised five marine surveys conducted on different ships (BGI, 2018), as shown in Table 3.1.

Table 3.1: The dataset comprises five marine surveys conducted by different ships

S/N	1	2	3	4	5
Survey No	Survey 61021051	Survey 61021332	Survey 61021790	Survey 65100022	Survey 65100023
Owners	Lamont Doherty Geological Observatory	Lamont Doherty Geological Observatory	Woods Hole Oceanographic Institution	Ifremer	Ifremer
Vessel name	Robert D. Conrad	Vema	Atlantis II	Jean Charcot	Jean Charcot
Project	Cruise 13, Leg 12	Cruise 29, Leg 07	Cruise 75, Leg 2	Oceanographic Cruises	Oceanographic Cruises
No of Data points	306	382	688	249	837
Chief Scientist	R. Leyden	Dr. Philip Rabinowitz	Dr. K. O. Emery	Roland Schlich	Vincent Renard
Begin and End of legs dates	02/9/1970 to 01/10/1970	21/05/1972 to 12/06/1972	10/02/1973 to 6/03/1973	04/09/1971 to 27/09/1971	19/07/1971 to 06/08/1971
Departure Port	Abidjan, Ivory coast	Luada, Angola	Dakar, Senegal	Abidjan	Luada, Angola
Arrival Port	Mossamedes, Angola	Abidjan, Ivory coast	Terma, Ghana	Dakar	Dakar, Senegal
Instrument type	Continuous recording sea gravimeter	GRAF-ASKANIA GSS2-12	vibrating string accelerometer (VSA) sea gravimeter	Unknown	Unknown
Positioning system	US Navy satellite system (TRANSIT)	Satellite/Sextant	satellite navigation and a gyroscope	US Transit satellite positioning system	US Transit satellite positioning system
Reference	(BGI, 2018; Wessel and Watts, 1988)	(BGI, 2018; Wessel and Watts, 1988)	(Unesco, 1973; Emery et al., 1975)	Schlich Roland (1971); Basile et al., 1996)	(Renard Vincent, 1971)

These surveys collectively covered a large part of the study area in the coastal region of Nigeria, with longitudes ranging from 2.5° E to 10° E, and latitudes ranging from 2.5° N to 6.5° N. A total of 2462 data points were collected, with shipborne gravity anomalies ranging from -84.40 mGal to 131.81 mGal and an average value of 15.17 mGal. Fig 3.3 illustrates the spatial distribution of the shipborne gravity data, and Fig 3.4 illustrates the different survey legs using different colors. The distribution of the shipborne gravity dataset in the study area was not homogeneous for geoid modelling research, with a significant data gap. To ensure the reliability of our analysis, we considered the possibility of residual errors in the shipborne gravity data used in this study arising from various sources, such as instrumental drifts, navigational errors, discrepancies in ties to harbor base stations, and inconsistent use of reference systems (Wessel and Watts, 1988; Denker and Roland, 2005).

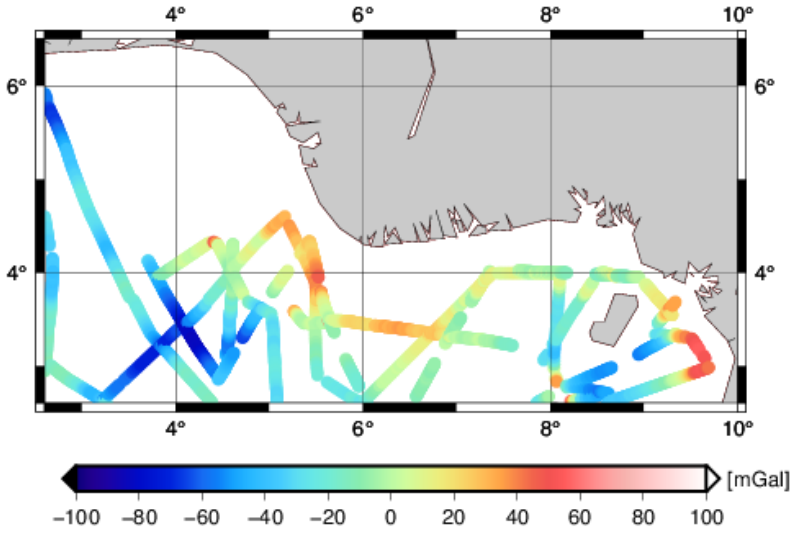

Fig 3.3. Distribution of the available shipborne gravity data over the coastal region of Nigeria.

Additionally, the accuracy of shipborne data is highly dependent on the quality of ship navigation. Hence, it is essential to thoroughly evaluate the consistency of these data and identify any outliers before integrating them with selected altimetry-derived gravity data (Bako and Kusche, 2024). The cruises mentioned above (Table 3.1) were linked to the local network with absolute gravity points on the land (Morelli, 1972). During the cruises, gravity data were collected using a GRAF-Askania GSS2-12, vibrating string accelerometer (VSA) sea gravimeter, and continuous recording sea gravimeter, which were equipped with navigational instruments such as satellite/sextant, satellite navigation and gyroscope, and the US Transit satellite positioning system, respectively (Unesco, 1973, Schlich Roland 1971, Renard Vincent 1971, Wessel & Watts, 1988).

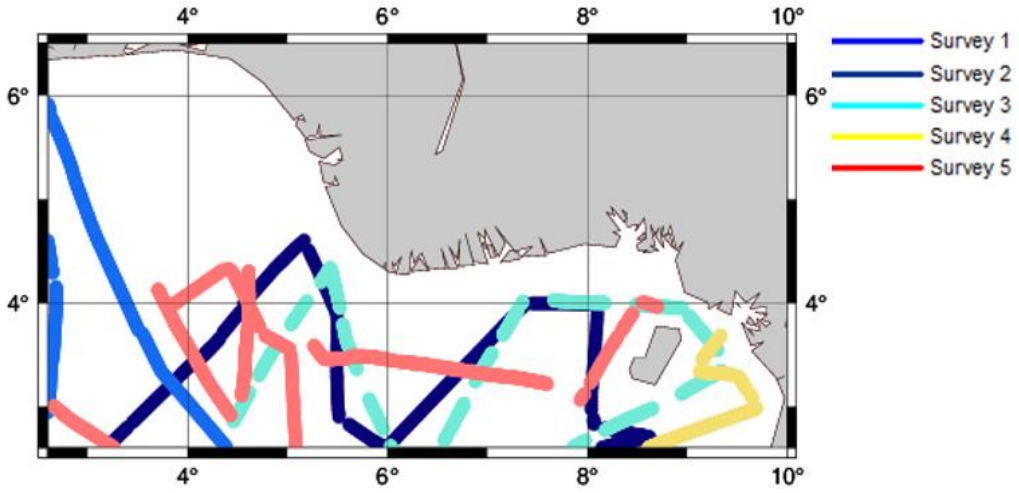

Fig 3.4: Geographical distribution of five surveys using different colours within the study area.

It is important to highlight that there are other shipborne gravimetry campaigns performed in the coastal region of Nigeria by the United States Geological Survey (USGS) between July 22 and August 20, 1987, utilizing the Lacoste Air-Sea gravimeter and Global Positioning System (GPS) technology in compliance with a request from the defense mapping agency, encompassing the African coast, with the aim of augmenting gravity coverage in areas where it has been insufficient or inadequate. However, this dataset is not publicly accessible (Folger et al., 1990).

3.2.2.3.2 Satellite altimetry derived-gravity data

In this study, we utilized marine satellite altimetry-derived gravity datasets, namely DTU21GRA (Andersen & Knudsen, 2021) and SSv29.1 data (Sand well et al., 2021), provided as grids with a 1-arc-minute resolution. EGM2008 (Pavlis et al., 2012) was employed as a reference field model to compute the DTU21GRA and SSv29.1. Among the DTU series models, DTU21GRA stands out for its focus on the near-coastal areas. Simultaneously, SSv29.1 distinguishes itself from other SS series models by incorporating two additional years of Sentinel-3A/B datasets in its computation. However, the critical difference between DTU21GRA and SSv29.1 lies in their choice of the estimation algorithm. DTU21GRA incorporates residual sea surface heights (SSHs) into its estimation method (Andersen & Knudsen, 2021) whereas SSv29.1 utilizes the residual slopes of the SSH obtained through mathematical differentiation of neighboring altimeter data (Sand well et al., 2021).

The SSv29.1 gravity model can be downloaded from ftp://topex.ucsd.edu/pub/archive/grav/. The DTU21GRA gravity model was obtained from https://ftp.space.dtu.dk/pub/. The DTU21GRA, SSv29.1 gravity model and their differences are illustrated in Fig. 3.5. The differences between DTU21GRA and SSv29.1 gravity values show a minimum, maximum,

mean offset and SD of −46.85, 79.93, 0.02 and 4.12 mGal, respectively. Larger differences were observed around coastal areas and islands, which demonstrates the poor accuracy of satellite altimetry near coastal areas (Bako and Kusche, 2024).

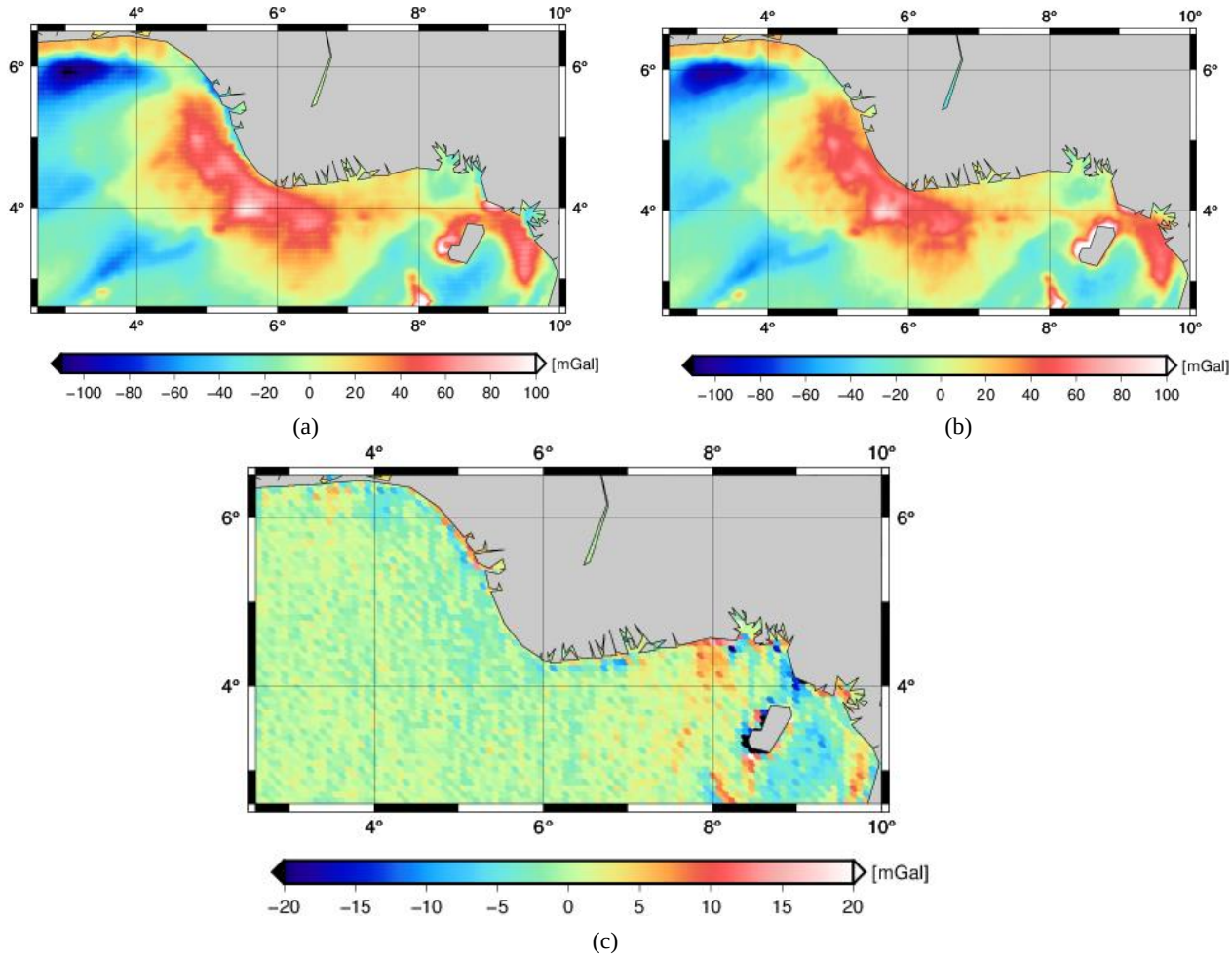

Fig. 3.5. Free-air gravity anomalies from the DTU21GRA model (a) SSv29.1 model (b) and the differences between DTU21GRA and SSv29.1 gravity values (c) in the coastal region of Nigeria

3.2.3 GNSS/levelling Data

Geometric heights obtained via GNSS and orthometric heights obtained via levelling were collected from the OSGoF across 90 GNSS/levelling sites distributed over Nigeria (Fig. 3.6). The study area ranges from 3° to 14° longitude and 4° to 14° latitude. GNSS observations were conducted at sites marked with concrete posts with official designation. As these points were recently established, they were not included in the computation of GGMs and were treated as independent datasets. Observations were performed using a dual-frequency Trimble differential global positioning system (DGPS) version R8, Model 4 instrument in static mode, with each station observed for five hours. The temperature during the measurements ranged

from 25°C to 38°C. Several precautions were taken to ensure accuracy during data collection, including setting the antenna height higher than the observer, maintaining a consistent five-hour observation session, ensuring a minimum of four satellites for each observation, and avoiding observations in areas under canopy coverage. The data in the receiver-independent exchange (Rinex) format from each benchmark station were processed using the Trimble Business Center software (TBC) set for the world geodetic system, 1984 (WGS84) reference ellipsoid. Precise ephemeris data from the International GNSS Service (IGS) orbit product and very low noise L1 and L2 carrier phase measurements were utilized to enhance the measurement precision (Bako et al., 2019). GNSS data were processed using the OSGoF Continuous Operating Reference Station (CORS) as a reference station (Bako et al., 2019).

The precise levelling data used in this study were obtained from the OSGoF. The heights of the control points across Nigeria were determined using geodetic spirit leveling. The reference point was established from the MSL height in Lagos, obtained through average tide gauge measurements of at least 19 years of observation at the Lagos datum station. This average tidal gauge measurement was employed to ascertain the heights of all the control points nationwide, including the Minna datum (L40). The heights obtained from geodetic levelling were derived after adjusting for various levelling loops. The leveling network comprises approximately 200 geodetic lines that are fairly uniformly distributed across the country, and a set of control points (benchmarks). Each leveling line started with fundamental benchmarks (FBM) or standard benchmarks (SBM) with intermediate benchmarks (IBM). A lower-order level network is tied to these (Fajemirokun, 1980; Opaluwa et al., 2010; Aleem et al., 2022).

Ezeigbo and Edoga (1980) observed that a systematic error of 0.9" existed in all geodetic azimuths computed at the Lagos datum (origin). In addition, (Ezeigbo, 1991; Agajelu, 1990) identified scale distortions between 1-3 ppm in the network owing to the absence of a geoid height model in northeastern Nigeria, as discussed by Aleem, 2014; Odumuso, 2019 and Bako et al., 2024.

3.2.4 High-resolution terrain data

In this study, the SRTM 30 data (USGS, 2017) serves as a critical component to address the spectral resolution disparity. It effectively bridges the gap between terrestrial data on one end and the GGMs on the other. This was achieved through the Spectral Enhancement Method (SEM) Forsberg (1985), Gruber (2009), Hirt et al. (2011), and Elsaka et al. (2016), as outlined in sections 2.5.3. The results from the RTM employing a 2.67 g/cm³ density on land and 1.86 g/cm³ on the sea within the Nigeria region yield a mean and SD of -0.24 and 0.98, respectively.

Plate 3.1 The student carried out a GNSS observation campaign

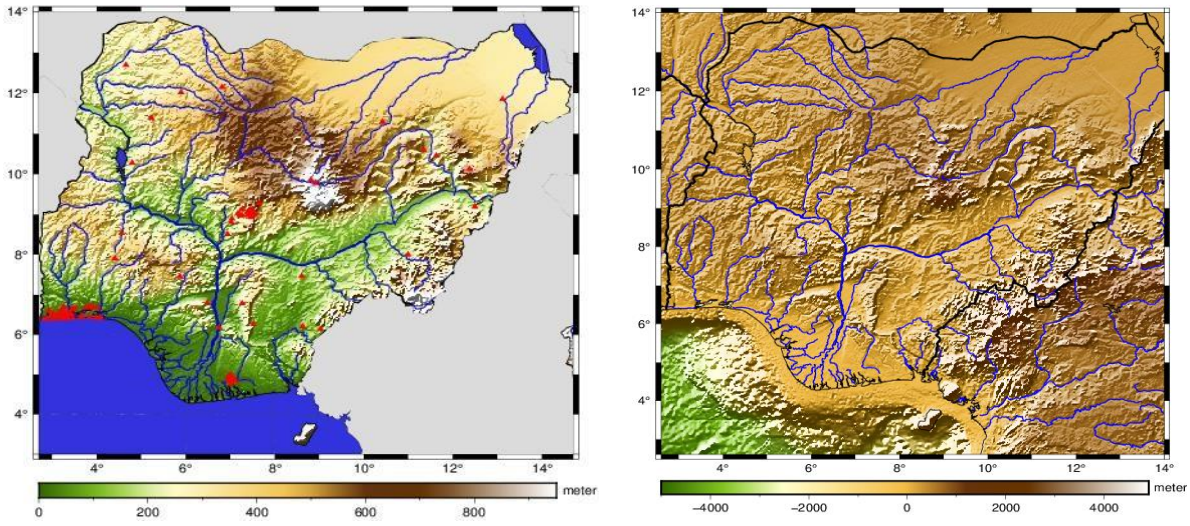

Fig 3.6: Terrain model of Nigeria based on the SRTM 30 data. Red points represent the positions of the GNSS/levelling observations (left) The terrain and bathymetry model covering the land and coastal region of Nigeria (right).

3.2.5 DTU21 MSS and CNES-CLS22 MDT

This study used the DTU21MSS model (Andersen et al., 2023) because it used five years of Sentinel-3A data and Sentinel-3B data for two years, respectively. Furthermore, the SAMOSA+ physical re-tracker, an advanced waveform re-tracker, was utilized for pre-processing CryoSat-2 data to compute DTU21MSS. The selection of the SAMOSA+ re-tracker over others, such as the MWaP re-tracker or empirical retrackers, is justified by its generally lower root-mean-square error (Villadsen et al., 2016). For validation purposes, the CNES-

CLS22 MDT (Jousset et al., 2022) was chosen because it uses the latest Gravity Observation Combination (GOCO06s) geoid model (Kvas et al., 2021), which is based on comprehensive reprocessing of the entire GOCE mission (Drinkwater et al., 2003) and 14 years of GRACE data (Tapley et al., 2004). This model also incorporated the new CNES-CLS 2022 MSS (Schaeffer et al., 2023). Overall, the precision analysis of the CNES-CLS22 MSS showed a 40% improvement compared with the 2015 model (Schaeffer et al., 2023). Additionally, in computing the CNES-CLS22 MDT, drifter and high-frequency radar data were processed to retain only geostrophic components (Jousset et al., 2022). The CNES-CLS22 MDT and DTU21 MSS datasets are shown in Fig. 3.7

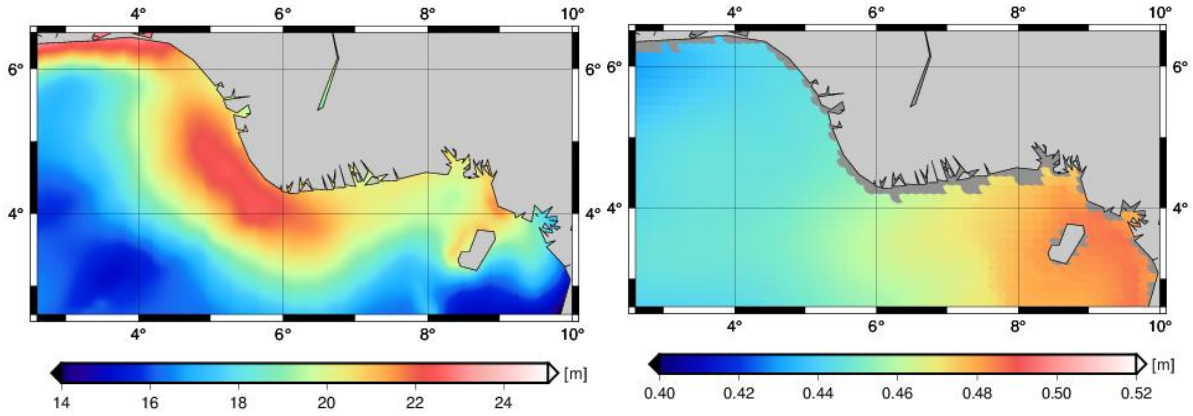

(a) (b)

Fig. 3.7 Mean Sea Surface data, DTU21MSS (a) and CNES-CLS22 MDT (b)

3.2.6 Gravimeter

The selection of gravimeters was dependent upon their availability and suitability for the study's objectives. Nigeria's field data collection process involved using the Scrintrex CG5 and the La Coste and Romberg gravimeter, sourced from the NGSA, as illustrated in Plates 3.2.

Plate 3.2: The Scrintrex CG5 gravimeter and The La Coste and Romberg Gravimeter

3.3 Methods

This study applied widely used geodetic methodologies documented in prior geodetic literature, adhering to established standards. This section outlines the steps undertaken to achieve the research objectives.

3.3.1 Validating the Geoid Heights from Global Geopotential Models using GNSS/levelling Data over Nigeria

This section outlines the research methodology used in this study. The objectives were: (1) evaluation of GGMs using GNSS/levelling data, (i) comparison without accounting for spectral consistency, (ii) comparison with accounting for spectral consistency, and (2) fittings of geoid heights from GGM to GNSS/levelling geoid heights.

3.3.1.1 Evaluation of GGM using GNSS/Levelling Data

The GGM assessment involved a comparison between the GGM-derived geoid heights and GNSS/levelling data. Two main scenarios were employed, with and without accounting for spectral consistency using SEM. The SEM is fundamentally designed to incorporate supplementary data and fill the spectral gap inherent in GOCE-based GGMs. This fusion serves to mitigate omission errors that may obscure the evaluations conducted between GOCE-based GGMs and GNSS/levelling data (see Fig. 3.8)**.**

3.3.1.1.1 Comparison without accounting for spectral consistency

In this study, GGM-derived geoid heights and 90 GNSS/levelling points were compared by interpolating the geoid height values from the GGMs into the positions of the GNSS/levelling

measurements using the GEOEGM toolbox of the GRAVSOFT package (Forsberg & Tscherning, 2008), and the results are plotted using Generic Mapping Tools (GMT) (Wessel et al., 2013). GGMs were evaluated in Nigeria at different spectral resolutions (i.e., different grids). Each GGM is bounded from SH degree 2 to N_{max} =100, 120, 140 …., 340, and 360 (20° steps), respectively. The evaluation was performed in terms of differences in the geoid height ΔN_1, as described in Eq. (3.1):

$$\Delta N_1 = N_{GNSS/\text{levelling}} - N_{GGM\,(\text{point})}\Big|_{2}^{N_{\max}} \tag{3.1}$$

3.3.1.1.2 Comparison with accounts of spectral consistency

Previous studies, including those referenced in Merry, (2009); Yilmaz et al., (2016) and Section 3.3.1.1.1, have overlooked the significance of incorporating short- and very short-wavelength gravity signals beyond maximum-degree GOCE-based GGMs (see Fig. 3.8). To mitigate omission errors that could obscure comparisons between GOCE-based GGMs and GNSS/levelling data, $N_{XGM\,2019e\_2159}$ term in Eq. (3.2), representing short-wavelength gravity signals from SH up to degree 2190, was added to N_{GOCE}. Additionally, the $N_{RTM,}$ which accounts for very short-wavelength gravity signals beyond SH degree 2190, was incorporated. The planar approximation is expressed in Eq. (2.63)

In this study, the computation of N_{RTM} incorporated SRTM30_PLUS data with a spatial resolution of approximately 0.9 km, and a calculation radius of 100 km was used. Therefore, the complete formula for comparison, which accounts for spectral consistency, is expressed by Forsberg, 1985; Gruber, 2009; Hirt et al., 2011; and Elsaka et al. 2015**.**

$$N_{GGM} = N_{GOCE\,(\text{point})2}^{N_{\max}} + N_{XGM\,2019e\_2159}{}_{N_{\max}+1}^{2190} + N_{RTM} \tag{3.2}$$

The major concern when comparing GGMs to GNSS/levelling data is spectral content difference (Hirt et al., 2011). In addition, GGMs have a wavelength spectrum limited by their maximum SH degree; therefore, they do not contain all the possible wavelength ranges. Omission errors occur when the Earth's gravitational field short-wavelength gravity signals are not captured in GGMs. Therefore, SEM is the best approach to facilitate the spectral gap between the GOCE-based GGMs and GNSS/levelling data, as represented in Eq. (3.3) and Fig. 3.8

$$\Delta N_2 = N_{GNSS/\text{levelling}} - N_{GGM} \tag{3.3}$$

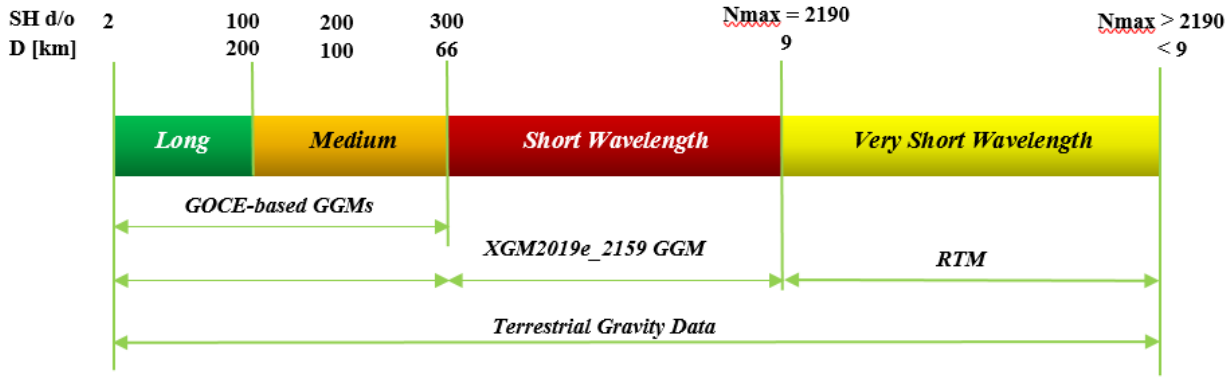

Fig. 3.8: The principle of the Spectral Enhancement Method (SEM) (Bako et al., 2024).

In this study, XGM2019e_2159 was used in the SEM assessment when evaluating the GOCE-based GGMs of the DIR_R6, SPW_R5, and TIM_R6 models up to d/o 300 and beyond for two reasons: the low SD value of 0.354 at SH d/o 2190 compared to other evaluated combined GGMs (see Table 4.1), and the observation that XGM2019e_2159 exhibited slightly improved behavior in the spectral band up to d/o 719 in the magnitude of a few mm RMS over land compared to prior models, such as EIGEN-6C4 and EGM2008. This improvement was evident when validated against independent geoid information derived from GNSS/levelling (Zingerle et al., 2020). However, it is essential to note that in the spectral range beyond d/o 719, the accuracy of XGM2109e_2159 experiences a slight decline because of the exclusive utilization of topographic forward modelling (Zingerle et al., 2020).

SEM can validate GGMs independently of the spatial distribution of GNSS/levelling data (Gruber, 2009; Hirt et al., 2011). This method is suitable for irregularly distributed ground observations, as in our case study (Nigeria), which had sparse GNSS/levelling data. Consequently, we used this method in our investigation.

3.3.1.2 Fittings of geoid height from GGM to GNSS/levelling geoid heights

The disparities between the geoid heights derived from GNSS/levelling data and GGMs lead to systematic errors (mean offset), commonly known as biases. The offset between the two equipotential surfaces created by GNSS/levelling-derived geoid heights and GGM geoid models may contribute to these biases or these disparities are presumably attributable to errors in the SH coefficients associated with long and medium wavelengths (Kotsakis & Katsambalos, 2010). To model systematic errors, least-squares parametric fitting was used. Four types of parameter transformation models, namely linear, four-, five-, and seven-parameter transformation models, were applied to eliminate these biases and accurately fit geoid heights from GGMs to GNSS/levelling-derived geoid heights over Nigeria.

These four transformation models were selected to address the biases and offsets between the GGMs and GNSS/levelling data. In addition, a parametric model with the smallest SDs across all GGMs was identified. The transformation models used are discussed in Bako et al., 2024. It represents the transformation models that adjust geoid heights, eliminate systematic errors, and improve the SD of the differences between GNSS/levelling-derived geoid heights and GGMs extended by XGM2019e_2159 and RTM. The transformation models involve parameters related to the ellipsoid eccentricity, random noise term, latitude, and longitude, and the transformation parameters (Bako et al., 2024).

3.3.2: Evaluation of the recent high-degree combined global gravity-field models for geoid modelling over Nigeria.

In this context, five combined GGMs (namely, SGG-UGM-2, XGM2019e_2159, GECO, EIGEN-6C4, and EGM2008) over the region of Nigeria were evaluated. This evaluation was performed using terrestrial gravity anomalies. Furthermore, an independent check was carried out using GPS/levelling data, albeit specifically over Abuja, Nigeria.

3.3.2.1 Evaluation of gravity anomalies from GGMs using terrestrial gravity data over Nigeria

The computation of free-air gravity anomalies considers the effects of atmospheric corrections, free-air reduction, and latitude correction, as expressed in Eq. (2.56). Given the significance of topography in the study region, topographic corrections based on the SRTM 30 dataset were considered when calculating the Bouguer anomaly, following the formulation presented in Eq (2.59). Furthermore, areas with relatively flat terrain and regions with significant topography were evaluated.

3.3.2.2 An independent check conducted using GPS/levelling data over Abuja

An independent check was conducted using GNSS/levelling data collected from 20 stations located in Abuja, Nigeria. To ensure a rigorous evaluation, it is imperative to account for very short gravity signals that extend beyond the maximum degree utilized in the combined GGMs. Therefore, including the residual terrain model N_{RTM}, which comprises very high-frequency gravity signals extending beyond the 2190 SH degree, into the combined GGMs is paramount.

3.3.3: Evaluation and homogenization of a marine gravity database from shipborne gravity and satellite-derived gravity data over the coastal region of Nigeria.

This section outlines the study's research methodology. The objectives were (i) accuracy assessment of shipborne and satellite altimetry-derived gravity data, (ii) comparison of refined shipborne and predicted gravity models, (iii) integration of refined shipborne and selected

altimetry-derived gravity data, and (iv) the effect on geoid determination. Fig. 3.9 provides an overview of our research methodology.

3.3.3.1: Accuracy assessment of shipborne and altimetry-derived gravity data

In this section, the fact that the survey was conducted by different institutions (see Table 3.1) over various years, using different instruments was addressed. Consequently, linear drift and systematic bias must be corrected before validation.

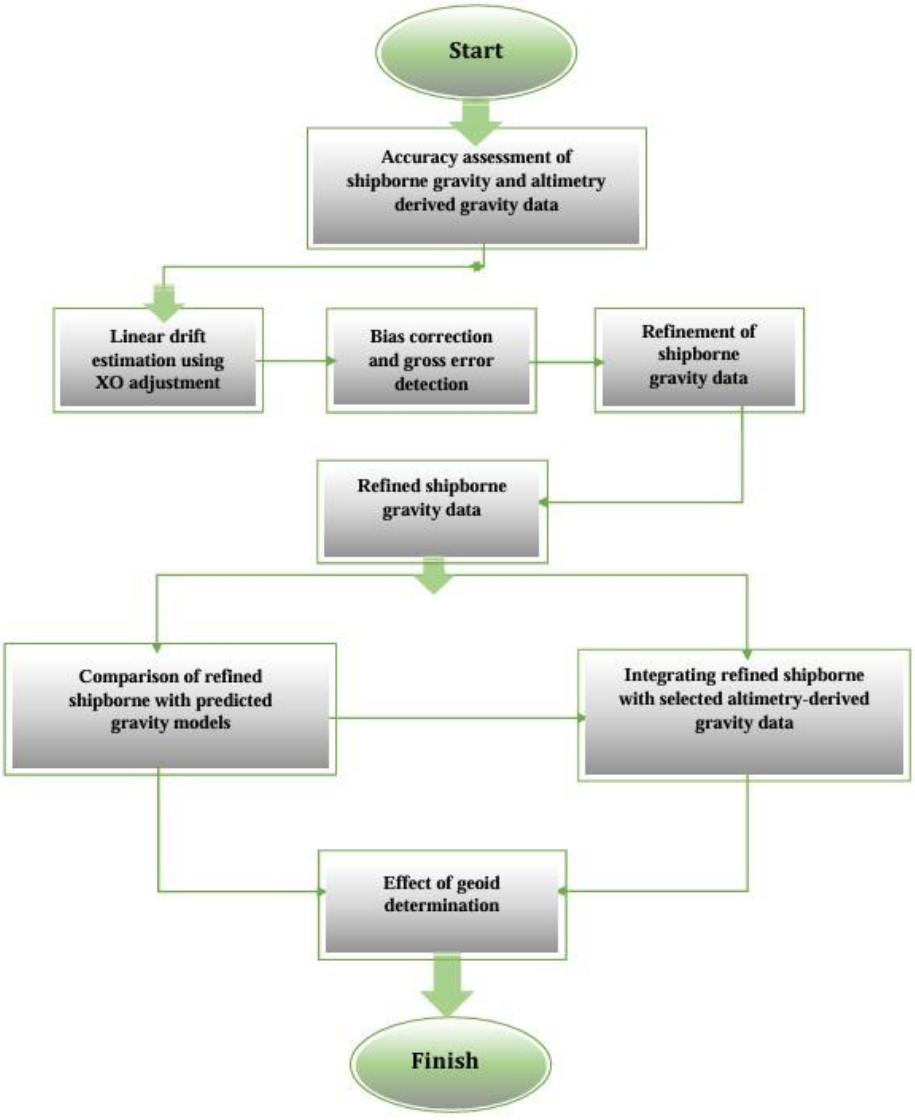

Fig 3.9: The framework of the research methodology (Bako and Kusche, 2024).

Additionally, these shipborne data contain several gross errors and outliers owing to varying measurement conditions. Therefore, it is necessary to eliminate these limitations based on preliminary evaluations using altimetry-derived gravity data (DTU21GRA and SSv29.1).

This assessment involves the adoption of a method similar to that outlined by Wessel and Watts (1988); Bako and Kusche, (2024), which addresses the inherent linear drifts within a shipborne

gravity dataset by utilizing crossover (XO) points that commonly arise because of temporal variations in gravimeters, thereby introducing systematic errors in gravity measurements as discussed by Bako and Kusche, (2024).

The conventional approach for mitigating this distortion involves connecting the gravimeter to the local network upon the conclusion of the cruise, followed by checking the differences between the meter readings and base station values. Any offset indicates potential linear drift.

To compute the drift error of a gravimeter utilizing XO points, the drift error was characterized as linear over time, and the drift factor was determined via least-squares adjustment based on multiple XO points. A design matrix '**A**' for the least-squares adjustment was formulated, where each row represents an XO point along with the measurement days and constant term. The XO points between the track segments were calculated by computing the differences between consecutive gravity measurement points, and a linear interpolation was applied at the crossover points.

As previously discussed, it is necessary to remove the systematic bias in shipborne gravity measurements from the BGI before validation. This method involves editing these data by comparing them with altimetry-derived gravity data. The discrepancies between the altimetry-derived gravity data and shipborne gravity measurements using linear interpolation was calculated.

To mitigate this systematic error (mean offset), linear corrective models were applied to the residual (Heisknen and Moritz, 1967). After eliminating linear drift and systematic bias, gross errors within each survey leg were identified and eliminated using rejection criteria. Specifically, data points showing residuals exceeding twice the average SD were identified as outliers and were subsequently removed from the dataset.

Finally, to ensure the reliability and accuracy of the remaining shipborne gravity data, a XV approach was adopted following the method described by Bako and Kusche, (2024). The XV method provides an unbiased statistical estimate of the error. This process involved excluding one observation at a time and utilizing each excluded point for validation. The remaining data were used for interpolation. The 2-sigma approach was used as a rejection criterion in which points exhibiting differences between the interpolated and observed values exceeding twice the SD of the residuals were removed as outliers. In this section, 436 data points were removed during the aforementioned process, representing 17.7% of the entire dataset (Bako and Kusche, 2024). This study used the Kriging interpolation method for the XV technique because it is a widely employed interpolation method for detecting biased values (Matheron, 1963).

3.3.3.2: Comparison of refined shipborne with predicted gravity models

The refined shipborne gravity measurements were compared with various estimated gravity models (DTU21GRA, SSv29.1, SGG-UGM-2, XGM2019e, GECO, EIGEN-6C4, and EGM2008) after eliminating linear drift, systematic bias, and outliers. The discrepancies between the shipborne free-air anomaly (FA) and the FA derived from various predicted gravity models were compared by interpolating the FA values from the various predicted gravity models into the positions of the shipborne FA measurements using linear interpolation. To identify the most suitable altimetry gravity model for integration, the model that exhibited the lowest SD and Root Mean Square (RMS) fit was selected.

3.3.3.3: Integrating the refined shipborne with DTU21GRA gravity data

This study focuses on establishing a coherent gravity field covering the coastal region of Nigeria by integrating shipborne gravity data with selected altimetry-derived gravity data, primarily for geoid modelling purposes.

Following the refinement process of the shipborne marine gravity data, which entailed the removal of data points (as elaborated in section 3.3.3.2), this refined shipborne gravity data was merged with the selected altimetry-derived gravity data (DTU21GRA). The DTU21GRA 1' × 1' marine dataset was converted into point data, where each record at the grid node was treated as an individual data point, resulting in 3371 records. The integration of refined shipborne data with the DTU21GRA (Andersen and Knudsen, 2021) marine gravity anomaly grid was accomplished using the LSC technique as reported by (Bako and Kusche, 2024), (Kamto et al. 2022), and (El-Fiky 2018). At any arbitrary point, the predicted value of the gravity anomaly, is given by Eq (2.38), as elaborated in section 2.4.1.3.

First, the residuals between the refined shipborne gravity data and DTU21GRA model was computed. Gridding of the resultant residuals was then performed using the LSC. The residuals were gridded onto a 1 arc-minute resolution, with the same resolution as the DTU21GRA grid. Consequently, a second-order Gauss-Markov covariance model with a 30-km correlation length and a white noise of 1 mGal was applied during the LSC after testing them over a range of 10-50 km and 1-5 mGal Zaki et al., 2018; Bako and Kusche, 2024.

Finally, the grid of the residuals was added to the pre-gridded DTU21GRA (Andersen and Knudsen, 2021) altimetry gravity anomaly values to obtain an enhanced altimetry dataset. GEOGRID toolbox within the GRAVSOFT package (Forsberg & Tscherning, 2008) was used for this purpose.

The validation was performed independently by examining the combined gravity datasets at randomly selected scattered shipborne gravity stations, accounting for approximately 5% of the data, which were not included in the LSC process. A total of 100 points were selected based on their geographical distributions in the northern, eastern, western, and southern regions of the study area. None of the 100 points selected for testing were considered outliers. This is because the test points were selected from the refined shipborne data and were not affected by outliers or gross errors.

3.3.3.4: The effect on geoid determinations over the coastal region of Nigeria.

In this section, two gravimetric geoid models for the study area are generated: one used refined shipborne data, and the other used the combined gravity dataset. MDT was computed using the DTU21MSS model (Andersen et al., 2023). This was validated using CNES-CLS22 MDT (Jousset et al., 2022). The computed gravimetric geoid model involved the adoption of a methodology similar to that outlined by El-Fiky, (2018); Bako and Kusche, (2024). The approach for gravimetric geoid modelling is based on the RCR technique, exemplified by (Sanso and Sideris, 2013; Hofmann-Wellnhof and Moritz 2006), coupled with the RTM reduction method (Forsberg, 1984). The RCR procedure was employed to compute the gravimetric geoid model for the coastal region of Nigeria. Within this procedure, the components of the short and very short wavelengths of the functional of the disturbing potential were derived from GGM and high-resolution General Bathymetric Chart of the Oceans (GEBCO) 15 arc seconds dataset, respectively. These effects were removed from shipborne gravity data and combined gravity data respectively, during the initial stage, resulting in residual gravity anomalies, as elaborated in section 3.3.4, Eq. (3.4) and (3.5).

Prior to geoid computation, the GGM is required as a reference model in the RCR procedures. Hence, the selection of the ideal GGMs is crucial to produce a precise marine geoid model. In this study, SGG-UGM-2 (Liang et al., 2020) GGM at SH degree truncated up to d/o 360 has been selected for the geoid computation to recover the long-to-short wavelength component of the gravity signal when modelling the gravimetric marine geoid, since it approximates the gravity field well over Nigeria (see Table 4.14 in section 4.4.2).

The computation of the marine geoid model involves the integration of reference geoid heights from the GGM, residual geoid heights, and the very short wavelength component of geoid heights. This computational task was carried out using the GRAVSOFT package (Forsberg & Tscherning, 2008).

3.3.4: Development of gravimetric geoid model for Nigeria

This section outlines the study's research methodology. The objectives were (1) develop a gravimetric geoid model for Nigeria, (2) fit the gravimetric geoid models with the National vertical datum, and (3) assess the accuracy of the developed gravimetric geoid model for Nigeria. Fig. 3.10 provides an overview of our research methodology.

The RCR procedure, as documented in prior research (Forsberg & Tscherning, 1981; Torge & Muller, 2012), was employed to compute the gravimetric geoid model. Within this procedure, the components of the short and very short wavelengths of the functional of the disturbing potential were derived from a GGM and high-resolution SRTM data (USGS, 2017), respectively. These effects were eliminated from the regional/local terrestrial gravity data during the initial stage, resulting in residual gravity anomalies. Δg_{res} (see Eq. 3.4).

$$\Delta g_{res} = \Delta g_{FA} - \Delta g_{GGM} - \Delta g_{RTM} \tag{3.4}$$

where Δg_{FA} represents the free-air terrestrial gravity anomaly, the long-to-short-wavelength component of the gravity anomaly computed from GGMs is Δg_{GGM} , and Δg_{RTM} is the very short-wavelength contribution of the gravity anomaly induced by local topography.

The determination of the very short-wavelength component of the gravity signal was achieved through the RTM method when employing a free-air gravity anomaly for geoid determination. Conversely, when utilizing the Faye anomalies, this component is omitted. The topographic masses previously underwent condensation and displacement to a geoid-aligned surface layer when computing Faye anomalies.

The resulting gravimetric quasi-geoid heights, N, generated using the RCR procedure are as follows:

$$\zeta = \zeta_{res} + \zeta_{GGM} + \zeta_{RTM} \tag{3.5}$$

where the reference geoid height is determined from the GGM ζ_{GGM} , that is, the short-wavelength component of the geoid height and the very-short-wavelength component of the geoid height ζ_{RTM} .

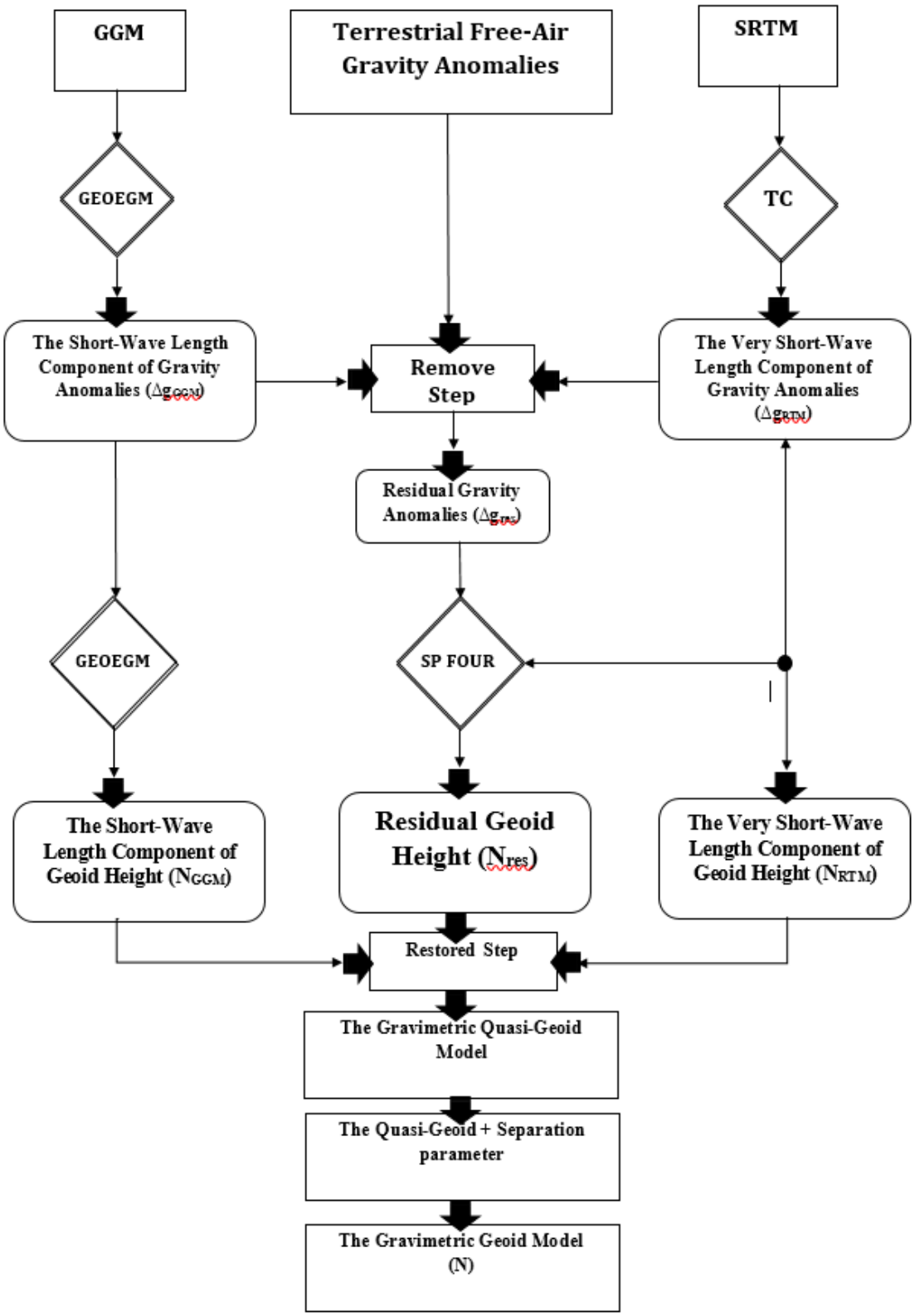

Fig 3.10: Flowchart illustrating computation of the gravimetric geoid model based on free-air gravity anomalies, the GGM and the SRTM.

The residual gravity anomaly is the basis for determining residual geoid height ζ_{res}. The modified Stokes integral was evaluated using the multiband spherical FFT technique (Forsberg & Sideris, 1993), specifically described in Section 2.4.1, and implemented using the GRAVSOFT software program SPFOUR. The computation of the gravimetric quasi- geoid model involves the integration of the reference geoid heights from the GGM, residual geoid heights, and the very short-wavelength component of the geoid heights. The quasi-geoid was converted to a gravimetric geoid using Brun's equation, as presented in Eq (2.64). This computational task was performed using the GRAVSOFT package (Forsberg & Tscherning, 2008).

The schematic representation of the computation steps for deriving the gravimetric geoid model, relying on free-air gravity anomalies, data from the SRTM, and GGM, are delineated as follows:

1. The free-air (FA) gravity anomaly was computed based on the gravity data.
2. Remove the long-to-short-wavelength component obtained from the GGM from the terrestrial free-air anomalies.
3. The short-wavelength component RTM was removed Δg_{RTM} from terrestrial free-air anomalies.
4. Compute the residual gravity anomalies as defined by the Eq (3.4).
5. Compute residual geoid heights using the FFT method ζ_{res}.
6. Restore the height anomalies contribution from the GGM ζ_{GGM}
7. Restore the height anomalies contribution from RTM ζ_{RTM}
8. Compute the gravimetric quasi-geoid height by summing up all the contributions
9. Estimate the gravimetric geoid height *N* as the sum of the quasi-geoid height and the separation parameter.

3.3.4.1: Fitting of the Gravimetric Geoid Models with the National vertical datum

When comparing the gravimetric and fitted geoid models, it is essential to note that the former geoid heights represent a surface that is exclusively associated with gravimetric data, lacks practical utility within the context of the MSL-based vertical reference system, and lacks connections to local or national height networks. In contrast, the fitted geoid model is a gravimetric geoid model adjusted to regional, national, or local levelling networks. The fitted

geoid surface functions as a transformation surface for converting ellipsoidal and physical heights, and is always linked to a specific vertical datum (Forsberg & Tscherning, 2008).

To fit the gravimetric geoid model NG-EGM2024, geoid undulations from 61 stations associated with Nigeria's national local vertical data were employed. A seven-parameter transformation (Fotopoulos, 2003) was implemented to mitigate data biases and enhance the differences between geoid heights derived from this research and those from GNSS/levelling data. The processing was conducted using MATLAB software. The discrepancies between the gravimetric geoid model NG-EGM2024 and the GNSS/levelling geoids were gridded via collocation using the GEOGRID module in GRAVSOFT. The final fitted gravimetric geoid is derived by adding the results obtained from the gridded residuals into the original gravimetric geoid model.

3.3.5: Accuracy assessment of the developed gravimetric geoid model for Nigeria.

The computed fitted gravimetric geoid model, NG-EGM2024, was validated using ten ground-based GNSS/levelling datasets that were not utilized in the fitting process. These discrepancies can be expressed as follows:

$$\Delta N = N_{NG-EGM\,2024} - N_{GNSS/levelling} \tag{3.6}$$

Where $N_{NG-EGM\,2024}$ represents the geoid heights derived from the fitted models, and $N_{GNSS/levelling}$ denotes the GNSS/levelling points. The accuracy assessment will also include comparing geoid heights derived from GGM to GNSS/levelling data at the selected 10 ground-based GNSS/levelling data.

Chapter 4

Results and Analysis

4.1 Introduction

This chapter, which comprises the presentation and analysis of the results, pertains to the fulfilment of research objective one to three. Most of the results shown in this chapter were published in Springer Journal of Studia Geodeatica et Geophysica and Journal of Applied Geodesy.

4.2 Results and Analysis (Objective One): Validating the geoid heights from GGMs using GNSS/levelling data over Nigeria.

4.2.1 Evaluation of GGMs using GNSS/levelling data

In this section, the results based on the method described in section 3.3.1 are presented. Our analysis reveals the importance of spectral consistency considerations for GOCE-based GGMs and fittings of geoid height from GGMs to GNSS/levelling geoid height.

4.2.1.1 Comparison without accounting for spectral consistency

The statistical summaries of the results are detailed in Tables 4.1 and 4.2, and the SD is graphically illustrated in Fig. 4.1. In Table 4.1, the arrangement of GGMs is structured from combined to GOCE-based satellite-only GGMs. As shown in Fig. 4.1, EGM2008 demonstrates the lowest SD, notably up to d/o 160, where GRACE data are incorporated into ITG-GRACE03s solutions (Mayer-Gürr et al., 2010). Beyond d/o 160, GOCE-based GGMs (DIR_R6, SPW_R5, and TIM_R6) provided valuable insights, particularly beyond d/o 200, in accordance with the spatial resolution objectives of the GOCE mission (Drinkwater et al., 2003). However, high-resolution GGMs performed better than the satellite-only model in terms of geoid height, specifically at medium wavelengths. The XGM2019e_2159 GGM provided the least SD of geoid heights of approximately 0.343 m at SH d/o 300, the improvement of XGM2019e_2159 over other GGMs at SH d/o 300 is due to the inclusion of satellite model GOCO06s in the longer wavelengths range up to d/o 300 combined with a ground gravity data in its computation (Zingerle et al., 2020).

GOCO05C, GECO, EIGEN-6C4, and SGG-UGM-2 at the same SH d/o 300 showed SD with geoid heights difference of approximately 0.353, 0.370, 0.395, and 0.413 m, respectively (see Table 3). At d/o 360, GOCO05C (Fecher et al., 2015) provided the lowest SD of geoid heights

of approximately 0.340 when compared to all evaluated GGMs. However, XGM2019e_2159 provided the least mean offset at the same 360 SH d/o compared with all evaluated GGMs.

Table 4.1: Statistical results of the differences between the observed GNSS/levelling and GOCE/GRACE and combined GGMs at 90 GNSS/levelling benchmarks (units are in meters).

Models	Max deg	Min	Max	Mean	SD
SGG-UGM-2	2190	0.041	1.623	0.831	0.432
XGM2019e_2159	2190	0.044	1.606	0.758	0.354
GECO	2190	−0.001	1.614	0.844	0.382
EIGEN-6C4	2190	0.027	1.723	0.874	0.416
EGM2008	2190	0.088	1.747	0.856	0.465
GOCO05C	720	−0.037	1.626	0.760	0.335
DIR_R6	300	0.126	1.920	0.879	0.369
SPW_R5	330	0.094	1.962	0.919	0.370
TIM_R6	300	0.078	1.939	0.925	0.369

Table 4.2: Statistics of differences between the GNSS/levelling and GOCE/GRACE and Combined GGMs at d/o 280, 300 and 360

d/o	**280**		**300**		**360**	
Combined GGMs	**Mean**	**SD**	**Mean**	**SD**	**Mean**	**SD**
SGG-UGM-2	0.886	0.411	0.872	0.413	0.810	0.462
XGM2019e_2159	0.807	0.349	0.782	0.343	0.731	0.371
GECO	0.897	0.373	0.882	0.370	0.824	0.406
EIGEN-6C4	0.921	0.401	0.910	0.395	0.855	0.438
EGM2008	0.909	0.449	0.896	0.449	0.836	0.493
GOCO05C	0.799	0.343	0.775	0.353	0.742	0.340
DIR_R6	0.870	0.362	0.879	0.369	-	-
SPW_R5	0.909	0.370	0.919	0.370	-	-
TIM_R6	0.828	0.362	0.925	0.369	-	-

Both the XGM2019e_2159 and GOCO05C models used DTU13GRA (Andersen et al., 2013) satellite altimetry data over the seas.

Furthermore, similar performances were provided regarding the SD of the geoid heights for all nine evaluated GGMs at their respective maximum SH degrees, as illustrated in Table. 4.1, the XGM2019e_2159 model (Zingerle et al., 2020) demonstrated the lowest SD of 0.354 m at SH d/o 2190 compared with all combined GGMs (GECO, EIGEN-6C4, SGG-UGM-2, and EGM2008). The GOCO05C model (illustrated by the yellow line) displayed the lowest SD among the nine evaluated models, with an SD of 0.335 m at its maximum SH d/o 720. The evaluation of GOCE-based GGMs such as DIR_R6, SPW_R5, and TIM_R6 against GNSS/levelling data showed that the SD of DIR_R6, SPW_R5, and TIM_R6 increased rapidly for all GOCE-based satellite-only GGMs solutions from d/o 150 onward because noise started

to dominate the GOCE signals. Hence, the TIM_R6 model exhibited better performance in terms of mean offset and SD with respect to the DIR_R6 and SPW_R5 GGMs at SH d/o 280.

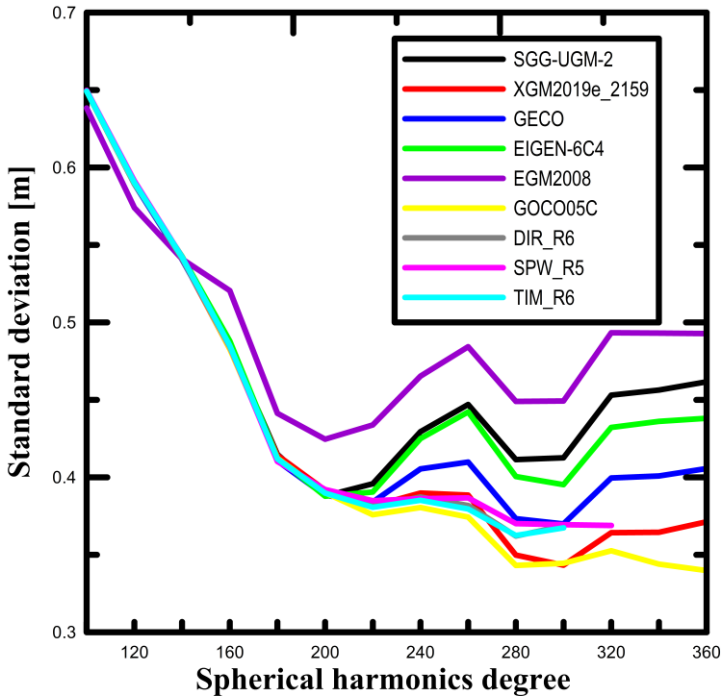

Fig. 4.1: Standard deviation of geoid height differences in meters obtained from GGMs and the corresponding ones from GNSS/levelling data over Nigeria territory.

However, when evaluated at their respective maximum SH degrees, the lowest SD was attained from the sixth-release GOCE-based GGMs of the DIR_R6 models at SH d/o 300, with mean offsets and SD of 0.879 m and 0.369 m, respectively. This was due to the inclusion of GRACE data in the computation of DIR_R6 (Bruinsma et al., 2014).

Finally, from Fig. 4.1, we can conclude that the SD of each model decreased when the SH degree increased. This is expected, because the higher the SH degree, the more accurately the model describes the gravitational field.

Residual point maps (that is, the results of Eq. 3.1) were used for the comparative evaluation of the investigated GGMs, as shown in Fig. 4.2, which indicate the occurrence and magnitude of the differences in the geoid heights. In Fig. 4.3 box plots are used for a graphical representation of the residuals. Visual analysis of the geoid heights via residual point maps revealed superior fitting in the southern region compared to the northern region of Nigeria. This distinction is likely attributable to the differences in topographic characteristics of each region. The XGM2019e_2159 (Zingerle et al., 2020) and DIR_R6 models (Bruinsma et al.,

2014) demonstrated a better fit over Nigeria than the other evaluated combined GGMs and GOCE-based GGMs.

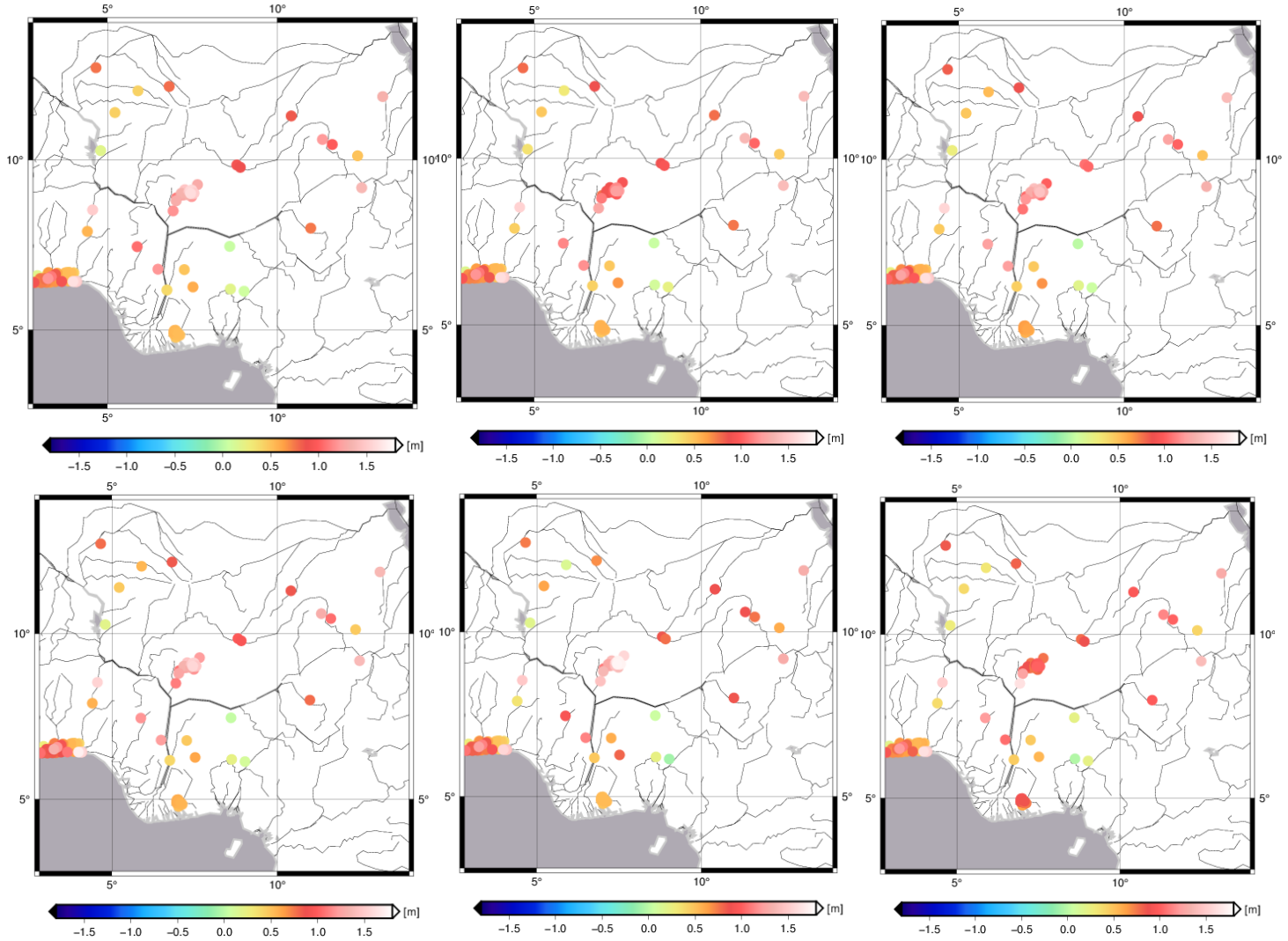

Fig. 4.2a: Residual maps between point-wise GNSS/levelling-derived geoid heights and those resulting from Combined GGMs, SGG-UGM-2 at d/o 2190 (top left); XGM2019e at d/o 2190 (top-middle); GECO at d/o 2190 (top right); EIGEN-6C4 at d/o 2190 (bottom-left); EGM2008 at d/o 2190 (bottom-middle); GOCO05c at d/o 720 (bottom left).

4.2.1.2 Comparison with Accounts of Spectral Consistency

The statistical results of the SEM are presented in Table 4.3 for the GOCE-based GGMs (DIR_R6, SPW_R5, and TIM_R6) at SH d/o of 180, 220, and 260 using Eq. (3.3). The SD values are shown in Fig. 4.5. Upon examination of Fig. 4.5 and Table 4.3, it is apparent that the smallest SD differences were observed in the sixth release of TIM_R6 (Brockmann et al., 2021) GOCE-based GGMs at SH d/o 260 when compared with DIR_R6 and TIM_R6 GGMs.

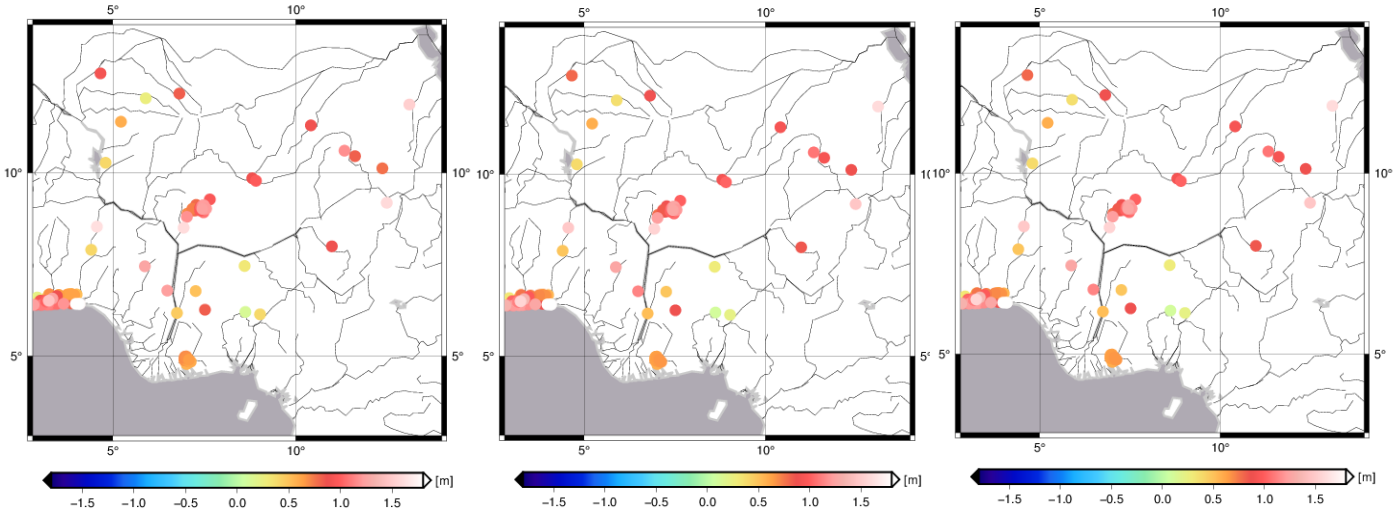

Fig. 4.2b: Residual maps between point-wise GNSS/levelling-derived geoid heights and those resulting from GOCE-based GGMs, DIR_R6 at d/o 300 (left); SPW_R5 at d/o 330 (middle); TIM_R6 at d/o 300 (right).

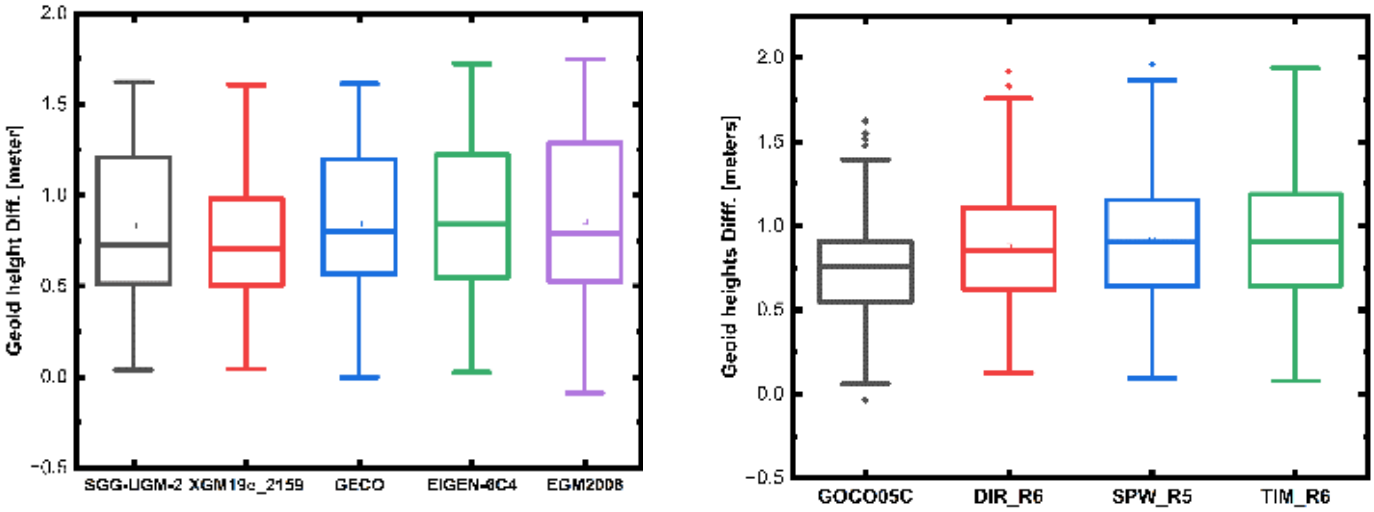

Fig. 4.3: Box plot of differences between GNSS/levelling-derived geoid heights and the corresponding ones from Combined GGMs at d/o 2190 (left) and GOCE/GRACE GGMs at their maximum d/o (right).

Table 4.3: Statistics of differences between the GNSS/levelling and GOCE-based GGMs at d/o 180, 220 and 260

d/o	180		220		260	
Models	**Mean**	**SD**	**Mean**	**SD**	**Mean**	**SD**
DIR_R6	0.803	0.349	0.809	0.358	0.858	0.346
SPW_R5	0.810	0.348	0.822	0.360	0.892	0.352
TIM_R6	0.768	0.351	0.769	0.358	0.809	0.342

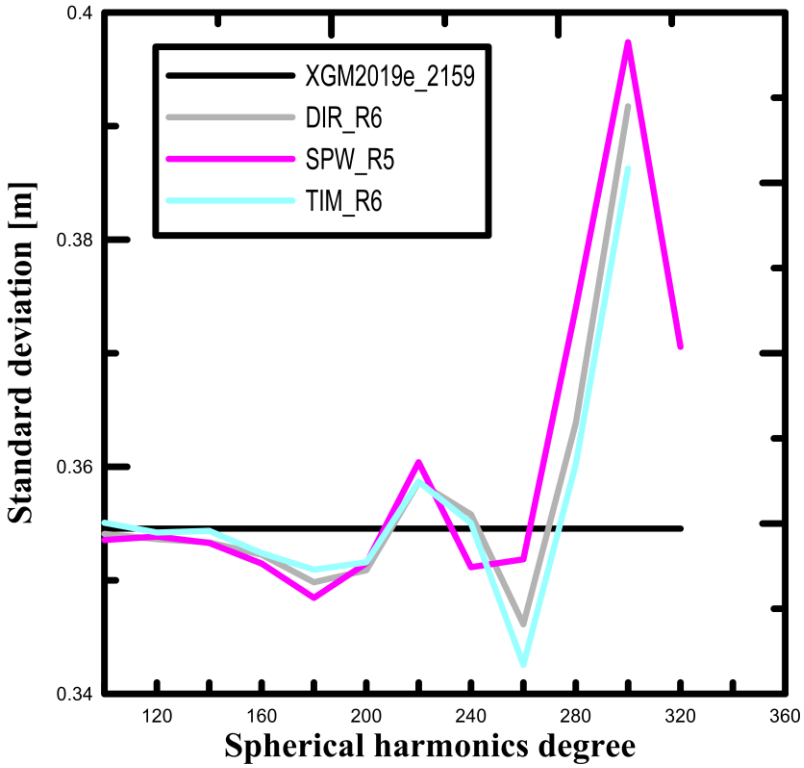

Fig. 4.4: Standard deviation of the differences between the GNSS/levelling and GOCE-based GGMs extended by XGM2019e_2159 and RTM as a function of the d/o spherical harmonics (after full application of the SEM principle).

However, it is worth noting that all the evaluated GOCE-based GGMs, such as DIR_R6, SPW_R5, and TIM_R6, exhibited similar behavior in the long-to-medium wavelength range from SH d/o 100-180, except for the SPW_R5 model (Gatti et al., 2016). The SPW_R5 model demonstrated the least SD differences in almost all the selected spectral contents from d/o 100 to 180, with an SD of 0.348 m at d/o 180, as illustrated in Table 4.3.

The implementation of SEM allows a more balanced comparison between GOCE-based GGMs (DIR_R6, SPW_R5, and TIM_R6) and GNSS/levelling data because the effect of the omitted short-wavelength gravity signals is mitigated in the comparison. Notably, a reduction of approximately 46.2% in the SD of geoid height differences is observed, from a SD of approximately 0.65 m to 0.35 m at SH d/o 100 for all models, after compensating for the medium/short and very short wavelength gravity signals using SEM (see Fig. 4.1 and Fig. 4.4 before and after SEM, respectively). The SEM is truncated at SH d/o 320 because DIR_R6 and TIM_R6 have a maximum SH d/o of 300, whereas SPW_R5 has a maximum SH d/o of 330 (see Fig. 4.4 and Table 4.3).

Among the three evaluated GOCE-based GGMs (DIR_R6, SPW_R5, and TIM_R6), the TIM_R6 model exhibited the least difference in SD at SH d/o 260 (0.342 m), representing a reduction of approximately 10% in the SD. Hence, TIM_R6 (Brockmann et al., 2021) appears

to be the most suitable GOCE-based GGM for estimating geoid heights across Nigeria at SH d/o 260 when compared with DIR_R6 and SPW_R5 at the same SH d/o.

4.2.2 Fitting of Geoid heights from GGMs to GNSS/levelling Geoid heights

Following the implementation of the aforementioned parametric correction models (Section 3.3.1.2) and the subsequent removal/mitigation of systematic errors (Bako et al., 2024), an improvement in the SD across all models was observed, as detailed in Table 4.5 Upon comparison of the employed parametric models, the seven-parameter model consistently yielded smaller SDs for all GGMs when compared to other parametric correction models. Thus, it was employed for the ranking of GGM performance with respect to geoid heights. In the overall assessment, XGM2019e_2159 (Zingerle et al., 2020) demonstrated an improvement compared to the other eight evaluated GGMs, with a SD of 0.30 m, representing a 15.3% improvement. However, GOCO05C (Fecher et al., 2015) exhibited an improved performance when employing the four-parameter model. The large SD values of 0.30 m obtained can be attributed to the parametric inconsistencies in the Nigeria height system. The histograms of the differences between the GGMs and GNSS/levelling derived geoid height before and after applying the SEM and fitting using the 7-parametric model are shown in Fig. 4.5. Table 4.4 illustrates the SD of the differences between the GNSS/levelling-derived geoid heights and the nine investigated GGMs extended by XGM2019e_2159 and RTM using various parametric correction models.

Table 4.4: Statistics of differences between the GNSS/levelling and GGMs extended by XGM2019e_2159 and RTM using different parametric models (units are in meters).

Models	***N*max**	**Parametric Model (No. of parameters)**			
		Linear	4	5	7
SGG-UGM-2	$2190 + RTM$	0.394	0.367	0.347	0.324
XGM2019e_2159	$2190 + RTM$	0.332	0.327	0.315	0.300
GECO	$2190 + RTM$	0.357	0.343	0.331	0.309
EIGEN-6C4	$2190 + RTM$	0.387	0.368	0.348	0.325
EGM2008	$2190 + RTM$	0.434	0.397	0.372	0.352
GOCO05C	$720 + XGM2019e\_2159_{721}^{2190} + RTM$	0.326	0.326	0.324	0.314
DIR_R6	$300 + XGM2019e\_2159_{301}^{2190} + RTM$	0.366	0.365	0.331	0.318
SPW_R5	$330 + XGM2019e\_2159_{331}^{2190} + RTM$	0.368	0.367	0.325	0.304
TIM_R6	$300 + XGM2019e\_2159_{301}^{2190} + RTM$	0.363	0.362	0.330	0.318

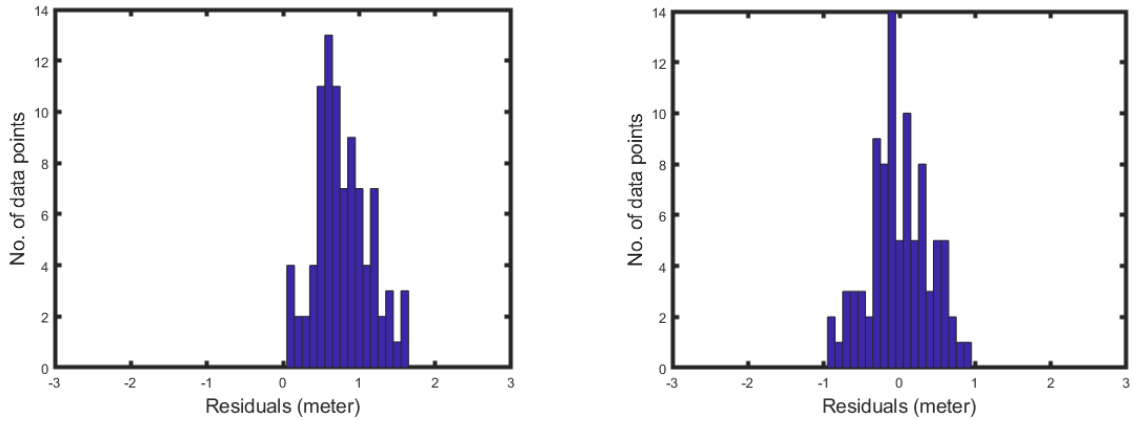

Fig. 4.5: Histograms of geoid height changes in meters between GGMs and GNSS/levelling data before eliminating the mean values (left) and after eliminating the mean values (right) using the 7-parameter transformation model.

4.3 Results and Analysis (Objective two): Evaluation of the recent high-degree combined global gravity-field models for geoid modelling over Nigeria.

4.3.1 Evaluation of gravity anomalies from GGMs using terrestrial gravity data over Nigeria

The statistical analysis, including minimum, maximum, SD, for the disparities between terrestrial gravity anomalies (both free-air and bouguer) and GGM-derived gravity anomalies, is presented in Tables 4.5 and 4.6.

Table 4.5: Statistics of the differences between the terrestrial gravity anomaly (free-air anomaly) and the gravity anomaly computed by GGMs at SH d/o 2190 (units are in mGal).

GGM	Minimum	Maximum	Mean	SD
SGG-UGM-2	−22.65	22.75	−0.61	6.92
XGM2019e	−22.64	22.76	−1.03	6.86
GECO	−23.42	22.83	−0.84	7.32
EIGEN-6C4	−22.22	25.57	−0.77	7.49
EGM2008	−21.85	24.43	−0.58	7.19

Table 4.6: Statistics of the differences between the terrestrial gravity anomaly (bouguer anomaly) and the gravity anomaly computed by GGMs at SH d/o 2190 (units are in mGal).

GGM	Minimum	Maximum	Mean	SD
SGG-UGM-2	−19.95	17.16	−0.58	6.26
XGM2019e	−17.81	17.18	−0.91	6.24
GECO	−19.82	18.25	−0.89	6.43
EIGEN-6C4	−19.49	18.59	−0.66	6.37
EGM2008	−19.95	17.60	−0.44	6.28

Tables 4.5 and 4.6, along with Fig. 4.6, illustrates the differences between terrestrial gravity data (both free-air and bouguer) and the gravity anomalies computed by the SGG-UGM-2,

XGM2019e_2159, GECO, EIGEN-6C4, and EGM2008 gravity field models, especially within the spectral range of d/o 720 to 2190. This phenomenon could be attributed to topographical variations in the study area.

The SD values in Table 4.5 indicate that, from d/o 300 to 359, all the assessed GGMs provide nearly equivalent results. However, XGM2019e_2159 slightly outperforms SGG-UGM-2 from degree 360 to 2190, followed by, EGM2008, GECO, and EIGEN-6C4 in sequential order. Among the evaluated GGMs, SGG-UGM-2 exhibits the least mean offset.

Likewise, in Table 4.6, the evaluation of bouguer anomalies reveals that XGM2019e_2159 performs marginally better than SGG-UGM-2, followed by EGM2008, GECO, and EIGEN-6C4, in that respective order. The assessment of gravity anomaly residuals indicates an SD ranging from 6.86 mGal to 7.49 mGal for the free-air gravity anomaly residual and 6.24 mGal to 6.43 mGal for the bouguer gravity anomaly residual.

Upon analyzing the results in Fig. 4.6, the free-air and bouguer gravity anomaly residuals reveal that XGM2019e_2159 (indicated by the orange-coloured line) consistently exhibits the lowest RMS. In the context of free-air gravity anomalies, the RMS values for the GGMs follow a descending order: XGM2019e_2159, SGG-UGM-2, EGM2008, EIGEN-6C4, and GECO, in that sequence. Similarly, for bouguer gravity anomaly residuals, XGM2019e_2159 again provides the smallest RMS, with the remaining models following a decreasing sequence: XGM2019e_2159, SGG-UGM-2, EGM2008, GECO and EIGEN-6C4,

The statistical summaries detailed in Table 4.5 further affirm that the more recently developed GGMs tend to exhibit better agreement with ground-based gravity measurements, especially when considering topographic and bouguer corrections. However, it is worth noting that EIGEN-6C4 performs slightly below the other models. Additionally, the SDs of bouguer gravity anomaly residuals in Table 4.6 are comparatively smaller than the SDs of free-air gravity anomaly residuals (as shown in Table 4.6 and Fig 4.6). This difference can be attributed to the anticipated smoother nature of bouguer gravity anomalies compared to free-air gravity anomalies. Comparing these five global gravity field models regarding SD values, XGM2019e_2159 is the most accurate model among the four evaluated in the study area.

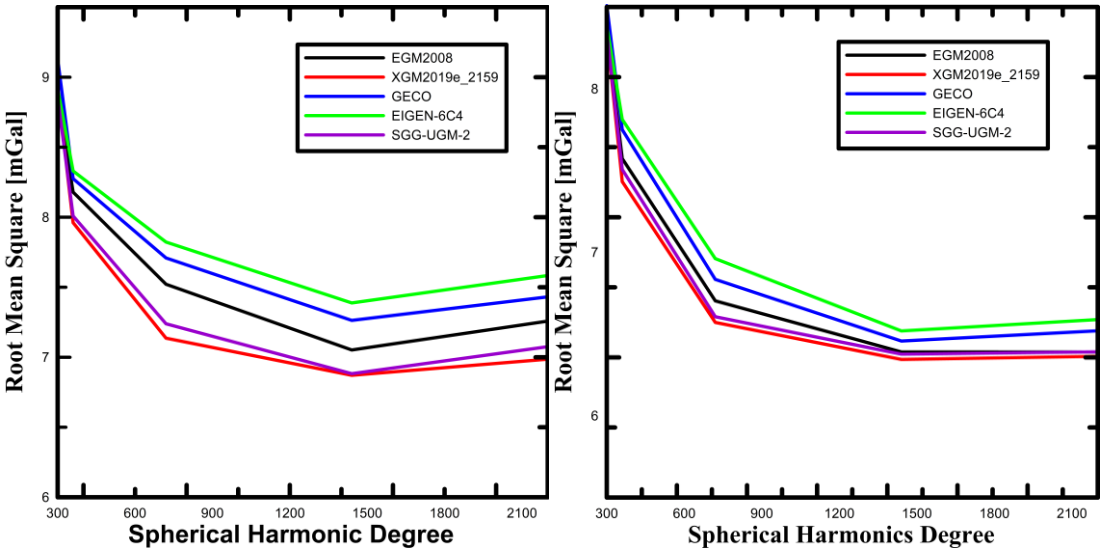

Fig 4.6: Differences between observed free-air gravity anomalies and GGM gravity anomalies (Left) Bouguer gravity anomalies and GGM gravity anomalies (right) in terms of RMS over Nigeria.

Table 4.7: Results obtained by other researchers

S/N	Country	Functionals	SD (mGal)	Researchers
1	Kenya	Gravity Anomalies	6.89	Nyoka et al., 2022
2	Turkey	Gravity Anomalies	8.05	Yilmaz et al., 2018
3	Kenya	Gravity Anomalies	10.3	Odera, 2020

It is worth noting that GECO and EGM2008 demonstrate nearly identical magnitudes, potentially attributed to their shared utilization of ground and altimetry data (as mentioned by Gilardoni et al. 2016) as reflected in the RMSE of GGM-derived gravity anomalies in relation to terrestrial gravity data (as illustrated in Figs. 4.6), the evaluation outcomes align with findings from diverse regions of similar characteristics, as presented in Table 4.7. These results regarding SD differences in GGM-computed gravity anomalies can be partially attributed to the various corrections applied to the observed terrestrial gravity data before comparing them with GGMs and the implementation of cross-validation techniques to remove gross errors and outliers.

4.3.2 Evaluation of flat regions differently from regions of significant topography

The statistical analysis comparing the terrestrial free-air gravity anomaly with the gravity anomaly computed by GGMs is presented in Table 4.8. Additionally, Fig 4.7 depicts residual box plots illustrating the disparities between observed free-air gravity anomalies and GGM-

derived anomalies in various regions of Nigeria: (a) flat region, (b) region characterized by significant topography, (c) northern region, and (d) southern region.

Table 4.8: Differences between terrestrial free-air gravity anomaly and GGMs over the different regions of Nigeria, unit: mGal.

Area/Data points	GGMs	Min.	Max.	Mean	SD
Flat areas	SGG-UGM-2	−12.68	13.04	0.17	4.70
	XGM2019e	−12.95	11.45	−0.79	4.96
	GECO	−14.44	13.50	−0.37	5.61
	EIGEN-6C4	−12.89	13.70	0.16	4.99
	EGM2008	−13.04	14.25	0.77	4.95
Region of Significant Topography	SGG-UGM-2	−6.36	14.38	2.49	5.76
	XGM2019e	−9.95	7.60	1.48	4.89
	GECO	−10.68	12.88	1.82	7.07
	EIGEN-6C4	−7.24	15.97	2.87	6.54
	EGM2008	−10.92	7.19	−1.54	4.91
Northern region	SGG-UGM-2	−12.93	13.76	−0.36	5.03
	XGM2019e	−15.47	13.59	−1.06	5.51
	GECO	−15.05	14.58	−0.58	5.59
	EIGEN-6C4	−15.40	13.70	−0.46	5.29
	EGM2008	−13.63	15.25	−0.08	5.46
Southern region	SGG-UGM-2	−21.09	21.90	−1.20	10.07
	XGM2019e	−20.90	18.27	−1.28	9.13
	GECO	−20.65	24.27	−1.48	10.04
	EIGEN-6C4	−20.95	22.55	−1.54	10.40
	EGM2008	−21.57	19.84	−1.64	9.15

The assessment of free-air gravity anomalies across the flat terrain of Nigeria reveals that when comparing five GGMs (SGG-UGM-2, XGM2019e, GECO, EIGEN-6C4, and EGM2008) with terrestrial gravity anomalies based on SD, SGG-UGM-2 demonstrates a slight advantage in the flat region. It exhibits the lowest mean offsets and SD values, measuring 0.17 and 4.70 mGal, respectively. Following SGG-UGM-2, the sequence in performance is XGM2019e_2159, EGM2008, and EIGEN-6C4. Notably, the more recent models generally exhibit improved performance, except for the GECO model, which performs less favorably. The evaluation results for the region with significant topography indicate that XGM2019e_2159 demonstrates the highest precision, with an SD of 4.89 mGal, followed by EGM2008, SGG-UGM-2, and EIGEN-6C4 (in that order). At the same time, the GECO model performs less favorably. In the Northern region, SGG-UGM-2 outperforms other GGMs, with a precision of 5.03 mGal, followed by EIGEN-6C4, EGM2008, XGM2019e_2159, and GECO (in that order).

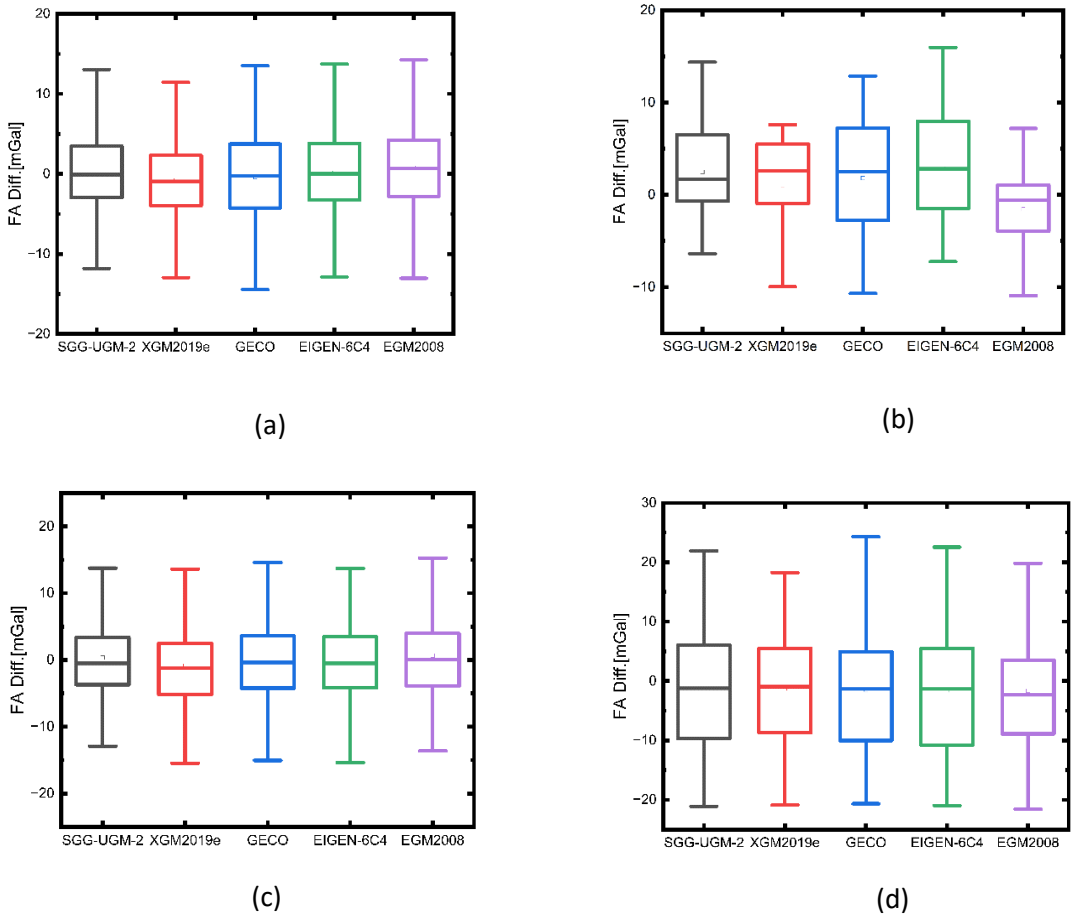

Fig 4.7: Residual box plot between observed free-air gravity anomalies and GGMs over Nigeria's (a) Flat region, (b) Region of significant topography, (c)Northern region, (d) Southern region.

However, in the Southern region, XGM2019e_2159 performs better than other GGMs, followed by EGM2008, GECO, SGG-UGM-2, and EIGEN-6C4 (in that order). It is worth noting that the GGMs exhibit relatively lower accuracy in the Southern region compared to the Northern region, as evident in the SD values across all investigated GGMs (refer to Table 4.8 and Fig 4.7). Considering the overall performance in all evaluation areas, XGM2019e_2159 and SGG-UGM-2 are considered the most suitable choices for geoid modelling in Nigeria.

4.3.3 An independent check conducted using GPS/levelling data over Abuja

In this section, geoid heights over FCT-Abuja, Nigeria, were compared to 20 GNSS/levelling points data, specifically over a small area, as an independent validation, building upon the results obtained from the evaluation of gravity anomalies (refer to sections 4.2.1 and 4.2.2). This comparative analysis was conducted both with and without considering spectral consistency (outlined in section 3.3.1.1).

The findings reveal that the application of the RTM reduction and a parametric correction model played a crucial role in assessing the quality of GGMs and ensuring a more coherent comparison, resulting in improved statistical outcomes. Notably, a 20% improvement in the SD of geoid heights was observed for XGM2019e_2159 at 2190 SH degree, measuring approximately 0.15 m (see Table 4.9) when spectral consistency was not considered. In contrast, after implementing the five-parametric correction model and RTM reduction (see Table 4.10 and Fig 4.8), the SD reduced to 0.12 m, signifying an improved performance.

Table 4.9. Statistics of comparison without RTM reductions and removing a parametric correction model using different GGM solutions as a function of maximum spherical degrees. N = GNSS/levelling geoid height. Units: meter

Comparison	Max. degree	Min	Max	Mean	SD
N- SGG-UGM-2	2190	1.107	1.604	1.286	0.1579
N- XGM2019e	2190	0.773	1.279	0.954	0.1490
N- GECO	2190	0.977	1.446	1.161	0.1494
N- EIGEN-6C4	2190	1.084	1.575	1.259	0.1595
N- EGM2008	2190	1.092	1.749	1.383	0.1964

Table 4.10 Statistics of RTM reductions and removing a parametric correction model using different GGM/RTM solutions as a function of maximum spherical degrees. N = GNSS/levelling geoid height.

Comparison	Max. degree	Min (meter)	Max (meter)	Mean (meter)	SD (meter)
N- (SGG-UGM-2+RTM)	2190	−0.264	0.192	0.000	0.128
N- (XGM2019e+RTM)	2190	−0.271	0.187	0.000	0.119
N- (GECO+RTM)	2190	−0.268	0.185	0.000	0.123
N- (EIGEN-6C4+RTM)	2190	−0.265	0.190	0.000	0.126
N- (EGM2008+RTM)	2190	−0.258	0.199	0.000	0.134

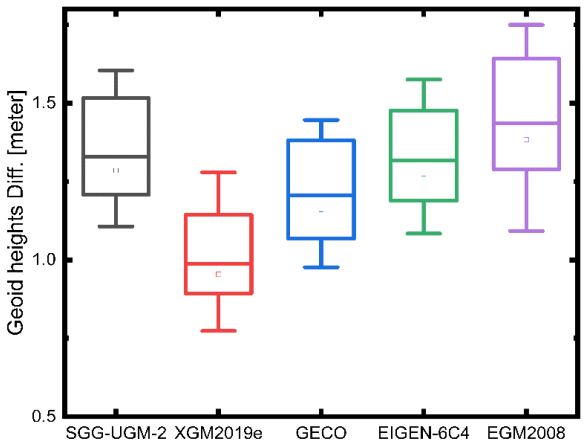

Fig 4.8: Residual box plot between GNSS/levelling-derived geoid heights and the corresponding heights from GGMs

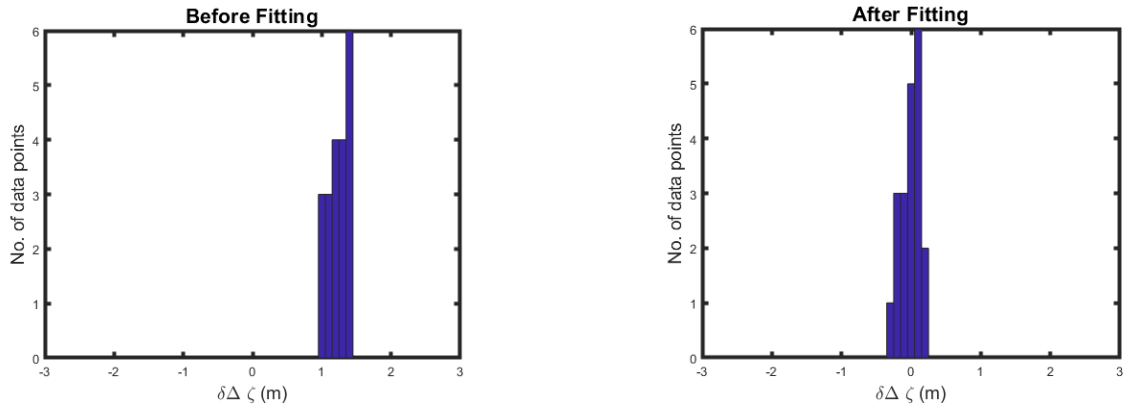

Fig 4.9: Histogram plots of geoid height changes in meters between GGMs and GNSS/levelling data before eliminating the mean values (left) and after eliminating the mean values (right) using the 5-parameter transformation model.

The comparative evaluation of the five combined models (SGG-UGM-2, XGM2019e, GECO, EIGEN-6C4, and EGM2008) used residual box plots (see Fig 4.8) to assess the magnitude and occurrence of differences in geoid height. The visual analysis of the residual maps pertaining to geoid heights indicates that XGM2019e_2159 exhibits a superior fit in the region compared to the other GGMs. These findings underscore the promising potential for the development of a precise gravimetric geoid model over Nigeria through the integration of local terrestrial gravity data, shipborne gravity, and satellite altimetry-derived gravity datasets within a remove-compute-restore framework, with a particular emphasis on employing XGM2019e_2159.

4.4 Evaluation and homogenization of a marine gravity database from shipborne and satellite altimetry-derived gravity data over the coastal region of Nigeria

4.4.1 Accuracy assessment of shipborne and altimetry-derived gravity data

In this section, the results based on the method described in section 3.3.3 were presented. Our analysis revealed that after the residual linear drifts inherent within the shipborne gravity dataset using crossover adjustment for each leg of the surveys were addressed, survey 1 demonstrated a noticeable drift of -0.185 mGal/day. Likewise, Surveys 2, 3, 4, and 5 exhibited drift behaviors, with drift rates recorded as -0.0082, -0.020, -0.028, and 0.070 mGal/day, respectively (see Fig. 4.10). The statistical results of the differences between each survey leg and altimetry-derived gravity data from the DTU21GRA (Andersen and Knudsen, 2021) and SSv29.1 (Sandwell et al., 2021) models before and after addressing the residual linear drift and data editing are listed in Tables 4.11 and 4.12, respectively. The use of XO adjustment to address linear drift and data editing resulted in subsequent elimination of linear drift, systematic errors (mean offset), and gross errors in each leg of the survey.

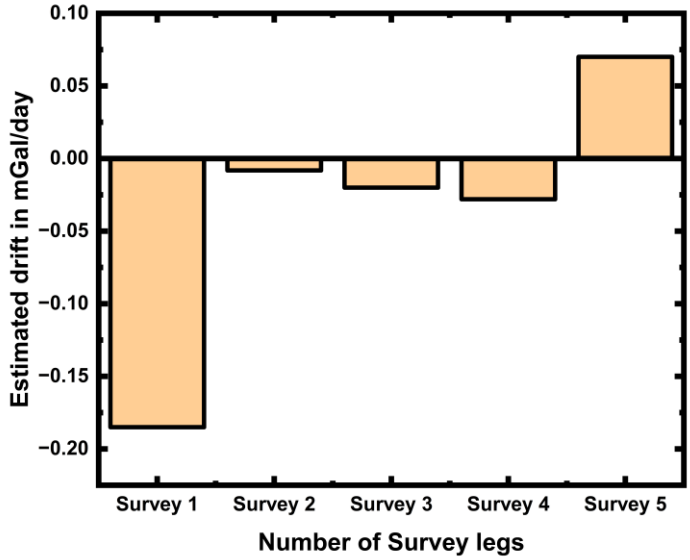

Fig 4.10: Bar chart of estimated drift rate in mGal/day for each survey legs

The mean offsets identified in Surveys 1, 3, and 5, initially measured at 14.16, 18.29, and 13.56 mGal for both altimetry gravity models (Table 4.10), have been eliminated (Table 4.12).

Table 4.11: Preliminary shipborne gravity data evaluated with DTU21GRA and SSv29.1 gravity model before applying all the corrections; Units [mGal].

Gravity model	Survey no	No of data	Min.	Max.	Mean	SD	RMS
	1	306	3.75	27.84	14.16	3.54	14.59
DTU21GRA	2	382	−6.27	5.50	−1.54	1.89	2.44
	3	688	5.94	25.76	18.29	2.61	18.48
	4	249	−5.79	10.89	2.33	3.001	3.79
	5	837	−37.09	43.13	13.563	10.49	17.14
	1	308	3.47	28.75	13.92	3.64	14.39
	2	382	−9.57	5.59	−1.51	2.07	2.56
	3	688	8.72	27.70	18.54	2.77	18.74
SSv29.1	4	249	−6.27	14.83	4.40	3.67	5.72
	5	837	−38.69	41.53	13.33	10.43	16.92

The large offsets observed in surveys 1, 3, and 5 may be attributed to incorrect ties to the land gravity datum or to different land gravity datum (Wessel & Watts, 1988).

This removal of the mean offset led to a reduction in the RMS values across all surveys (Table 4.12). Notably, the RMS values for Surveys 1, 3, and 5, which were originally around 14.59 mGal, 18.48 mGal, and 17.14 mGal for both models, have dropped to approximately 2.78 mGal, 2.32 mGal, and 4.67 mGal, respectively.

Table 4.12: Shipborne gravity data evaluated with DTU21GRA and SSv29.1 gravity model after all the corrections were applied; Units [mGal].

Gravity model	Survey no	No of Outlier	No remaining data	Min.	Max.	Mean	SD	RMS
	1	65	241	−6.71	8.80	−0.00	2.79	2.78
DTU21GRA	2	30	352	−6.60	4.51	−0.00	1.79	1.78
	3	31	657	−7.09	6.95	0.00	2.37	2.37
	4	10	239	−6.07	6.50	0.00	2.47	2.47
	5	222	615	−9.84	9.71	1.58	4.40	4.67
	1	65	241	−7.03	9.09	0.19	2.90	2.91
	2	30	352	−6.69	4.85	0.02	1.84	1.85
	3	31	656	−9.03	8.13	−0.27	2.69	2.70
SSv29.1	4	10	239	−9.94	4.94	−2.09	2.79	3.48
	5	222	615	−11.2	11.56	−1.83	4.32	4.68

These findings demonstrate that by addressing linear drift using XO adjustment and data editing, even a fifty-year old shipborne dataset can be corrected to attain accuracy within a few mGal, rendering it suitable for combination with modern satellite data. Through this process, 358 shipborne gravity measurement points were eliminated from five survey legs. The remaining shipborne gravity dataset after removing the outliers, consisting of 2104 points, demonstrates a mean and SD of −2.33, and 27.81 mGal, respectively. Consequently, all marine ship surveys are deemed acceptable and can be used for the next stage of refinement of shipborne gravity data using XV techniques. Seventy-eight (78) shipborne gravity points with residual values greater than twice the SD were identified as gross errors, and outliers were removed after the XV method was applied. Following the XV procedure, 2026 refined shipborne gravity data remain. Table 4.13 summarizes the statistical analyses conducted on the shipborne gravity data.

Table 4.13: Statistics of the shipborne gravity data before and after removing the gross errors and outliers; unit [mGal]

Data type	No. of Values	Min	Max	Mean	SD
Before cross-validation	2104	−68.92	62.47	−2.33	27.81
Residuals	2104	−17.38	11.19	−0.02	0.98
After cross-validation	2026	−68.91	60.99	−2.86	27.79
Residuals	2026	−13.63	8.75	−0.01	0.78

4.4.2 Comparison of refined shipborne with predicted gravity models

The evaluation results for the refined shipborne and gravity models are listed in Table 4.14. Among the gravity models, the DTU21GRA (Andersen and Knudsen, 2021) gravity model demonstrated better agreement in fitting the shipborne gravity data, with the least SD and RMS

differences of 3.14 and 3.17 mGal, respectively. On the other hand, the EIGEN-6C4 (Förste et al., 2014) model produced the largest SD and RMS values of 4.50 and 4.51 mGal, respectively. The findings of this study highlight the consistency of altimetry-derived gravity data with existing refined shipborne gravity data in the coastal region of Nigeria, which is attributed to the use of new satellite data and advanced data processing techniques. Compared with other models, we found that DTU21GRA (Andersen and Knudsen, 2021) outperformed the other models in the same region when compared with shipborne data.

Table 4.14: The differences between the refined shipborne dataset and the gravity models.

Gravity model	Degree/ Resolution	Type	No of data	Min	Max	Mean	SD	RMS
DTU21	1 minute	Altimetry	2026	−9.84	9.71	0.43	3.14	3.17
SSv29.1	1 minute	Altmetrey	2026	−11.20	11.56	0.22	3.39	3.39
SGG-UGM-2	2190	GGM	2026	−12.11	12.56	−0.04	3.69	3.69
XGM2019e_2159	2190	GGM	2026	−19.61	15.20	0.17	4.24	4.35
GECO	2190	GGM	2026	−20.43	11.91	−0.09	4.25	4.25
EIGEN-6C4	2190	GGM	2026	−14.82	12.98	−0.29	4.50	4.51
EGM2008	2190	GGM	2026	−18.22	12.12	−0.13	4.14	4.14

Consequently, DTU21GRA (Andersen and Knudsen, 2021) was chosen as the preferred altimetry-derived gravity model for further integration with refined shipborne gravity data for two reasons: the low SD value of 3.14, and the algorithm used to obtain gravity data from altimetric observations, that is, sea surface height (SSH). The DTU21GRA (Andersen and Knudsen, 2021) is the only gravity model that integrates Sentinel-3A/B SAR altimeter measurements in the coastal region of Nigeria. Abdallah et al. (2022) obtained similar findings in the Red Sea when they compared shipborne gravity data with satellite altimetry-derived gravity data (DTU21GRA and SS v29.1). Their analysis revealed that the DTU21GRA model outperformed the SS v29.1 model, with SD and RMS values of 7.37 mGal and 8.73 mGal, respectively. In this study, when we compared our results with the results of Abdallah et al. (2022), our results showed an improvement of approximately 57.4% in term of SD, which is attributed to the processing strategy applied to the shipborne gravity data in our research.

4.4.3 Integrating the refined shipborne with DTU21GRA gravity data

In this section, the results based on the method described in section 3.3.3 were presented. The refined shipborne data were integrated into the DTU21GRA (Andersen and Knudsen, 2021) marine gravity anomaly grid by using the LSC technique. This analysis utilized 1926 records obtained by excluding 78 outliers identified through XV procedures and 100 points reserved for validation from the original dataset of 2104 refined shipborne gravity (Table 4.13 and Fig

4.12). The statistical results of these data before and after the integration process reflect an improvement gained by employing the LSC, as shown in Table 4.15. Where the SD dropped from 30.83 mGal to 26.84 mGal.

Table 4.15: Marine surface gravity data before and after applying LSC; units [mGal]

Marine Gravity data	No data points	**Min**	**Max**	**Mean**	**SD**
DTU21GRA gravity	3371	−104.07	151.66	−3.20	30.83
Shipborne gravity	1926	−68.92	60.99	−2.89	27.72
Combine dataset	1 min	−114.82	152.3	−1.96	26.84

The free-air gravity anomalies from the DTU21GRA (Andersen and Knudsen, 2021) and the combined dataset with their differences are illustrated in Fig. 4.11. The results of their differences exhibit minimum, maximum, mean and SD of −10.46, 10.64, 0.35 mGal, and 1.11 mGal, respectively.

The comparison between the selected 100 shipborne observations (Fig. 4.11d) and the DTU21GRA (Andersen and Knudsen, 2021) before and after the LSC procedures demonstrated an improvement in the fit, as shown in Table 4.16. The SD values drop from 2.91 to 2.24 mGal. On the other hand, Table 4.17 shows the comparison between the complete refined shipborne gravity data and DTU21GRA (Andersen and Knudsen, 2021) before and after the integration process.

Both the mean offset and the SD values decreased from 0.43 to −0.02 mGal and 3.14 to 2.69 mGal, respectively, which reveal an improvement in the final combined data. This combination established a unified and consistent gravity field over the coastal region of Nigeria, ensuring the absence of data voids (Fig. 4.11b).

Table 4.16: The differences between 100 randomly selected shipborne stations and combined gravity data before and after the integration process; units [mGal].

Integration	**Min**	**Max**	**Mean**	**SD**	**RMS**
Before	−6.17	9.27	0.17	2.91	2.90
After	−8.96	6.72	−0.05	2.24	2.25

Table 4.17: The differences between the entire 2026 refined shipborne stations and and combined gravity data before and after the integration process; units [mGal].

Integration	**Min**	**Max**	**Mean**	**SD**	**RMS**
Before	−9.84	9.70	0.43	3.14	3.17
After	−8.96	8.59	−0.02	2.69	2.69

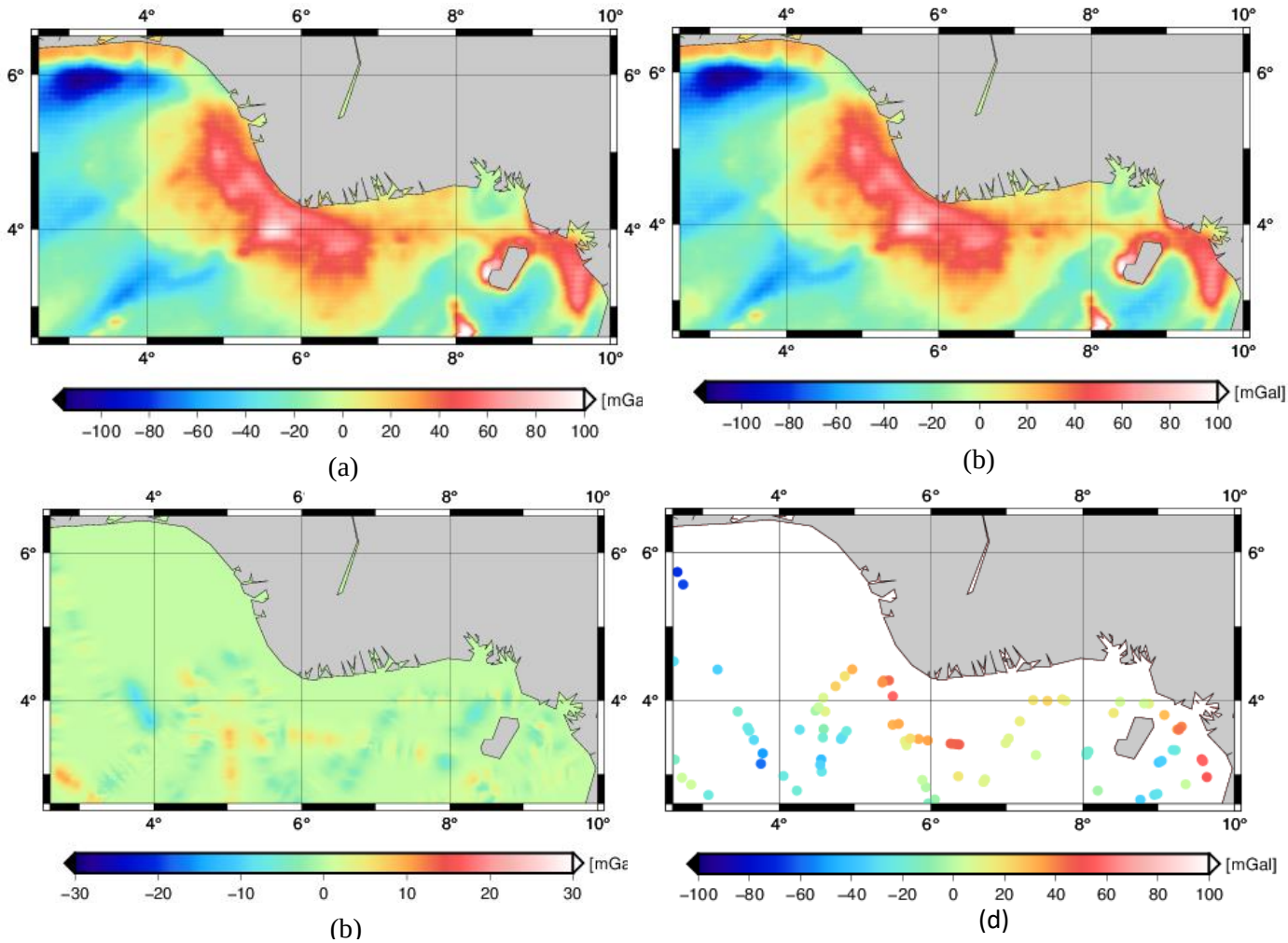

Fig. 4.11: Free-air gravity anomalies from the DTU21GRA model (a), Combined gravity data (b) Differences between the two models (c) and the distribution of 100 testing shipborne station (d) over the coastal region of Nigeria: units [mGal].

4.4.4 The effect on geoid determinations over the coastal region of Nigeria.

In this section, the results based on the method described in section 3.3.4 were presented.

The marine geoid model computed using refined shipborne gravity data utilized the DTU21 MSS (Andersen et al., 2023) to calculate the refined MDT. Similarly, the marine geoid model computed using the combined gravity datasets employed DTU21 MSS to calculate the combined MDT. Table 10 presents a comparison between the refined MDT and the combined MDT against the CNES-CLS22 MDT (Jousset et al., 2022). Fig 4.12 illustrates the marine geoid computed using the combined datasets.

Both the mean offset and SD values decreased from 0.924 to 0.923 m and from 0.021 to 0.015 ml, respectively, indicating an improvement in the SD when evaluated against the CLS22 MDT (Jousset et al., 2022).

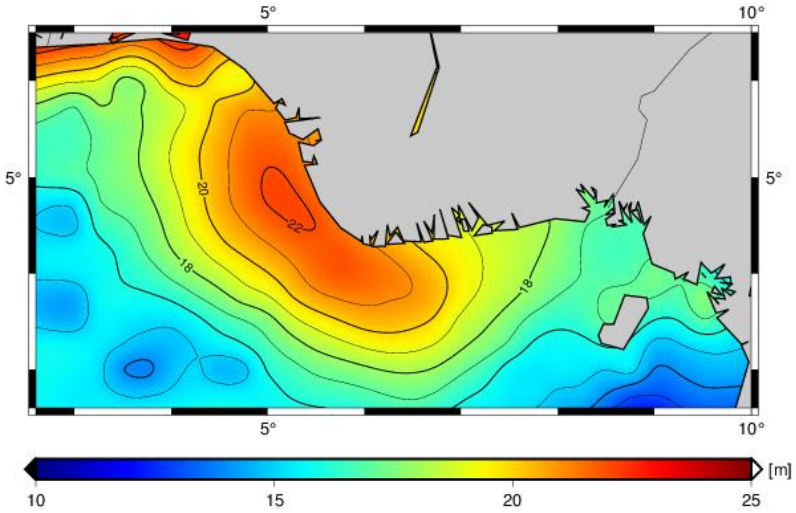

Fig. 4.12 Marine geoid model computed with combined gravity dataset. Contour interval: 1m

Table 4.18: Validation of computed geoid model over the over the coastal region of Nigeria (Away from the coastline and island)

Differences between CLS22 MDT and Computed MDT	Min. (meter)	Max (meter)	Mean (meter)	STD (meter)
CLS22MDT - Refined MDT	0.859	0.989	0.924	0.021
CLS22MDT - Combined MDT	0.872	0.974	0.923	0.015

These outcomes affirm the efficacy of incorporating recently published satellite altimeter-derived gravity data (DTU21GRA) into the regional geoid modelling process, which is particularly beneficial in island regions, as pointed out by (Wu et al., 2022). Additionally, including Sentinel-3A/3B SAR altimetry data in the computation of DTU21GRA (Andersen and Knudsen, 2021) further augments regional accuracy, thereby contributing to the observed improvements.

4.5 Summary

This chapter presents the results and analysis pertaining to objectives one to three. The outcomes of objective one was first discussed. The findings confirmed that applying the SEM enhances the assessment of solutions derived from GOCE-based GGMs in a more unbiased manner. The investigation reveals that augmenting the absent high-frequency component of geoid heights in GOCE-based GGMs by integrating XGM2019e_2159 and SRTM data leads to an approximately 10% improvement in reducing the SD of differences. This improvement is demonstrated by TIM_R6 at SH d/o 260, which shows a reduction from 0.380 m without SEM application to 0.342 m with SEM implementation**.** Additionally, an evaluation was conducted on four transformation models: linear, four-parameter, five-parameter, and seven-

parameter. The objective of this investigation was to mitigate reference system offsets between the GNSS/levelling data and the GOCE/GRACE and combined GGMs and to compare the efficacy of the utilized parametric models to ascertain which yielded smaller SDs across all GGMs. This effort resulted in the reduction of misfits of GGMs to GNSS/levelling to 0.30 m, representing a 15.3% decrease in SD. Notably, the XGM2019e_2159 model provides this improvement.

The second objective conducts an assessment of recent high-degree combined global gravity-field models for geoid modelling in the context of Nigeria. The findings of this evaluation reveal essential insights. In the comparison of these five GGMs, namely SGG-UGM-2, XGM2019e_2159, GECO, EIGEN-6C4, and EGM2008, with terrestrial free-air gravity anomalies, XGM2019e_2159 exhibits a slight advantage in the study area in term of SD. SGG-UGM-2 demonstrated the next best performance, while the EGM2008 and EIGEN-6C4 models exhibit similar levels of precision. On the other hand, the GECO model performs at a relatively lower level.

When the terrain and bouguer correction are taken into account alongside free-air and latitude corrections in bouguer gravity anomaly computation, the evaluation of terrestrial gravity anomalies and GGMs indicates that terrain and bouguer correction contribute to an improvement in precision of approximately 1 mGal across all investigated models. XGM2019e_2159 continues to lead with the best precision, achieving 6.36 mGal. In addition, the evaluation of flat regions differently from regions of significant topography reveals that when taking into account the overall performance in all evaluation areas, XGM2019e_2159 and SGG-UGM-2 are considered the most suitable choices for geoid modelling in Nigeria. Furthermore, an independent check was conducted using 20 GPS/levelling data over Abuja. The results underscore the promising potential for the development of a precise gravimetric geoid model over Nigeria through the integration of local terrestrial gravity data, shipborne gravity, and satellite altimetry-derived gravity datasets within a remove-compute-restore framework, with a particular emphasis on employing XGM2019e_2159.

Finally, the research results involve evaluating and homogenizing a marine gravity database utilizing shipborne and satellite altimetry-derived gravity data over the coastal region of Nigeria were presented. This study aims to develop homogenized gravity data for the region. We began by comparing the shipborne gravity data available at the BGI with the gravity data predicted from the DTU21GRA, SSv29.1, SGG-UGM-2, XGM2019e, GECO, EIGEN-6C4, and EGM2008 models. The research findings showed that the altimetry models exhibited similar characteristics in the region, with DTU21GRA demonstrating superior performance in

SD, RMS and mean offset values compared to shipborne gravity data. To ensure data accuracy, we addressed residual linear drifts inherent within the shipborne gravity dataset using cross-over adjustment for each leg of the surveys. Concurrently, the gross errors within each survey leg were identify and eliminate by employing the 2-sigma method as the rejection criterion and implemented a stringent pre-refinement process for ship marine surveys using the DTU2GRA model as a reference. Furthermore, the leave-one-out cross-validation techniques were applied to detect and eliminate outliers across the entirety of the shipborne gravity data, resulting in a refined shipborne gravity dataset with improved consistency and accuracy. The refined shipborne gravity data were merged with the DTU21GRA data using LSC to create a combined gravity dataset. The results of comparison between the complete refined shipborne gravity data and DTU21GRA before and after the integration process, shows that both the mean offset and the SD values decreased from 0.43 to -0.02 mGal and 3.14 to 2.69 mGal, respectively, which reveal an improvement in the final combined data. The geoid model constructed using the combined gravity data before and after the integration process, showed an improvement in the mean values, decreasing from 0.924 to 0.923 m when evaluated against the CNES-CLS22 MDT.

Chapter 5

Geoid modelling Results and Analysis

5.1 Introduction

This chapter is dedicated to presenting and analyzing the results of objectives four and five. Objective four pertains to the computation of a new experimental gravimetric geoid model for Nigeria, whereas objective five involves validating the newly computed gravimetric geoid model for Nigeria.

5.2 Results and Analysis (Objective four): The computation of a new experimental gravimetric geoid model for Nigeria

5.2.1 Development of gravimetric geoid model for Nigeria

In this study, a gravimetric geoid model specific to the Nigerian region was developed using RCR and FFT methods, as described in Section 3.3.4. Terrestrial free-air gravity anomalies underwent a subtraction process to remove short- and very-short-wavelength components, generating residual gravity anomalies.

In this study, the XGM2019e_2159 (Zingerle et al., 2019) GGM at SH up to d/o 360 was selected for geoid computation to recover the long-to-short wavelength component of the gravity signal when modelling the gravimetric geoid, as it approximates the gravity field well over Nigeria Bako et al. (2024). In addition, it should be noted that only d/o 360 of XGM2019e_2159 was applied (and not 2190) over Nigeria, because beyond d/o 715, XGM2019e_2159 is mostly based on topography (Zingerle et al., 2019).

Conversely, the computation of the very short-wavelength component of the gravity signal was performed using the SRTM data through the RCR method specified in Section 3.3.4. Fig 5.1 illustrates the reduced anomalies for the NG-EGM2024 geoid model computed using Eq. (3.4).

Table 5.1: Statistics of free-air gravity anomalies reduction and residuals [mGal]

Anomaly	Min	Max	Mean	SD
Δg_{FA}	−73.23	70.65	2.76	27.02
$\Delta g_{FA} - \Delta g_{GGM}$	−63.59	56.69	−2.04	13.01
$\Delta g_{FA} - \Delta g_{GGM} - \Delta g_{RTM}$	−63.94	39.73	−2.29	13.11

These results indicate that removing the long-to-short-wavelength components of the gravity signal from the free-air gravity anomalies results in a substantial smoothing effect. The SD of

the differences has been reduced from 27.02 mGal to 13.01 mGal, representing approximately 51.85% compared to the original terrestrial free-air gravity anomalies (see Table 5.1). However, this smoothing effect was relatively modest when the short-wavelength components representing the impact of local topography were removed. This limited additional smoothing can be attributed to the nature of the available terrestrial free-air gravity anomalies in Nigeria, where much of the region exhibits smooth and flat topography.

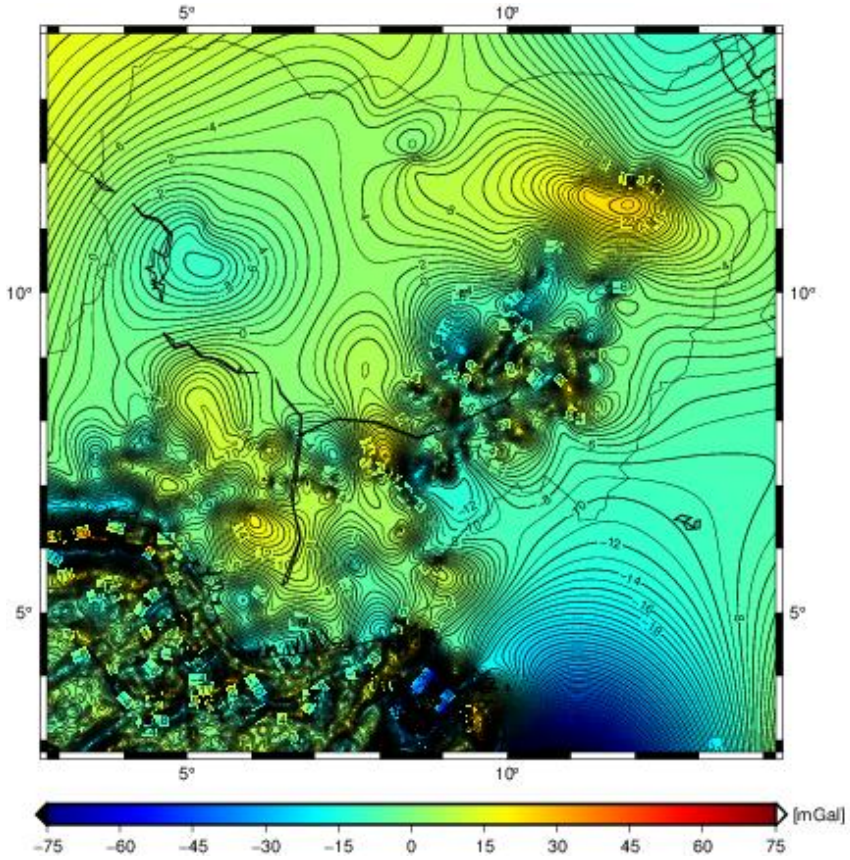

Fig. 5.1: The reduced gravity anomalies for the NG-EGM2024 geoid model. Units: [mGal]

Residual gravity anomalies were interpolated onto a 15 × 15 grid. These residual gravity anomalies ranged from $-63 \cdot 94$ mGal to $39 \cdot 73$ mGal, with a mean of $-2 \cdot 29$ mGal and an SD of $13 \cdot 11$ mGal.

The reference geoid heights were derived from XGM2019e_2159 GGM truncated to d/o 360, using Eq. (2.25). Furthermore, the topographic influence on the geoid height was accounted for as a residual terrain effect and computed using the RTM method described in Eq. (2.63). Subsequently, the gravimetric geoid model, designated NG-GM2024, for the Nigerian region was computed by converting the quasi-geoid model to the gravimetric geoid model using Brun's equation, as presented in Eq. 2.64. Fig. 5.2 depicts the gravimetric geoid model NG-

EGM2024 for Nigeria on a 15 × 15 grid. The values of NG-EGM2024 prior to the fitting process range from 5.11 m to 25.71 m, with a mean of 18.97 m and a SD of 3.53 m.

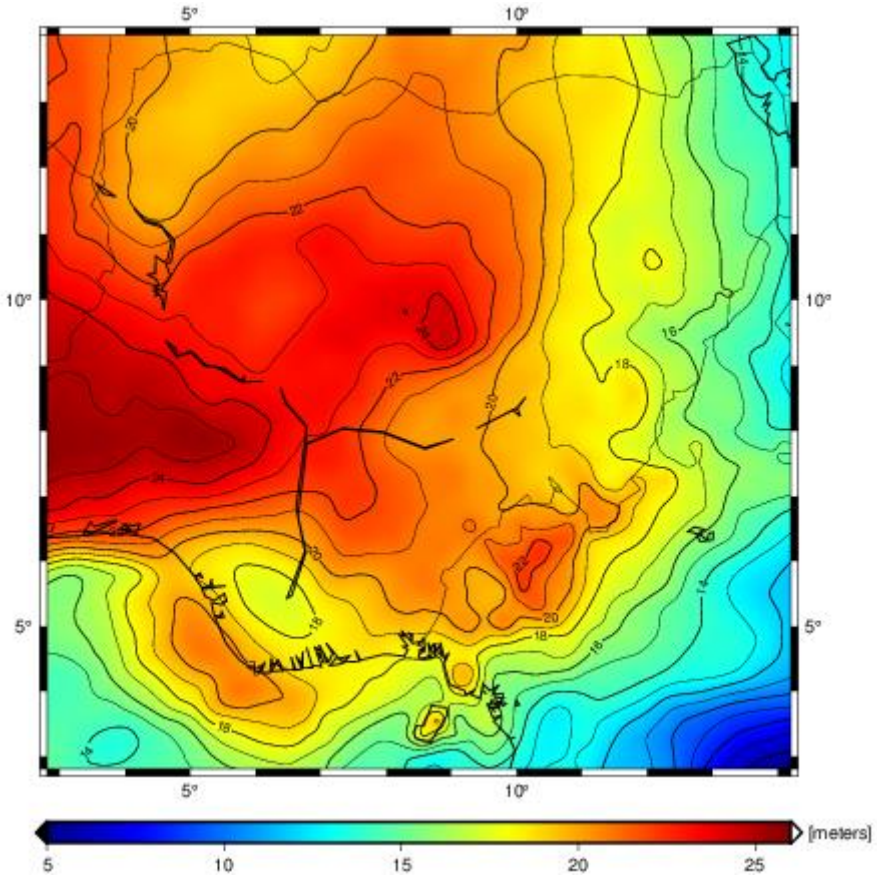

Fig. 5.2: NG-EGM2024 Geoid model before fitting. Contour interval: 2m

The residual geoid heights correspond to the short-wavelength component of the geoid heights beyond d/o 361. The impacts of residual terrain on geoid heights on range from −6.0 cm to 5.2 cm, with a mean of 0.23 cm and a SD of 1.28 cm across Nigeria land and −0.27 cm to 4.37 cm, with a mean of 0.15 cm an SD of 1.11 cm over the coastal region of Nigeria.

5.2.2 Fitting of the Gravimetric Geoid Models with the National vertical datum

Based on terrestrial, shipborne, and altimetric-derived gravity data, geoid computation yields the gravimetric geoid, which is associated with a global reference system, specifically, the global center of mass. Typically, a country's vertical datum is related to the local or regional MSL, which differs from the global zero vertical datum owing to the sea surface topography. Engineers and geodesists use GNSS to determine orthometric heights within a local vertical datum. To ensure consistency with existing levelling data, it is essential to adjust the gravimetric geoid to the local level.

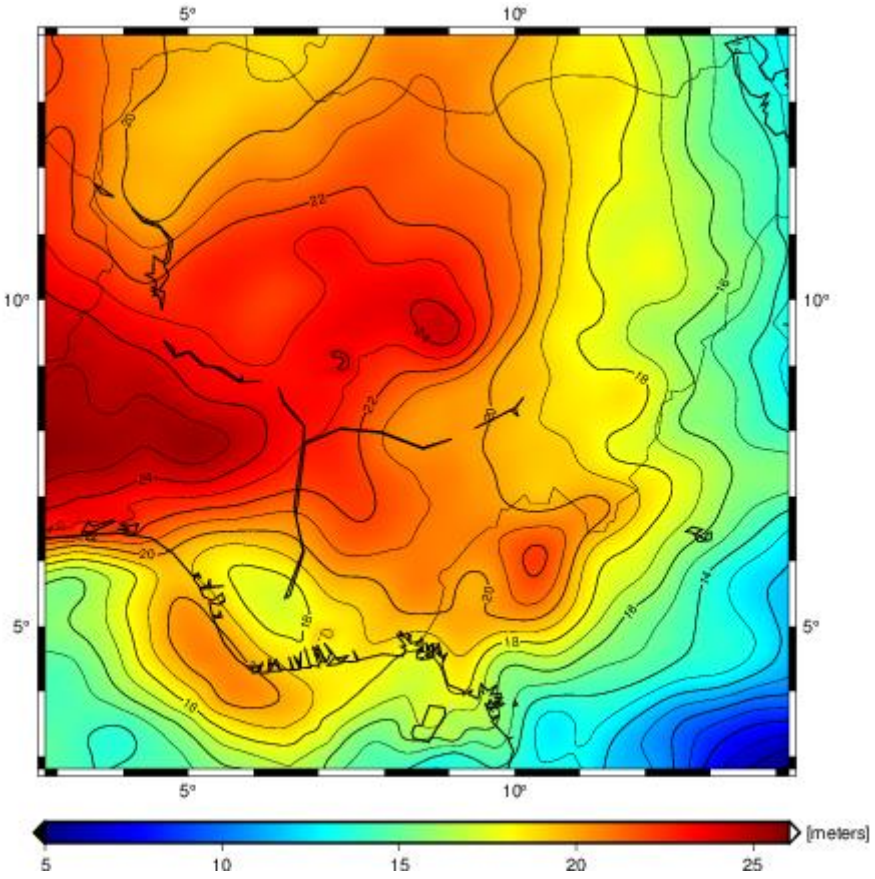

Fig. 5.3: Fitted NG-EGM2024 Geoid model. Contour interval: 2m

The fitted gravimetric geoid, as depicted in Fig 5.3, is expected to help aligned the gravimetric geoid with the GNSS/leveling results. The gravimetric geoid was adjusted using the GNSS/levelling observation data at 61 locations. It is essential to note that not all of the 90 GNSS/levelling stations used in section 4.1 are included in the gravimetric geoid fitting process. Out of the 90 stations, 61 are used for fitting, while 10 were preserved for validation purposes (see Fig 5.4). The remaining 19 GNSS/levelling points exhibited relatively large residuals exceeding ±1m and were identified as outliers and subsequently excluded. This large difference is likely attributable to a combination of inaccurately observed geodetic (GNSS height) and orthometric heights (levelling), as it is highly unlikely that the geoid would differ from the benchmarks at that level.

5.3 Results and Analysis (Objective five): Accuracy assessment of the developed fitted gravimetric geoid model for Nigeria NG-EGM2024 using the GNSS/levelling data

In this section, the results of the validation of the fitted gravimetric geoid model at 10 randomly selected GNSS/levelling stations, which were not considered during the fitting process, are presented. The findings revealed that the discrepancies in geoid heights between the 10 GNSS/levelling points not included in the fitting of the gravimetric geoid model NG-EGM2024

exhibited an improvement of 10.8 cm compared to other GGMs. This underscores the improvement achieved by the newly computed experimental gravimetric geoid model, NG-EGM2024, which has improved geoid heights by approximately 32.4% to 62.7% over Nigeria compared to the five assessed GGMs (SGG-UGM-2, XGM2019e_2159, GECO, EIGEN-6C4, and EGM2008). However, even when different GNSS/levelling points were used for the validation, the differences were negligible.

Table 5.2: The differences between the developed NG-EGM2024 Geoid model for Nigeria and the corresponding ones from the 10 GPS/levelling data (m) as well as GGMs.

Statistics	**Min**	**Max.**	**Mean**	**SD**
$N_{GNSS/levelling} - N_{NG-EGM\,2024}$	0.473	0.736	0.626	**0.108**
$N_{GNSS/levelling} - N_{SGG-UGM-2}$	0.121	1.296	0.725	0.339
$N_{GNSS/levelling} - N_{XGM\,2019e\_2159}$	0.100	0.890	0.641	0.226
$N_{GNSS/levelling} - N_{GECO}$	0.174	1.268	0.770	0.303
$N_{GNSS/levelling} - N_{EIGEN-6C4}$	0.241	1.295	0.790	0.312
$N_{GNSS/levelling} - N_{EGM\,2008}$	0.144	1.229	0.739	0.329

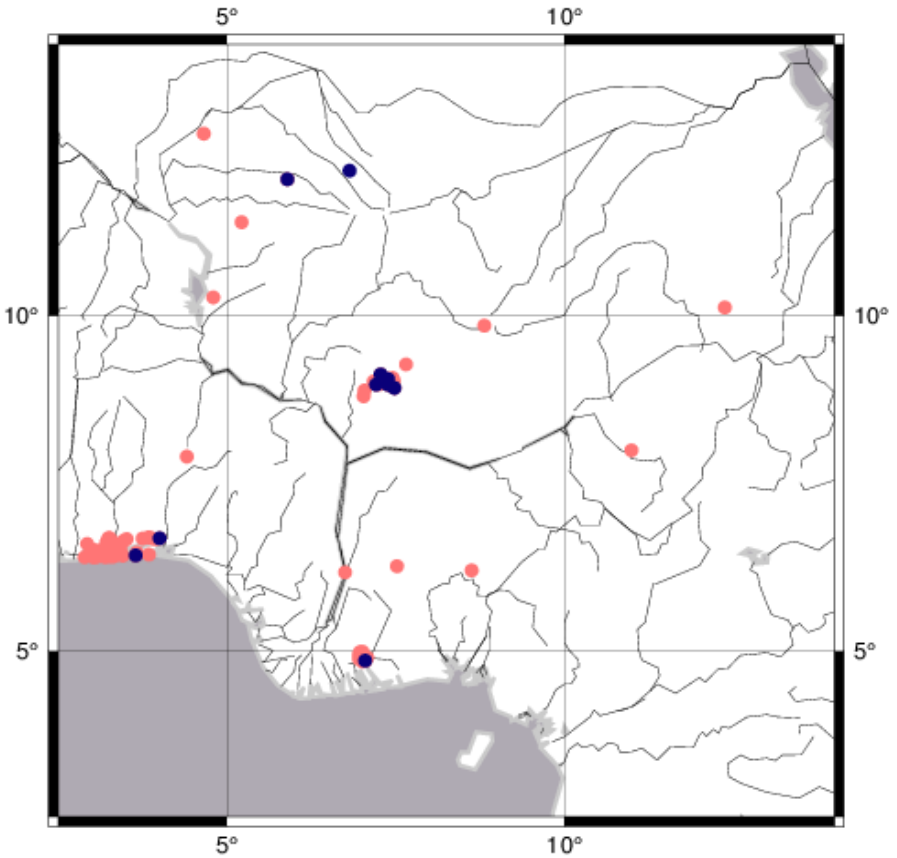

Fig 5.4: Distribution of 61 GNSS/levelling stations used for the fittings (red) and 10 GNSS/levelling check points not used in the fitting process (blue).

5.4 Summary

The aim of the study is to develop a fitted gravimetric geoid model for Nigeria, using the FFT method. The RCR technique was applied using various datasets, including terrestrial, shipborne, and satellite altimetry-derived gravity data. The shipborne gravity data, when integrated with satellite altimetry-derived gravity data, provided an improvement of approximately 30% in the combined gravity dataset over the coastal region of Nigeria. In addition, datasets comprising the gravity contributions from XGM2019e_2159, GNSS/levelling data, and high-resolution topographic information from SRTM30_Plus for land areas and GEBCO bathymetry for coastal areas of Nigeria were used in the geoid computation.

To model the gravimetric geoid heights, a combined GGM (XGM2019e_2159) ranging from d/o 2 to 360 was used to eliminate the long-to-short-wavelength component from gravity anomalies. Additionally, the very short-wavelength component of the gravity signal was removed from the terrestrial gravity anomalies using the RCR technique. In the computational step, the FFT method was employed to predict the residual geoid height from the residual gravity anomalies. Furthermore, gravimetric geoid models were fitted to Nigeria's national local vertical datum by using 61 GNSS/levelling stations. The accuracy of the fitted gravimetric geoid models for Nigeria, denoted as NG-EGM2024, was evaluated by assessing geoid undulations from 10 GPS/leveling stations that were not considered in the fitting process. The discrepancies in geoid heights between the 10 GNSS/leveling stations and the NG-EGM2024 model were approximately 10.8 cm. The NG-EGM2024 model, when compared to five evaluated combined GGMs (SGG-UGM-2, XGM2019e_2159, GECO, EIGEN-6C4, and EGM2008), has shown an improvement in geoid heights ranging from about 32.4% to 62.7% over Nigeria. Therefore, the NG-EGM2024 model is recommended as a suitable model for improving geoid heights across Nigeria.

Chapter 6

Conclusions and Recommendations

6.1 Conclusions

This dissertation has detailed the development of an experimental gravimetric geoid model, designated NG-EGM2024, tailored for Nigeria. The computation of the model involved the application of the FFT and RCR procedures. Different datasets were integrated, including terrestrial, shipborne, and satellite altimetry-derived gravity data from DTU21GRA (Andersen and Knudsen, 2021). The shipborne gravity data, when integrated with satellite altimetry-derived gravity data, provided an improvement over the coastal region of Nigeria (Bako and Kusche, 2024). In addition, datasets comprising the gravity contributions from XGM2019e_2159 (Zingerle et al., 2020), GNSS/levelling data, and high-resolution topographic information from SRTM30_Plus for land areas and GEBCO bathymetry for coastal areas of Nigeria were used in the geoid computation.

To ensure precise outcomes in local/regional geoid modelling, ground-based gravity measurements and GNSS/levelling observations were evaluated. Five distinct evaluation methodologies were employed: validation of geoid height using GNSS/levelling data compared to GGMs and assessment of free-air and bouguer gravity anomalies using terrestrial gravity data. The XGM2019e_2159 model was selected as the reference model because of its fidelity to the gravity field in Nigeria. In addition, a marine gravity database was established to encompass the maritime domain within Nigeria, incorporating shipborne and satellite altimetry-derived gravity data.

The gravimetric geoid was determined using the RCR methodology, wherein a reference GGM, XGM2019e_2159 up to d/o 360, was employed to subtract the long-and short-wavelength components from the terrestrial gravity anomalies. XGM2019e_2159 used the satellite model GOCO06s (Kvas et al., 2021), in the longer-wavelength range up to d/o 300 combined with ground gravity data obtained from the United States (US) National Geospatial-Intelligence Agency (NGA) over Nigeria's Land and DTU13GRA (Andersen et al., 2013) satellite altimetry data over the coastal region of Nigeria. Concurrently, the very short-wavelength component of the gravity signal was eliminated from the terrestrial gravity data using the RTM method.

In the computational step, the FFT method was employed to predict the residual geoid height from the residual gravity anomalies. Furthermore, gravimetric geoid models were fitted to Nigeria's national local vertical datum by using 61 GNSS/levelling stations. The accuracy of the fitted gravimetric geoid models for Nigeria, denoted as NG-EGM2024, was evaluated by assessing geoid undulations from 10 GPS/leveling stations that were not considered in the fitting process. The discrepancies in geoid heights between the 10 GNSS/leveling stations and the NG-EGM2024 model were approximately 10.8 cm. The NG-EGM2024 model, when compared to five evaluated combined GGMs (SGG-UGM-2, XGM2019e_2159, GECO, EIGEN-6C4, and EGM2008), has shown an improvement in geoid heights ranging from about 32.4% to 62.7% over Nigeria. Therefore, the NG-EGM2024 model is recommended as a suitable model for improving geoid heights across Nigeria. Considering these findings, the NG-EGM2024 model is recommended as a suitable model that provides more accurate geoid heights in Nigeria than other geoid solutions.

6.2 Recommendations:

Numerous challenges and constraints were identified throughout this dissertation, warranting further scrutiny in subsequent research. In this section, several suggestions for future research was present.

1. Insufficiency in the number and distribution of gravimetric stations, particularly in Northern Nigeria, is a critical factor. Achieving a uniform and high-quality gravimetric geoid model requires establishing a consistent distribution of terrestrial gravity data. However, collecting gravity data over the northern region of Nigeria is extremely challenging because of logistics and insecurity.
2. Given Nigeria's extensive and diverse terrain, encompassing flat areas, rugged terrains, mountains, and coastal regions, the acquisition of terrestrial gravity measurements is a formidable task. Therefore, it is strongly recommended to employ airborne gravimetry to augment the quantity and quality of the gravity data.
3. Establishing and maintaining the levelling network would significantly contribute to the further refinement and improvement of gravimetric geoid models for Nigeria.

Bibliography

Abdallah, M., Abd El Ghany, R., Rabah, M., & Zaki, A. (2022). Comparison of recently released satellite altimetric gravity models with shipborne gravity over the Red Sea. *The Egypt. Journal of Remote Sensing and Space Science, 25*(2), 579-592. https://doi.org 1016/j.ejrs.2022.03.016.

Abulaitijiang, A., Andersen, O. B., & Stenseng, L. (2015). Coastal sea level from inland CryoSat-2 interferometric SAR altimetry. *Geophysical Research Letters, 42*(6), 1841-1847.

Abd-Elmotaal, H. A., Seitz, K., Kuhtreiber, N., & Heck, B. (2019). AFRgeo_v1.0: a geoid model for Africa. *karlsruher institute fur Technologie (KIT) f*.

Agajelu, S. (1990). The geoidal heights for Nigeria. *Survey Review* 30 (235), 229-236.

Aleem, K.F., & Abubakar, A.F. (2022). The review and development of the Nigeria geodetic control network. *Journal of Geospatial Survey* 2(2). 22-29, https://doi.org/10.4038/ jgs. v2i2.4

Aleem, K.F. (2014). *Adaptation of a Global Orthometric Height Model to Local Height Datum using 'Sat level Collocation* (Doctoral dissertation, University of Lagos, Nigeria).

Andersen O.B. and Knudsen P. (1998). Global marine gravity field from the ERS-1 and Geosat geodetic mission altimetry. *Journal of Geophysical and Reserach*, 103, 8129 – 8137.

Andersen, O. B., Knudsen, P., & Berry, P. A. (2010). The DNSC08GRA global marine gravity field from double-tracked satellite altimetry. *Journal of Geodesy, 84*, 191-199. doi:10.1007/s0019-009-0355-9.

Andersen, O.B., Knudsen, P., Kenyon, S., Factor, J., & Holmes, S. (2013). The DTU13 global marine gravity field-first evaluation. *Ocean Surface Topographic science Team Meeting, Boulder, Colorado*. (http://www.aviso.altimetry.fr/fileadmin/documents /OSTST/2013/oral/Andersen_DTU13GRA.pdf)

Andersen, O.B., Knudsen, P., Kenyon, S., Factor, J., & Holmes, S. (2017). Global gravity field from recent satellite (DTU15) –Arctic improvements. *First Break*, 35, 37-40, doi: 10.3997/1365-2397.2017022.

Andersen, O.B and Knudsen, P (2019). The DTU17 global marine gravity field: First validation results, *International Association of Geodesy Symposia. Springer*, pp. 83–87. https://doi.org/10.1007/1345_2019_65.

Andersen O.B and Knudsen P (2021). The DTU 21 global marine gravity field-first evaluation. *Ocean Surface Topographic Science Team Meeting, Boulder, Colorado*. Ftp.space.dtu.dk/pub/Altimetry/CUNDERLIK.

Andersen, O.B., Rose, S.K., Abulaitijiang, A., and Zhang, S., Fleury, S. (2023). The DTU21 global mean sea surface and first evaluation. *Earth System Science Data Discussion*, 2023, 1-19. doi: https://doi.org/10.5194/essd-/15-4065-2023.

Arlot, S., and A. Celisse. 2010. A survey of cross-validation procedures for model selection. *Statistics Survey.* 4:40–79. doi:10.1214/09-SS054.

Bako, M., Ojigi L.M and Dodo J.D (2019). An Evaluation of Different GNSS Orbit Solutions for Precise Point Positioning in the Federal Capital Territory, Abuja. *Journal of Geoinformation and Earth Science* 1, 1-8.

Bako, M., Zitta, N., Saliu, A. M., & Ibrahim, A. (2020). Land Surface Topographic Change Detection Using Remote Sensing Techniques. *Environmental Technology & Science J*ournal 11, (2), 65-73.

Bako, M., & Kusche, J. (2024). Evaluation and homogenization of a marine gravity database from shipborne and satellite altimetry-derived gravity data over the coastal region of Nigeria. *Journal of Applied Geod*esy doi: 10.1515/jag-2024-0059.

Bako, M., Elsaka B., Kusche, J., and Feboglio-Marc, L. (2024). Evaluation of GOC/GRACE and combined global geopotential models using GNSS/levelling data over Nigeria. *Studia Geophysica et Geod*etica https:/doi.org/10.1007/s11200-023-0804-6.

Balmino, G., (1978). Introduction to least squares collocation, in: H. Moritz, H. Sunkel (Eds) Approximation methods in geodesy, lecture delivered at *2nd Int. Summer School in the Mountains on Mathematical Methods in Physical Geodesy*, Ramsau, Austria, 23 August – 2 September 1977, 47-88.

Basile, C., Mascle, J., Sage, F., Lamarche, G., & Pontoise, B. (1996). Precruise and site surveys: a synthesis of marine geological and geophysical data on the Côte d'Ivoire-Ghana Transform Margin. In *Mascle, J., Lohmann, GP, Clift, PD, et al., Proc. ODP, Init. Repts* (159), 47-60.

Barzaghi, R., Carrion, D., Kamguia, J., Kande, L.H., Yap, L., & Betti, B (2021). Estimating gravity field and quasi-geoid in Cameroon (CGM20). *Journal of African Earth Science*, 184, 104377.

Bjerhammer, A., (1975). Discrete solutions of the boundary value problem in physical geodesy, Tellus, 27 (2), 97-106.

Brockmann, J. M., Schubert, T., & Schuh, W. D. (2021). An improved model of the Earth's static gravity field solely derived from reprocessed GOCE data. *Survey in Geophyics, 42*, 277-316. doi:10.1007/s10712-020-09626-0.

Bruinsma, S., Förste, C., Abrikosov, O., Lemoine, J., Marty, J., Mulet, S., Rio, M. and Bonvalot, S. (2014). ESA's satellite-only gravity field model via the direct approach based on all GOCE data; *Geophysica Research Letters*, Vol 41, No. 21, p. 7508-7514, doi: 10.1002/2014GL062045.

Bureau Gravimetrique International, 2018. Marine gravity data Available from: http://bgi.omp.obs-mip.fr/data-products/Gravity-Databases/Marine-Gravity-data.

Calafat, F. M., Cipollini, P., Bouffard, J., Snaith, H., & Féménias, P. (2017). Evaluation of new CryoSat-2 products over the ocean. *Remote Sensing of Environ.*, *191*, 131-144.

Chen, W., Tenzer, R., & Gu, X. (2014). Sediment stripping correction to marine gravity data. *Marine Geodesy*, *37*(4), 419-439.

Denker, H., & Roland, M. (2005). Compilation and evaluation of a consistent marine gravity data set surrounding Europe. In *A Window on the Future of Geodesy: Proceedings of the International Association of Geodesy IAG General Assembly Sapporo,* 248-253. Berlin, Heidelberg: Springer Berlin Heidelberg, doi:10.1007/3-540-27432-4_42.

Dorschel, B. et al. (2022). The International Bathymetric Chart of the Southern Ocean Version 2. *Scientific Data* 9, 275, https://doi.org/10.1038/s41597-022-01366-7.

Drinkwater M, Floberghagen R, Haagmans R, Muzi D, Popescu A (2003). GOCE: ESA's first Earth explorer core mission. *Space Science Review,* 108:419−32.

El-Fiky, G. S., Kato T., and Y. Fujii, (1997), "Distribution of the vertical crustal movements rates in the Tohoko district, Japan, predicted by least-squares collocation" *Journal of Geodesy,* 71, 7, pp. 432-442.

El-Fiky, G. (2018). Satellite Gradiometry for Modeling Sea Current Circulation (*Doctoral dissertation, Zagazig University*).

Elsaka, B., Alothman, A., & Godah, W. (2015). On the contribution of GOCE satellite-based GGMs to improve GNSS/leveling geoid heights determination in Saudi Arabia. *IEEE Journal of Selected Topics in Appl. Earth Observations and Remote Sens., 9*(12), 5842-5850. doi:10.1109/JSTARS.2015.2495193.

Emery, K. O., Uchupi, E., Phillips, J., Bowin, C., & Mascle, J. (1975). Continental margin off western Africa: Angola to Sierra Leone. *AAPG Bulletin, 59*(12), 2209-2265.

Ezeigbo, C. U. & Edoga, A. C. (1980). The scale and Orientation problems in Geodetic Positioning in Nigeria. *Proceeding of International Workshop on Geodetic Positioning*, University of Lagos, Nigeria.

Ezeigbo, C.U. (1991). Estimation Models of Geoid in Nigeria Using Doppler Satellite Observation. Determination of Geoid. *Springer*, 230-240. https://doi.org/10.1007/978-1-4612-3104-2.

Ezeigbo, C.U., 1989. Estimate Models of Geoid in Nigeria using Doppler Satellite Observation. *Journal of Geodesy, pp. 78-86.*

Fajemirokun, F. A. (1980). The Nigeria Geodetic Control System: An Appraisal. *Proceedings* of the XVth Annual General Meeting of the Nigeria Institution of Surveyors held in Abeokuta. April 22-24.

Fashir, H, Majid, A. and Kadir, A. (1998). African regional gravimetric geoid: Stokesian approach. *Bulletin of the International Geoid Service*, 8, 65-84.

Fecher, T., Pail, R., & Gruber, T. (2015). Global gravity field modeling based on GOCE and complementary gravity data. *International Journal of Applied Earth Observation and Geoinformation, 35*, 120-127. doi: 10.1016/j.jag.2013.10.005.

Flechtner F, Dahle C, Neumayer KH, König R, Förste C. (2010). The release of champ and grace eigen gravity field models. In: *System Earth* via geodetic-geophysical space techniques; pp. 41−58.

Folger, D. W., Irwin, B. J., McCullough, J. R., Driscoll, G. R., & Polloni, C. F. (1990). Map showing free-air gravity anomalies off the western coast of Africa Senegal (south of 15° north latitude) to Sierra Leone (No. 2098-D). US Geological Survey.

Fotopoulos, G. (2003) *An Analysis of the Optimal Combination of Geoid, Orthometric and Ellipsoidal Height Data. Department of Geomatics Engineering*, University of Calgary, Calgary, Canada, UCGE Reports No. 20185 (PhD Thesis).

Forsberg, R. (1984). A study of terrain reductions, density anomalies and geophysical inversion methods in gravity field modelling. *Report 355*, Department of Geodetic Science and Surveying, Ohio State University, Columbus.

Forsberg, R. (1985). Gravity field terrain effect computations by FFT. *Bulletin Geodesique*, 59, 342–360, doi:10.1007/ BF02521068.

Forsberg, R., & Tscherning, C. C. (1981). The use of height data in gravity field approximation by collocation. *Journal of Geophysical Research.: Solid Earth, 86*(B9), 7843-7854. doi:10.1029/JB086iB09p07843.

Forsberg, R., and Tscherning, C. C. (2008). An overview manual for the GRAVSOFT geodetic gravity field modelling programs. DRAFT 1 ed. Copenhagen: *Contract report for JUPEM.*

Förste, C., Bruinsma S. L., Abrikosov, O., Lemoine, J. M., Schaller, T., Gotze, H., Ebbing, J., Marty, J. C., Flechtner, F., Balmino, G. and Biancale, R. (2014). EIGEN-6C4 The latest combined global gravity field model including GOCE data up to degree and order 2190 of GFZ Potsdam and GRGS Toulouse. *GFZ Data Services*. https://doi.org/10.5880/icgem.2015.1

Gatti, A., Reguzzoni, M., Migliaccio, F., & Sansò, F. (2016). Computation and assessment of the fifth release of the GOCE-only space-wise solution. In *The 1st joint commission 2 and IGFS meeting* (pp. 19-23).

Gilardoni, M., Reguzzoni, M., & Sampietro, D. (2016). GECO: a global gravity model by locally combining GOCE data and EGM2008. *Stud Geophysica et Geodeatica, 60*, 228-247. doi:10.1007/s11200-015-1114-4.

Gruber, T. (2009). Evaluation of the EGM2008 gravity field using GPS-levelling and sea surface topography solutions; External evaluation reports of EGM2008. *Newton's Bulletin*, 4, 3–17, Bureau Gravimétrique International (BGI)/International Geoid Service (IGeS), ISSN 1810-8555.

Hackney, R.I. and Featherson, W. E. (2003). Geodetic versus geophysical perspectives of the gravity anomaly. *Geophysical Journal International*, 154 (1), 35 -43.

Heiskanen W.A., Moritz, H. (1967). *Physical geodesy* W.H. Freeman, San Francisco.

Hirt, C., Gruber, T. and Featherstone, W.E. (2011). Evaluation of the first GOCE static gravity field models using terrestrial gravity, vertical deflections and EGM2008 quasi geoid heights. *Journal of Geodesy*, 85, 723–740, http://dx.doi.org/10.1007/s00190-011-0482-y

Hofmann-Wellenhof, B. & Moritz, H., (2005). Physical geodesy. Springer Science & Business Media. Printed in Austria.

Ilk, K.H., J. Flury, R. Rummel, P. Schwintzer, W. Bosch, C. Haas, J. Schroter, D. Stammer, W. Zahel, H. Miller, R. Dietrich, P. Huybrechts, H. Schmeling, D. Wolf, H.J. Gotze, J. Riegger, A. Bardossy, A. Bardossy, A. Guntner and T. Gruber (2005) Mass transport and mass distribution in the Earth system – *contribution of new generation of satellite gravity and altimetry missions to geosciences*. Proposal for a German priority research program. GOCE-Projektburo Deutschland, Technische Universitat Munchen, Potsdam.

Idowu T. O (2005). *Determination and utilization of optimum residuals gravity anomalies for mineral utilization*. PhD dissertation of the department of surveying and Geoinformatics, University of Lagos, Nigeria.

ISIK, M. S., Cevikalp, M. R., Erol, B., & Erol, S. (2022). Improvement of GOCE-Based Global Geopotential Models for Gravimetric geoid Modeling in Turkey. *Geosciences*, 12(12),432.

Ince, E. S., Barthelmes, F., Reißland, S., Elger, K., Förste, C., Flechtner, F., & Schuh, H. (2019). ICGEM–15 years of successful collection and distribution of global gravitational models, associated services, and plans. doi: http://doi.org/10.5194/essd-11-647-2019.

Jekeli, C., Lee, J. K. And Kwon, J. H. (2007). On the computation and approximation of ultra-high-degree spherical harmonic series. *Journal of Geodesy*, 81: 603.

https://doi.org/10.1007/s00190-006-0123-z.

Jousset, S., Mulet, S., Greiner, E., Wilkin, J., Vidar, L., Dibarboure, G., & Picot, N. (2023). New global Mean Dynamic Topography CNES-CLS-22 combining drifters, hydrological profiles and high-frequency radar data. *Authorea Preprints*. https://doi.org/10.24400/527896/a03-2022.3292.

Kamguia, J., Tabod, C. T., Nouayou, R., Tadjou, J. M., Manguelle-Dicoum, E., & Kande, H. L. (2007). The Local Geoid Model of Cameroon: CGM05. *Nordic J. surveying and real estate res.*, 4 (2), 7-23.

Kamto, P.G., Yap, L., Nguiya, S., Kande, L.H., & Kamguia, J. (2022). Evaluation of latest marine gravity field models derived from satellite altimetry over the Gulf of Guinea (Central Africa) with shipborne gravity data. *Studia Geophysica et Geodeatica*, 66(1), 23-37.

Kornfeld, R.P., Arnold, B.W., Gross, M.A., Dahya, N.T., Klipstein, W.M., Gath, P.F., et al. (2019) Grace-fo: the gravity recovery and climate experiment follow-on mission. *Journal of Spacecraft Rockets*; 56, 931−51.

Kotsakis, C., Katsambalos, K, (2010). Quality analysis of global geopotential models at 1542 GPS/levelling benchmarks over the Hellenic mainland. *Survey Review* 42, 327-344.

Kvas, A., Brockmann, J. M., Krauss, S., Schubert, T., Gruber, T., Meyer, U., ... & Pail, R. (2021). GOCO06s–a satellite-only global gravity field model. *Earth System Science Data Discussions*, 1-31. https://doi.org/10.5194/essd-13-99-2021.

Li, Q., Bao, L., & Wang, Y. (2021). Accuracy evaluation of altimeter-derived gravity field models in offshore and coastal regions of China. *Frontiers in Earth Science*, *9*, 722019.

Liang, W., Li, J., Xu, X., Zhang, S., & Zhao, Y. (2020). A high-resolution Earth's gravity field model SGG-UGM-2 from GOCE, GRACE, satellite altimetry, and EGM2008. *Engineering*, *6*(8), 860-878. doi 10.1016/j.eng.2020.05.008.

Mahmud, B., Dirssu, O. Y., Albert, N. I., Bako, M and Solomon, F.O (2023). Estimation of sea level anomaly across the Nigeria coastal region using satellite altimetry technique. *Journal of Geomatics and Environmental Research*, 6 (1), 16-31. https://www.unilorinjoger.com.

Martensen, E., and Ritter, S., (1997). Potential theory. In Lecture Notes in Earth Sciences, vol. 65, Geodetic Boundary Value Problems in view of the 214 One Centimeter Geoid, pp. 19-66, Eds. Sanso and R. Rummel, *Springer*-Verlag, Berlin.

Matheron, G. (1963). Principles of geostatistics. Economic Geology 58 (8):1246–1266. doi:10.2113/gsecongeo.58.8.1246.

Mayer-Gurr, T., K.H. ILK, A.Eicker and M. Feuchtinger (2010) ITG-CHAMP01: A CHAMP gravity field model from short kinematical arcs of a one-year observation period. *Journal of Geodesy*, 78:462-480.

Moritz, H., (1980). Geodetic Reference System 1980, Bull. Geod., 54, 395-405. Moritz, H (1976). Covariance functions in Least squares collocation. Department of Geodetic Science Report 240, Ohio State University, Columbus, OH.

Merry, C. L., Blitzkow, D., Abd-Elmotaal, H., Fashir, H. H., John, S., Podmore, F., & Fairhead, J. D. (2005). A preliminary geoid model for Africa. In *A Window on the Future of Geodesy: Proceedings of the International Association of Geodesy IAG General Assembly Sapporo, Japan June 30–July 11, 2003* (pp. 374-379). Springer Berlin Heidelberg.

Merry, C. (2009). EGM2008 evaluation for Africa. *Newton's Bulletin*, *4*, 200-206.

Moka, E. C, Jackson, K., & Lawrence, H. (2018) Development of a Gravimetric Geoid model for Nigeria. *Nigeria Journal of Geodesy*. 1, (1), 1-9. Special Issue.

Morelli, C., Gantar, C., McConnell, R. K., Szabo, B., & Uotila, U. (1972). The International Gravity Standardization Net (IGSN 71). *DTIC Document*. https://apps.dtic.mil/sti/pdfs/ADA006203.pdf.

Molodenskii, M. S., Eremeev, V. F., and Yurkina, M. I. (1962). Methods for Study of the External Gravitational Field and Figure of the Earth. Jerusalem: Translated from the Russian by the Israel Program. For Sc. Transl.

Nielsen k, Stenseng L, Andersen OB, Villadsen H, Knudsen P. Validation of cryosat-2 sar mode-based lakes. *Remote Sensing Environment*, (171), 162-170.

Nwilo, P. C. (2013). Technological advancements in surveying and mapping: The Nigeria adaptation. FIG working week 2015 ''From the wisdom of the ages to the challenges of the modern world'', Bulgaria, 17th -21st May 2015. Sofia, FIG publications.

Odumuso, J.O. (2019). *Determination and Utilization of a homogenized gravity dataset for the development of a gravimetric geoid for South Western Zone of Nigeria*, A PhD thesis submitted to the School of Postgraduate, Federal University of Technology, Minna, Nigeria.

Opaluwa, Y.D., and Quadri A.A. (2010). Derivation of orthometric heights from GPS measured heights using geometric techniques and EGM96 model. *FUTY Journal of Environmental* 5, (1) 80-93

Pavlis N.K., Holmes S.A., Kenyon S.C., Factor JK, (2012). The development and evaluation of the Earth gravitational model 2008 (EGM2008). *Journal of Geophysical Research* 117(B04406), 1–38.

Renard Vincent (1971) Walda-004 CH21 cruise, RV Jean Charcot, https://doi.org/10.17600/71003611.

Reigber, C., Schwintzer, P., & Luhr, H. (1999). The CHAMP geopotential mission. *Boll. Geof. Teor. Appl*, 40(3-4), 285-289.

Saadon, A, Mohamed El-Ashquer, Basem Elsaka and Gamal El-Fiky (2021). Determination of local Gravimetric Geoid Models over Egypt using LSC and FFT Estimation Techniques based on Different Satellite- and Ground-based Datasets. https://www.tandfonline.com/doi/full/10.1080/00396265.2021.1932148.

Sandwell, D. T., and Smith, W. H. F. (1997). Marine Gravity Anomaly from Geosat and ERS Satellite Altimetry. *Journal of Geophysical Research* 102 (B5), 10039–10054. doi:10.1029/96JB03223

Sandwell, D. T., Harper, H., Tozer, B., and Smith, W. H. F. (2021). Gravity Field Recovery from Geodetic Altimeter Missions. *Advanced Space Research* 68, 1059–1072. doi 10.1016/j.asr.2019.09.011

Sanso, F. & Sideris, M. G, (2013). Geoid determination: theory and methods, Springer Science & Business Media.

Schaeffer, P., Pujol, M.I., Veillard, P., Faugere, Y., Dangneaux, Q., Dibarboure, G., & Picot, N. (2023). The CNES CLS 2022 mean sea surface: short wavelength improvements from cryostat-2 and SARAL/Altika high-sampled altimeter data. *Remote Sensing., 15(11),* 2910.

Schlich Roland (1971) Benin 1971 cruise, RV Jean Charcot,

https://doi.org/10.17600/71003811
Tapley, B., Bettadpur, S., Watkins, M., Reigber, C. (2004). The Gravity Recovery and Climate Experiment: Mission Overview and Early Results. *Geophysical Research Letters*, Vol. 31, Issue 9, doi:10.1029/2004GL019779.
Torge, W., (2001). Geodesy, 3rd ed.de Gruyter, Berlin/New York.
Torge, W. and Muller, J., (2012). Geodesy, 4th Edition, Walter de Gruyter. Berlin. https:/doi .org/10.1515/9783110250008.
Tscherning, C.C., and Rapp, R.H., (1974). Closed Covariance Expressions for Gravity Anomalies, Geoid Undularion, and Deflections of the Vertical Implied by Anomaly Degree-Variance Models, Reports of the Department of Geodetic Science No. 208, The Ohio State University, Columbus, Ohio.
Unesco. (1973). Intergovernmental Oceanographic Commission Technical Series. Presented at the eighth Session at the IOC Assembly Unesco, Paris 5-17 November 1973, PP 52-54. unesdoc.unesco.org/in/rest/annotationSVC/DownloadWatermarkedAttachment/attach _import_6ecf4695-d2b2-4dfb-b275-ede3c437fcac? _=016074engo.pdf&to=64&from=1
USGS. 2017. Shuttle Radar Topography Mission, https://Earthexplorer.usgs.gov.

Villadsen, H., Deng, X., Andersen, O. B., Stenseng, L., Nielsen, K., & knudsen, P. (2016). Improved inland water levels from SAR altimetry using novel empirical and physical retrackers. *Journal of hydrology*, 537, 234-247.
Wessel, P., Smith, W. H. F. Scharroo, R. Luis, J. F. & Wobbe, F. (2013). Generic Mapping Tools: Improved version released, EOS Trans. *AGU*, 94, 409-410.

Wessel, P., & Watts, A. B. (1988). On the accuracy of marine gravity measurements. *Journal of Geophysical Reearch.: Solid Earth*, *93*(B1), 393-413.
Wu, Y., Wang, J., Abulaitijiang, A., He, X., Luo, Z., Shi, H., Wang, H., Ding, Y. Local Enhancement of Marine Gravity Field over the Spratly Islands by Combining Satellite SAR Altimeter-Derived Gravity Data. *Remote Sensing*. 2022, 14, 474. https://doi.org/10.3390/rs14030474.
Yilmaz, M., Yilmaz, I., & Uysal, M. (2018). The evaluation of gravity anomalies based on global models by land gravity data. *International Journal Geological and Environmental Engineering*, *12*(11), 814-820.
Yilmaz, M., Turgut, B., Gullu, M., & Yilmaz, I. (2016). Evaluation of recent global geopotential models by GNSS/Levelling data: internal Aegean region. *International J. Engineering and Geoscience.*, 1, 15-19.
Zamri, A. N. M., Pa'Suya, M. F., Din, A. H. M., Azmin, N. S. H. N., & Othman, N. A. (2024). Optimizing the Integration of Gravity Data Inputs for Geoid Modelling over Peninsular Malaysia. In *2024 20th IEEE International Colloquium on Signal Processing & Its Applications (CSPA)* (pp. 41-46). IEEE.
Zaki, A., Mansi, A. H., Selim, M., Rabah, M., & El-Fiky, G. (2018). Comparison of satellite altimetric gravity and global geopotential models with shipborne gravity in the Red Sea. *Marine geodesy*, *41*(3), 258-269. DOI: 10.1080/01490419.2017.1414088

Zaki, A., Magdy, M., Rabah, M., & Saber, A. (2021). Establishing a marine gravity database around Egypt from satellite altimetry-derived and shipborne gravity data. *Marine Geodesy, 45*(2), 101-120. DOI: 10.1080/01490419.2021.2020185.

Zhang, S., Sandwell, D. T., Jin, T., & Li, D. (2017). Inversion of marine gravity anomalies over southeastern China seas from multi-satellite altimeter vertical deflections. *Journal of Applied Geophysics., 137*, 128-137. doi:10.1016/j. jappgeo.2016.12.014.

Zingerle, P., Pail, R., Gruber, T., & Oikonomidou, X. (2020). The combined global gravity field model XGM2019e. *Journal of geodesy, 94*, 1-12. https://doi.org/10.1007 /s00190-02001398-0.